Utilization of Multispectral-UAV system for Rice Crop Management

A dissertation submitted to the
Graduate School of Bioagricultural Sciences
Nagoya University
in partial fulfillment of the requirements for the degree of
Doctor of Bioagricultural Sciences

By

Maria Victoria Rabaca Bascon

Laboratory of Information Sciences in Agricultural Lands

Department of Plant Production Sciences

Graduate School of Bioagricultural Sciences

Nagoya University

Chikusa, Nagoya Japan

September 2022

Table of Contents

Abstract

Remote sensing using unmanned aerial vehicles (UAVs) and satellites is a rapidly growing technology in rice crop management today. While satellites are expected to cover a wide area at the national level and become an important platform for future agriculture, they have a low temporal and spatial resolution, making it difficult to develop technology for farmland. Therefore, there is a need to develop technology that can be applied to wide-area monitoring using UAVs, which can acquire crop data with higher temporal and spatial resolution, using satellites.

Crop parameters such as above-ground biomass (AGB) and leaf area index (LAI) of paddy rice are indicators of productivity and can be used to evaluate rice crop management for optimal grain yield and agricultural decision making. Previous studies have shown that LAI and AGB of rice can be estimated using the vegetation index (VI) derived from spectral reflectance. Assuming that the development of a good LAI and AGB estimation model would be useful in predicting grain yield of paddy rice, this study improved the LAI and AGB estimation method using UAV-derived multispectral images and developed a grain yield estimation method using them.

In general, the accuracy of crop prediction models depends on the type of feature variables, model algorithms, and timing of data measurement, and these factors need to be considered in developing accurate crop prediction models. Therefore, the following four items were considered in this study.

(1) Evaluation of the impact of the use of texture variables on the accuracy of LAI-VI estimation models

(2) Evaluation of the impact of feature selection methods and the use of vegetation fraction (VF) on the rice AGB estimation model

3) Development of a grain yield prediction model using VI variables

4) Evaluation of optimal timing of data acquisition for grain yield prediction.

Experimental trials were conducted for two fertilizer trials and five rice cultivars during the 2020 and 2021 rice seasons. Multispectral images and the data of LAI, AGB, and grain yield were measured at four growth stage for each cultivar. UAV-derived variables such as VI and texture features calculated from the gray-level co-occurrence matrix (GLCM) were used as explanatory variables in the models. Feature selection methods such as Recursive Feature Elimination (RFE),

M-statistics, and z-tests were used in AGB estimation model while Exhaustive Feature Selection (EFS), variance threshold, and Variance Inflation Factor (VIF) were used in LAI estimation model to reduce the dimensions of the models by selecting parameters. For regression models, we evaluated the machine learning methods Support Vector Regression (SVR), Random Forest (RF), and Extreme Gradient Boost (XGBoost) for AGB estimation model while Multiple Linear Regression (MLR), SVR, RF, and Ridge Regression for LAI estimation model.

The results showed that RF gave stable results for LAI estimation of rice (R^2 = 0.60–0.62, RMSE = 0.68–0.73, m^2 / m^2), suggesting that feature selection had little effect on the performance of this model. Furthermore, combining specific reflectance data (RVI, GRVI) with texture data (DTI(NIR,R), RTI(NIR,G)) improved the accuracy of LAI estimation for all five cultivars tested (R^2 = 0.68–0.82). This clearly shows that the use of texture and appropriate reflectance data can improve the accuracy of LAI estimation for rice.

We also considered the use of VF, a known alternative indicator of LAI, in the AGB estimation model. However, it is difficult to develop a model that stably distinguishes between plant and non-plant areas under outdoor conditions in this study, and no significant improvement in AGB estimation accuracy was observed even when VF was used as an additional explanatory variable. We also developed a model to predict grain yield using time-specific VI measured at tillering, stem elongation, booting, and heading stages. Correlations between VI and grain yield showed that it was low among growth stages (r = 0.07–0.39). To improve the accuracy of grain yield prediction using VI as an explanatory variable, a multivariate regression model was selected. The results showed that RF performed the best among the regression models used in this study, including SVR, MLR, and Ridge regression, and the grain yield prediction using five VIs, including the normalized VI with Red Edge as an explanatory variable, was moderately weak (R^2 = 0.35 and RMSE = 0.78 ton/ha). The normalized VI with Red Edge contributes to grain yield prediction by providing optimal variability to the model. On the other hand, grain yield prediction was not substantially improved (R^2 = 0.39, RMSE = 0.75 ton/ha) when VI for the booting and heading stages were added as explanatory variables. When prediction models were created for each cultivar, better performance was observed for the cultivars Hatsushimo (R^2 = 0.50, RMSE = 0.84 ton/ha) and Nikomaru (R^2 = 0.50, RMSE = 0.53 ton/ha).

AGB and LAI estimations using multi-temporal VI were redeveloped in the XGBoost model and simulated throughout the growing season using Gompertz curves to determine the optimal timing of data acquisition for grain yield prediction for each cultivar. A single-day linear regression model was also constructed to examine prediction performance using simulated AGB and LAI values. The results showed that AGB and LAI could be estimated from VI (R^2 = 0.56–0.83, 0.57–0.73), and that the optimal timing of UAV flight varied from 4 to 31 days between the tillering and early heading periods for each cultivar. These findings are expected to help researchers save resources and time for numerous UAV flights to predict rice grain yield.

These results suggest that LAI and AGB estimates for two fertilizer trials and five varieties in a two-year experiment can be reasonably estimated using UAV-derived variables and machine learning models. Furthermore, direct prediction of grain yield using the cumulative VI provides comparable or better predictions than that of the estimated AGB and LAI using VI for some cultivars. Even variables with low correlation to crop parameters can be employed as explanatory variables indicating that a variety of inputs are essential for improved prediction.

In summary, our results showed that rice grain yield could be predicted before the heading stage using either VI or VI-estimated AGB and LAI, although it is cultivar-dependent. The analysis of the suitable timing of observations, which has not been evaluated in previous reports, allowed us to identify when yield estimation by satellite remote sensing can be used, and we believe this will contribute to the future widespread use of agricultural remote sensing.

List of Abbreviations

AGB	Aboveground biomass
AIC	Akaike Information Criterion
EFS	Exhaustive Feature Selection
XGBoost	Extreme Gradient Boost
GLCM	Gray Level Co-occurrence Matrix
GY	grain yield
LAI	leaf area index
ML	machine learning
MLR	Multple Linear Regression
NIR	near infrared
PLS	Partial Least Square
RF	Random Forest
RFE	Recursive Feature Elimination
SVR	Support Vector Regression
TI	Texture index
UAV	Unmanned Aerial Vehicle
VIF	Variance Inflation Factor
VT	Variance Threshold
VF	Vegetation Fraction
VI	Vegetation Index

Index

Chapter I: Background of the Study

Abstract: Remote sensing using UAVs in agriculture is a fast-expanding technique in crop management today. UAVs have the potential to provide crop data with higher temporal and spatial resolution. Thus, the suitability of UAV-derived multispectral images in crop prediction must be evaluated. Past research shows that leaf area index and aboveground biomass can be estimated using vegetation index derived from spectral reflectance measured by different sensors. The accuracy of the estimation or prediction model depends on the type of feature variables, the model algorithm, and the timing of data measurement. Developing a crop prediction model with high accuracy must consider these factors.

---

1. Rationale

The primary purpose of agriculture in producing food for the world's population encompasses practices that positively and negatively impact the environment. Pollution and degradation of soil, water, and air are inevitable effects of agriculture but are mitigated using appropriate farming practices. Such farming practices promote a precise, cost-effective, and sustainable way of producing crops. One possible approach is the use of the remote sensing method.

Remote sensing is used in agriculture to monitor vegetation cover, evaluate crop health and nutrient demand, and assess crop pests and diseases. Thus, it can help reduce the effect of problems in agriculture, such as improper use of fertilizers and pesticides, labor cost and shortage, and unstable approximations of crop parameters.

Remote sensing product such as vegetation index (VI) acts as a proxy to crop parameters such as leaf area index (LAI) used to evaluate crop nutrient management. Proxy variables allow faster evaluation and decision-making, which is critical because of the relatively short crop growth duration. However, the availability of these proxy variables depends on the remote sensing platform. The revisiting time of a satellite takes 10 to 14 days. Thus, missed information in the interval is highly possible and crucial for the success of its implementation. The unmanned aerial vehicle (UAV) system can provide this missed information at an even higher spatial resolution.

Moreover, the difference in spatial resolution indicates a different quality from the satellite-derived remote sensing products. It requires optimization of proxy variables from UAV-derived images for proper usage. The need to validate and optimize remote sensing methods shall further improve its applicability in the field.

The remote sensing method is also a potential approach for crop predictive modeling due to its high temporal and spatial resolution. Crop prediction models provide researchers with a guide on the crop growth dynamics while proactively facilitating crop management for the farmers. The continuous improvement of computing machines allows researchers to estimate and predict crop agronomic traits using a high volume of data from numerous farm fields on a regional and national scale. Using machine learning (ML) to find patterns in the data and consequently use these patterns to predict a crop estimate made the crop prediction model a much faster task to accomplish.

Rice production is characterized by small pieces of land with different water and soil fertility regimes. The cultural practices and cultivars used are highly diverse, indicating possible grain yield variation. Accordingly, it has been shown that site-specific rice crop nutrient management contributes to more cost-effective production due to higher grain yield [1]. Crop yield improvement involves optimizing the light interception of the foliage, converting the photosynthetic product into assimilates, and partitioning the assimilates into grains. Estimating crop parameters such as leaf area index and aboveground biomass (AGB) is an alternative method to assess crop grain yield improvement [2].

The most common way of rice crop prediction is using VI, usually derived from RGB and multispectral sensors. The potential use of AGB and LAI estimates from VIs in predicting grain yieldmust also be investigated to relate the pre-harvest crop productivity indicators to grain yield.

Research conducted by [3] using multitemporal RGB and multispectral images to predict rice grain yield found that the initial heading stage is the optimum time for grain yield prediction, which may have 5-7 days. According to [4], the assimilated reserves of the rice plant until the heading stage is the product assimilated during the ripening period. Moreover, N redistribution, which is the N found in the leaves and stems at the maturity stage, significantly correlates with grain yield. Its value depends on the N content of the biomass at the heading stage [5]. As mentioned by [6], the assimilation of the plant before heading is highly correlated with the high-yielding rice variety.

On the other hand, an LAI increase exponentially decrease tillering rate for a given N level, which affects the number of panicles, a grain yield component [7]. LAI was also positively correlated with rice grain yield [8]. LAI reaches its maximum value at the heading stage [9]. Thus, the number of panicles produced is achieved at the heading stage.

However, the satellite may not capture this short period of the heading stage. Thus, using UAV is an alternative to increase the temporal resolution of vegetation indices that can capture the optimum time window for grain yield prediction. The higher temporal resolution of UAV can confirm if the optimum time window for a cultivar's grain yield prediction can be extended beyond the satellite's revisiting time of 5 days.

2. Statement of the Problem

Previous research about the prediction model of AGB, LAI, and grain yield were developed separately and were not integrated to produce a prediction system for the whole agricultural production.

Thus, the suitability of a proxy variable such as VI is limited in future use. This study attempted to develop prediction models for AGB, LAI, and grain yield from remotely sensed products of the same rice field trials using machine learning algorithms. The study aimed to develop a model prediction workflow that can integrate the three crop parameters, AGB, LAI, and grain yield. The study hypothesized that an integrated model prediction system could reduce the dimensionality and noise of the prediction model while expanding its applicability to estimate different crop parameters, thus improving its performance.

3. Objectives of the Study

The major objective of this study is to develop prediction models for rice crop parameters such as AGB, LAI, and grain yield. Specifically, the study attempted to achieve the following:

1. Evaluate the impact of vegetation fraction cover on estimating rice AGB.
2. Determine the effect of texture-based variables on the rice LAI-VI estimation model.
3. Determine the effect of vegetation index (VI) variables on predicting rice grain yield
4. Determine the optimum time window of UAV flight for rice grain yield prediction

4. Literature Review

4.1. Remote Sensing

4.1.1 Principle of Remote Sensing

Remote sensing measures an object from afar without physical contact using reflected or emitted electromagnetic energy [10]. It uses the electromagnetic spectrum in the visible, infrared, and microwave regions. Target objects such as bare soil, water, and vegetation vary in their responses to these wavelengths, providing a method to distinguish these target objects for the assessment of the earth's surfaces [11]

Specifically, it is the method of detecting and recording the radiant energy reflected by surface material. Every surface material reflects different amounts of energy in the different bands along the electromagnetic spectrum. The reflectance property depends on the reflecting surface's structural, chemical, and physical properties. Other factors such as angle of incidence, intensity, and wavelength of the radiant energy also affect the reflectance value of a surface material [12]

The basic process of remote sensing consists of the following: (1) emission of electromagnetic radiation from the source such as the sun, (2) transmission, absorption, and scattering of the radiant energy from the source to the surface material, (3) interaction of the source and the surface material, characterized as the reflection of the energy source and emission of the energy from the surface material, (4) transmission of the reflected energy from the surface to the remote sensor and (5) processing of the remote sensor output [12]. The transmission of the reflected energy from the surface to the remote sensor is possible, with the property of the sun being the source of radiation and illumination. With these properties, camera sensors can capture the reflected energy [12].

When electromagnetic radiation interacts with the surface material, its magnitude, direction, and polarization change, these changes are detected by the remote sensors, allowing extraction of information about the surface material. This information is spatial (size, shape, and orientation) and spectral (tone, color, and spectral signature) [13]. The spectral band from 0.3 to 3.0 um is the reflective region whose radiation the remote sensor senses is due to the sun, reflected by the surface material [14].

Surface reflection occurs when the light radiation is redirected as it hits the non-transparent surface. The reflection intensity depends on the absorption coefficient, surface refractive index, and

angle of incidence. Transmission occurs when the radiation passes through a surface material without significantly decreasing intensity. The transmission level measured as transmittance depends on the surface thickness [13].

Spectral reflectance is the ratio of reflectance energy to incident energy as a function of wavelength. The spectral signature of an object refers to the value of reflectance averaged over different, well-defined wavelength intervals [13]. The spectral reflectance value of an object depends on the wavelength, whereby spectral reflectance is

$$\rho(\lambda) = [ER(\lambda) / EI(\lambda)] \times 100$$

where, ρ(λ) = Spectral reflectance (reflectivity) at a particular wavelength. ER(λ) = Energy of wavelength reflected from object EI (λ) = Energy of wavelength incident upon the object.

4.2 Radiation Properties of Earth's Surface

The spectral reflectance curve of a surface feature is its reflectance values along the electromagnetic spectrum. The curve varies with the surface feature's chemical composition and physical condition. Comparing the spectral signature of these surface features can distinguish them from each other as surface features are similar in the reflectance at a particular wavelength but different in another. The earth's surface feature has three types: vegetation, water, and soil [13].

4. 2.1. Vegetation

The spectral characteristics of vegetation differ with wavelength. Chlorophyll-containing plant part absorbs radiation in the red and blue wavelengths but reflects green wavelength. The palisade layer of healthy leaves reflects near-infrared wavelength. This is the basis for determining the health status of vegetation via remote sensing [13].

Vegetation differences can be observed in near-infrared reflectance [10]. When combined with the reflectances in the visible region, the reflectances in the near-infrared region up to 0.9 um and shortwave infrared beyond 0.9 um can provide data for vegetation identification and classification [13].

4.2.2. Soil

The incident radiation of a soil surface is reflected chiefly or absorbed. Its reflectivity factors are moisture content, organic matter content, texture, structure, and iron oxide content [13]. Soil characteristics such as chemical and soil texture components correlate highly with the spectral reflectance gathered in the laboratory [15]. Spectral indices developed to estimate chlorophyll content correlate with soil organic matter [16]. Spectral reflectance at visible and NIR bands were the most related in estimating soil reflectance can be extended to estimating the physical properties of paddy soil [17,18].

4.2.3. Water

Most incident radiation that hits the water surface is either absorbed or transmitted, and water absorbs longer visible and near-infrared radiation than shorter visible radiation. Factors such as water depth, particles within the water, and surface roughness of water affect its reflectivity [13]. Estimating soil water content using a water-based spectral index is only sensitive at the top soil water status and more appropriate in areas with drought or water as its limiting factor for yield production [19].

4.2.4. Atmosphere

Electromagnetic radiation passes through the atmosphere twice. First is the direct electromagnetic radiation from the sun travels to the earth's surface, and second, when reflected light from the surface passes through the sensor. The interaction between the direct and reflected radiation is called atmospheric effects, which contain information about the atmosphere itself. Moreover, in the process, the atmosphere may change the reflected radiation's direction and absorb and scatter the reflected radiation [13].

The scattering of the reflected radiation depends on the particles present in the atmosphere and the time and season. Thus, the effect of scattering the reflected radiation will vary from time to time [13].

4.3. Unmanned Aerial Vehicle (UAV)

An unmanned aerial vehicle (UAV) is an aircraft design with no pilot on board, more commonly known as a drone. In contrast, the unmanned aerial system integrates UAVs, sensors, and the ground

control point system, enabling location identification necessary for data acquisition, such as reflectance maps [20]. Generally, UAVs are involved in agricultural tasks such as monitoring agricultural areas, assessment of crop status, and forecasting crop yields. UAVs are flown at lower altitudes. Thus, cloud penetration from the sensors on board is not necessary. The most recent common type of UAV used in agricultural surveys and monitoring is the multi-rotor wing type or quadcopter. [21]. This type of UAV has good maneuverability, is portable, and has an interchangeable payload. Third-party sensors can be onboard a UAV [22]. However, the flight time is shorter.

4.4. Vegetation Index as Proxy Variable

The vegetation index is used as a proxy variable in crop monitoring and estimation with the premise that the spectral signature of vegetation is correlated with biophysical characteristics. Combining different spectral bands in the form of a ratio or linear transformation may accurately estimate biophysical plant parameters such as leaf area index and aboveground biomass [23]. The vegetation index provides a good characterization of crop growth and condition [11].

There are different types of vegetation index: (1) simple, intrinsic index, (2) index with soil line, and (3) atmospherically-corrected index. The simple vegetation indices include difference vegetation index (DVI), normalized difference vegetation index (NDVI), and ratio vegetation index (RVI). NDVI is the most common VI used. It has values ranging from 0 to 1 due to the normalization of the reflectance values. Ratio Vegetation Index (RVI) is the ratio between red and NIR bands assuming that plants absorb more in the red band than in the NIR band. This index, however, is sensitive to atmospheric effects. Difference Vegetation Index (DVI) is the difference between NIR and red bands, which is a solution to the sensitivity of RVI in atmospheric effects. DVI, on the other hand, is sensitive to soil background.

The vegetation index with soil line can distinguish vegetation from the soil background. This is possible by determining the soil line, the linear relationship between red and NIR reflectance observed from the soil spectral reflectances. The background soil effect is established to adjust the value of normalized VIs sensitive to background effects. Atmospherically-corrected VI was also developed to improve biomass estimation of NDVI [24]. The atmospherically corrected Vis uses a

blue band to regulate the atmospheric effects, while the difference between red and blue bands relates to the atmospheric effects in the reflectance.

4.5. Aboveground Biomass Estimation

Aboveground biomass (AGB) in rice is estimated by destructive sampling and weighed as either fresh biomass or dry matter after oven-drying [38]. It is the most accurate yet labor-intensive and time-consuming method to estimate AGB. Indirect estimation of AGB was developed using image analysis of remote sensing data that is fast, time, and cost-effective. The traditional remote sensing method in estimating AGB is the extraction of VIs. AGB in rice is estimated to estimate carbon stock in the plant as most of the biomass accumulation in plants is made up of carbon. It is the most frequently used indicator of crop productivity. The development of rice AGB estimation commonly consisted of improving feature variable extraction, determining the optimum time of measurement, and evaluating different estimation models based on a particular set of experimental variables.

4.5.1. Model Selection varies with Growth Stage and Type of Feature Variables

The relationship between rice AGB and VIs varies with the source of reflectance images, growth stage, and given field conditions of the experiment. The complexity of an experiment inhibits simple regression models from generating conclusive relationships among the variables. Thus, using other machine learning (ML) algorithms allows multiple data sources to uncover relationships between variables. Selecting which algorithm to use primarily depends on the similarity of the variables used between ML algorithms. A comparison of ML was conducted by [39] to evaluate which algorithm best estimates dry AGB of rice using VIs derived from different satellites. When the model developed were according to rice growth stages, the results showed that decision-tree-based models such as gradient boost decision tree (GBDT) and random forest (RF) performed best at a pre-heading stage, while Support Vector Regression (SVR) and k-Nearest Neighbor (k-NNN) performed best at the post-heading stage. On the other hand, when a single source of VIs is used in a study, the estimation results of different machine learning methods are comparable. Even the combination of different UAV-related variables resulted in similar estimation results, as observed in research done by [40], where

different regression methods using a combination of spectral, structural, and meteorological feature variables had similar estimation results.

4.5.2. AGB Estimation is Improved by Combining VI with other UAV-related Variables

Estimation of AGB using VI depends on the correlation between VI and AGB, which may vary depending on how the VI was extracted and adjusted to enhance the AGB-VI relationship. Estimating rice AGB using VI alone has shown good performance, as seen from the high correlation of AGB with RGB images at different growth stages [31]. The color index, VARI, can estimate grain yield using a log relationship at R^2 = 0.71. On the other hand, NDVI from multispectral images showed a linear relationship with grain yield at R^2 = 0.75. OSAVI also gave reasonable AGB estimates throughout the growing season [41]. Likewise, optimization of the spectral band for VI calculation using a spectroradiometer can result in a difference in the accuracy of AGB estimation. First-derivative-based VI is best performed at the booting and heading stages, while second-derivative-based VI is best performed at the stem elongation stage [42]. Given the VIs mentioned above, the accurate extraction of VIs from UAV-derived images is critical.

Two feature extraction methods were developed by [43] to extract the vegetation component of a UAV image accurately. These are GFKuts, an image filtering method to extract VI based on a Gaussian model, Montecarlo-based K means, and Graph-Based Fusion (GBF), a feature extraction method that does not depend on canopy reflectance. AGB estimates from these feature extraction methods resulted in improved AGB estimation.

Another option to estimate AGB other than using VI is the Digital Surface Model (DSM). Canopy height (CH) is estimated using DSM by determining the difference between each DSM and the first DSM after transplanting. A high R^2 (> 0.90) was observed in AGB estimation using the DSM-CH model. This relatively high prediction performance using DSM was due to the less influence of weather on DSM [44]. Moreover, using total dry biomass as the ground truth representative of AGB may present limitations in using VI. For example, chlorophyll indices may not perform well when estimating AGB derived from total dry biomass. Thus, the dry matter index (DMI) will likely better estimate AGB. One such research was conducted by [45]. The DMI group of vegetation index resulted in better estimation than the use of chlorophyll index like CI-red edge.

Textural information was also employed in AGB estimation. The Gray Level Co-Occurrence Matrix (GLCM) is the most commonly used textural analysis, and it is a statistical method of calculating a statistical metric of two neighboring gray-level pixels. The texture metric, Mean using NIR and its corresponding NDTI texture using NIR and Red bands, had the highest estimation accuracy (R^2 = 0.65 to 0.84) [41]. Using full band textures in AGB estimation also improved AGB estimation, particularly at the tillering stage [46].

4.5.3. Timing of AGB Estimation relies on the Optimum Feature Variable

Timing for AGB estimation using VIs depends on the feature variable used in the model. Generally, rice AGB is estimated using VI, where the image's greenness indicates vegetation. This assumption is usually at the early growth stage until the maximum canopy stage [47]. However, good estimation results can still be observed when the VI is optimized in each stage. AGB estimation using VI derived from first derivative reflectance performed best at booting and heading stages, while second derivative reflectance performed best at stem elongation stage [42]. Also, when the VI value is adjusted by removing the non-canopy area in the image, AGB can be estimated for each growth stage. One example is the combined method of optimal VI and object-oriented segmentation, wherein the VI most correlated with AGB is adjusted using an image segmentation method that merges canopy and non-canopy areas based on the spectrum and textural characteristics of the image [37].

4.6. Leaf Area Index Estimation

LAI is essential as it indicates the total canopy area that can absorb light for photosynthesis. It estimates the photosynthetic potential of the crop and influences the microclimate in the canopy being the medium for the gas exchanges. Estimating LAI can be a substitute for identifying the photosynthetic productivity of the crop, as well as the foliar damage of pests and diseases. It can also estimate grain yield as it directly correlates with grain yield. However, LAI estimation using the traditional destructive approach is time-consuming, even though most accurate. Thus, developing a regression model between LAI and VI will fasten LAI phenotyping.

4.6.1 Model performance depends on the type of algrorithm and feature variable

Different regression algorithms were used to develop the LAI estimation model with its performance depending on the type of the feature variable. Support Vector Regression (SVR) and Random Forest (RF) showed to have higher accuracy in LAI estimation when the LAI of the whole rice crop growth duration was used in training the model and were trained on Vis derived from first-derivative spectra [25]. Combining bands and VIs can improve XGBoost and RF models in estimating rice LAI [26]. Other rice LAI estimation models showed that an extreme learning machine (ELM) is also better than RF when RGB and multispectral images were combined [27]. The appropriateness of a regression algorithm to estimate a rice LAI may depend on the structural characteristics of the canopy indicative of the growth stage and may not always mean superiority of the algorithm throughout the crop growth duration. For example, simpler models, such as the univariate regression model, performed better when LAI was estimated at the vegetation growth stage [25]. Nevertheless, as the canopy becomes more complex at the ripening stage, machine learning models such as SVR and RF proved to have higher accuracy than simple regression models. This presents flexibility in the prediction process where all aspects of estimation are not considered.

4.6.2. Feature Selection to Reduce Model Dimension

Selection of feature variable is a method used to reduce the dimension of the model. Several feature selection methods could be applied. Models such as RF and XGBoost have built-in feature selection methods making them robust against multicollinearity. SVR models in estimating maize LAI can be improved against these models by incorporating feature selection methods such as Principal Component Analysis (PCA) and correlation analysis [28]. In rice, PCA detects a relationship between VI and LAI when single VI information could not estimate the LAI [29].

4.6.3. Type of Variable Affects Model Performance

Earlier research on LAI estimation using reflectance data dealt with identifying optimal waveband for further spectral transformation. Although the selected optimal bands were evaluated using the correlation-coefficient method using hyperspectral images, the selected bands have a

counterpart in established VI, thereby making the established VI still applicable for LAI estimation when hyperspectral reflectance data is not available [30].

Rice LAI highly correlates with visible-NIR images at different growth stages [31]. RF and XGBoost models were improved using NIR + red spectral transformation as variables [26]. Even the use of NDVI at a single growth stage VI model gave the best rice LAI prediction at the vegetative stage [25]. This only supports claims that the fusion of RGB and multi-spectral images resulted in better rice LAI prediction [27]. Better rice LAI prediction was also observed when the VI was adjusted based on the growth stage. The VI measured throughout the growth duration was divided into clusters, and then the clusters were converted as another variable [23].

However, other research has shown that a combination of red-edge and NIR images is more optimal in generating vegetation indices such as DVI, NDVI, and RVI, whether about the whole crop growth stage or single growth stage [25]. This is further proven by the effectiveness of red edge-based VI, MTCI, and CIred edge in estimating green LAI, the photosynthetic component of LAI. These VI performed better than EVI, a soil background-insensitive VI, indicating that these VI are not affected by the soil background. However, MTCI is sensitive to crop type with varying leaf canopy structures, while CIrededge is not [32]. A global dataset from the Landsat satellite of LAI estimates from different VIs showed that LAI-VI relationships are crop-specific and non-linear. However, in the same global dataset, EVI/EVI2 was found to be the most effective LAI estimate [33].

Other research on rice LAI estimation using UAV showed a weak correlation between rice LAI and VIs throughout the growing season due to the hysteresis relationship of VI vs. LAI from heading to post-heading stages. However, the inclusion of canopy height with OSAVI reduced the hysteresis effect, thereby improving LAI estimation [34].

Including non-remote sensed variables in the LAI estimation model did not improve the model. Earlier research using a radiometer showed that adding variables such as plant chlorophyll content, paddy depth, water sediment load, and bottom layer color did not improve the model [23].

In other crops, such as maize, the spectral and textural features of UAV-derived images were used to estimate LAI. Results show that LAI estimation can be improved by combining VI and texture-based indices. Texture-based indices combine two texture features (i.e., variance and entropy) of the same band. [28]. In rice LAI, the texture of the UAV images was also explored. The Local Binary

Pattern (LBP) and Variance (VAR) texture of a spectral image were combined. Then, the combined LBP-VAR was combined with the corresponding spectral reflectance. This feature variable performed better than VI alone in estimating LAI [35]. Another texture-based rice LAI estimation model was developed by creating a normalized difference texture index from two spectral bands with the same texture features (i.e., Red variance, Blue variance) using the 3 x 3 window size. Results show that texture features mean from Red and Green improved LAI estimation [36].

Optimization of the vegetation component extracted from a Region of Interest (ROI) was also investigated in rice LAI estimation. The use of optimal VI (OVI) and object-oriented segmentation (OS) to remove the non-canopy component increase LAI estimation, although not substantial, regardless of the growth stage used [37].

4.6.4. Timing of Estimation

The accuracy of LAI estimation depends on the type of variables used in the model. However, there is an optimum time for LAI estimation when a single set or type of variable is used. This is due to the limitation of a feature variable to approximate the actual crop parameter being estimated. The most common reason is the saturation of VI with the red spectral band. This is because leaf pigments highly absorb energy at the red band, resulting in lower red reflectance and remaining unchanged even at higher canopy coverage (i.e., leaf area index). Thus, the estimation of LAI at the vegetative stage had higher accuracy than at the ripening stage. The initial jointing stage is the best time for LAI estimation [27]. A similar result was also found by [37].

4.7. Integrating AGB and LAI to grain yield

As indicators of crop growth and productivity, AGB and LAI can be utilized in predicting rice grain yield. The precision of using the leaf area index estimated from the vegetation index in estimating grain yield depends on the radiation-use efficiency (RUE). The spectral information indicated in the VI may not reflect the actual photosynthetic activity in the canopy. Nevertheless, using leaf area dynamics can improve yield estimation [49]. Using the Random Forest model, the estimation of plant growth parameters using RGB images can have similar performance using multispectral images.

On the other hand, the use of multispectral images in simple linear models is more effective than RGB images [31]. The optimized value of LAI and leaf nitrogen accumulation gave better grain yield prediction [50]. Data from the SPOT satellite and leaf area index had a high R^2 of 0.945 in estimating grain yield [51].

4.8. Present Challenges

The instability of prediction results from developing grain yield can be reduced by increasing the accuracy of biomass estimation and harvest index [56]. The accuracy of prediction models requires the availability of different datasets that can characterize the sources of variation of the target variables, such as AGB, LAI, and grain yield. However, no single standard is applied in developing a crop prediction model. Thus, despite the availability of different machine learning and feature selection methods, crop prediction models are still a vast task in crop management. Thus, proper optimization of all the components of a crop prediction model must be done for suitability in farm management.

5. References

1. Wang, G.; Dobermann, A.; Witt, C.; Sun, Q.; Fu, R. Performance of Site-Specific Nutrient Management for Irrigated Rice in Southeast China. *Agronomy Journal.* **2001**, *93(4)*, 869–878, https://doi.org/10.2134/agronj2001.934869x.
2. Gifford, R. M.; Thorne, J. H.; Hitz, W. D.; Giaquinta, R. T. Crop productivity and photoassimilate partitioning. *Science*. **1984**, *225*(4664), 801-808, doi/10.1126/science.225.4664.801.
3. Wan, L.; Cen, H.; Zhu, J.; Zhang, J.; Zhu, Y.; Sun, D.; Du, X.; Zhai, L.; Weng, H.; Li, Y.; et al. Grain Yield Prediction of Rice Using Multi-Temporal UAV-Based RGB and Multispectral Images and Model Transfer – a Case Study of Small Farmlands in the South of China. *Agricultural and Forest Meteorology.* **2020**, *291*, 108096, doi:10.1016/j.agrformet.2020.108096.
4. Weng, J. H.; Takeda, T.; Agata, W.; Hakoyama, S. Studies on dry matter and grain production of rice plants: I. Influence of the reserved carbohydrate until heading stage and the assimilation products during the ripening period on grain production. *Japanese Journal of Crop Science*. **1982**, *51(4)*, 500-509, https://doi.org/10.1626/jcs.51.500.
5. Zhang, Y.L.; Fan, J.B.; Wang, D.S.; Shen, Q.R. Genotypic Differences in Grain Yield and Physiological Nitrogen Use Efficiency Among Rice Cultivars. *Pedosphere.* **2009**, *19(6)*, 681–691, doi:10.1016/S1002-0160(09)60163-6.
6. Laza, Ma.R.; Peng, S.; Akita, S.; Saka, H. Contribution of Biomass Partitioning and Translocation to Grain Yield under Sub-Optimum Growing Conditions in Irrigated Rice. *Plant Production Science.* **2003**. *6(1)*, 28–35, https://doi.org/10.1626/pps.6.28.
7. Zhong, X.; Peng, S.; Sheehy, J.E.; Visperas, R.M.; Liu, H. Relationship between Tillering and Leaf Area Index: Quantifying Critical Leaf Area Index for Tillering in Rice. *Journal of Agricultural Science.* **2002**, *138(3)*, 269–279, doi:10.1017/S0021859601001903.
8. Zhu, G.; Ren, Z.; Liu, Y.; Lu, F.; Gu, L.; Shi, Y.; Liu, J.; Zhou, G.; Nimir, N.E.A.; Mohapatra, P.K. Optimization of Leaf Properties and Plant Phenotype through Yield-Based Genetic Improvement of Rice over a Period of Seventy Years in the Yangtze River Basin of China. *Food and Energy Security.* **2020**, *9(3)*, e223, https://doi.org/10.1002/fes3.223.
9. Hussain, S.; Fujii, T.; McGoey, S.; Yamada, M.; Ramzan, M.; Akmal, M. Evaluation of different rice varieties for growth and yield characteristics. *JAPS: The Journal of Animal and Plant Sciences*. **2014**, *24*(5), 1504-1510.
10. Goetz, A.F.H.; Rock, B.N.; Rowan, L.C. Remote Sensing for Exploration: An Overview. *Economic Geology.* **1983**, *78(4)*, 573–590, https://doi.org/10.2113/gsecongeo.78.4.573.
11. Palanisamy, S.; Selvaraj, R.; Ramesh, T.; Ponnusamy, J. Applications of Remote Sensing in Agriculture - A Review. *International Journal of Current Microbiolology and Applied Sciences.* **2019**, *8(1)*, 2270–2283, doi:10.20546/ijcmas.2019.801.238.
12. Aggarwal, S. Principles of remote sensing. *Satellite remote sensing and GIS applications in agricultural meteorology*. **2004**, *23*(2), 23-28, https://citeseerx.ist.psu.edu/viewdoc/summary?doi=10.1.1.536.9991.
13. Bian, L.; Walsh, S. J. Scale Dependencies of Vegetation and Topography in a Mountainous Environment of Montana. *The Professional Geographer.* **1993**, *45(1)*, 1–11, https://doi.org/10.1111/j.0033-0124.1993.00001.x.
14. Marceau, D.; Hay, G. Remote Sensing Contributions to the Scale Issue. *Canadian Journal of Remote Sensing.* **1999**, *25(4)*, 357–366, https://doi.org/10.1080/07038992.1999.10874735.
15. Nanni, M.R.; Demattê, J.A.M. Spectral Reflectance Methodology in Comparison to Traditional Soil Analysis. *Soil Science Society of American Journal.* **2006**, *70(2)*, 393–407, doi:10.2136/sssaj2003.0285.
16. Bartholomeus, H.M.; Schaepman, M.E.; Kooistra, L.; Stevens, A.; Hoogmoed, W.B.; Spaargaren, O.S.P. Spectral Reflectance Based Indices for Soil Organic Carbon Quantification. *Geoderm.* **2008**, *145(1-2)*, 28–36, doi:10.1016/j.geoderma.2008.01.010.

17. Post, D.F.; Fimbres, A.; Matthias, A.D.; Sano, E.E.; Accioly, L.; Batchily, A.K.; Ferreira, L.G. Predicting Soil Albedo from Soil Color and Spectral Reflectance Data. *Soil Science Society of American Journal.* **2000**, *64(3)*, 1027–1034, doi:10.2136/sssaj2000.6431027x.
18. Gholizadeh, A.; Amin, M.S.M.; Borůvka, L.; Saberioon, M.M. Models for Estimating the Physical Properties of Paddy Soil Using Visible and Near Infrared Reflectance Spectroscopy. *Journal of Applied Spectroscopy.* **2014**, *81(3)*, 534–540, doi:10.1007/s10812-014-9966-x.
19. Ma, S.; Zhou, Y.; Gowda, P.H.; Dong, J.; Zhang, G.; Kakani, V.G.; Wagle, P.; Chen, L.; Flynn, K.C.; Jiang, W. Application of the Water-Related Spectral Reflectance Indices: A Review. *Ecological Indicators.* **2019**, *98*, 68–79, doi:10.1016/j.ecolind.2018.10.049.
20. Nex, F.; Remondino, F. UAV for 3D Mapping Applications: A Review. *Applied Geomatics.* **2014**, *6(1)*, 1–15, doi:10.1007/s12518-013-0120-x.
21. Kim, J.; Kim, S.; Ju, C.; Son, H.I. Unmanned Aerial Vehicles in Agriculture: A Review of Perspective of Platform, Control, and Applications. *IEEE Access.* **2019**, *7*, 105100–105115, doi:10.1109/ACCESS.2019.2932119.
22. del Cerro, J.; Cruz Ulloa, C.; Barrientos, A.; de León Rivas, J. Unmanned Aerial Vehicles in Agriculture: A Survey. *Agronomy.* **2021**, *11(2)*, 203, https://doi.org/10.3390/agronomy11020203.
23. Vaesen, K.; Gilliams, S.; Nackaerts, K.; Coppin, P. Ground-Measured Spectral Signatures as Indicators of Ground Cover and Leaf Area Index: The Case of Paddy Rice. *Field Crops Research.* **2001**, *69(1)*, 13–25, https://doi.org/10.1016/S0378-4290(00)00129-5.
24. Xue, J.; Su, B. Significant Remote Sensing Vegetation Indices: A Review of Developments and Applications. *Journal of Sensors.* **2017**, *2017*, 1353691, https://doi.org/10.1155/2017/1353691.
25. Wang, L.; Chang, Q.; Li, F.; Yan, L.; Huang, Y.; Wang, Q.; Luo, L. Effects of Growth Stage Development on Paddy Rice Leaf Area Index Prediction Models. *Remote Sensing.* **2019**, *11(3)*, 361, https://doi.org/10.3390/rs11030361.
26. Liu, S.; Zeng, W.; Wu, L.; Lei, G.; Chen, H.; Gaiser, T.; Srivastava, A.K. Simulating the Leaf Area Index of Rice from Multispectral Images. *Remote Sensing.* **2021**, *13(18)*, 3663, https://doi.org/10.3390/rs13183663.
27. Du, X.; Wan, L.; Cen, H.; Chen, S.; Zhu, J.; Wang, H.; He, Y. Multi-Temporal Monitoring of Leaf Area Index in Rice under Different Nitrogen Treatments Using UAV Images. *International Journal of Precision Agricultural Aviation.* **2018**, *1(1)*, 11–18, doi:10.33440/j.ijpaa.20200301.57.
28. Zhang, X.; Zhang, K.; Sun, Y.; Zhao, Y.; Zhuang, H.; Ban, W.; Chen, Y.; Fu, E.; Chen, S.; Liu, J.; Hao, Y. Combining Spectral and Texture Features of UAS-Based Multispectral Images for Maize Leaf Area Index Estimation. *Remote Sensing.* **2022**, *14(2)*, 331, https://doi.org/10.3390/rs14020331.
29. Yan Y.; Qing-jiu T. Principal Component Analysis Method for Retrieving Leaf Area Index of Rice from Hyperspectral Data. *Remote Sensing for Natural Resources.* **2007**, 3, 47-50,61, doi:10.3969/j.issn.1001-070X.2007.03.011.
30. Wang, F.; Huang, J.; Zhou, Q.; Wang, X. Optimal Waveband Identification for Estimation of Leaf Area Index of Paddy Rice. *Journal of Zhejiang University SCIENCE B.* **2008**, *9(12)*, 953–963, doi:10.1631/jzus.B0820211.
31. Qiu, Z.; Ma, F.; Li, Z.; Xu, X.; Du, C. Development of Prediction Models for Estimating Key Rice Growth Variables Using Visible and NIR Images from Unmanned Aerial Systems. *Remote Sensing.* **2022**, *14(6)*, 1384, doi:10.3390/rs14061384.
32. Viña, A.; Gitelson, A.A.; Nguy-Robertson, A.L.; Peng, Y. Comparison of Different Vegetation Indices for the Remote Assessment of Green Leaf Area Index of Crops. *Remote Sensing of Environment.* **2011**, *115(12)*, 3468–3478, doi:10.1016/j.rse.2011.08.010.
33. Kang, Y.; Özdoğan, M.; Zipper, S.C.; Román, M.O.; Walker, J.; Hong, S.Y.; Marshall, M.; Magliulo, V.; Moreno, J.; Alonso, L.; Miyata, A.; Kimball, B.; Loheide, S.P. How Universal Is the Relationship between Remotely Sensed Vegetation Indices and Crop Leaf Area Index? A Global Assessment. *Remote Sensing.* **2016**, *8(7)*, 597, doi:10.3390/rs8070597.

34. Gong, Y.; Yang, K.; Lin, Z.; Fang, S.; Wu, X.; Zhu, R.; Peng, Y. Remote Estimation of Leaf Area Index (LAI) with Unmanned Aerial Vehicle (UAV) Imaging for Different Rice Cultivars throughout the Entire Growing Season. *Plant Methods* **2021**, *17(1)*, 88, doi:10.1186/s13007-021-00789-4.
35. Yang, K.; Gong, Y.; Fang, S.; Duan, B.; Yuan, N.; Peng, Y.; Wu, X.; Zhu, R. Combining Spectral and Texture Features of UAV Images for the Remote Estimation of Rice LAI throughout the Entire Growing Season. *Remote Sensing.* **2021**, *13(5)*, 3001, doi:10.3390/rs13153001.
36. Li, S.; Yuan, F.; Ata-UI-Karim, S.T.; Zheng, H.; Cheng, T.; Liu, X.; Tian, Y.; Zhu, Y.; Cao, W.; Cao, Q. Combining Color Indices and Textures of UAV-Based Digital Imagery for Rice LAI Estimation. *Remote Sensing.* **2019**, *11(15)*, 1763, doi:10.3390/rs11151763.
37. Qiu, Z.; Xiang, H.; Ma, F.; Du, C. Qualifications of Rice Growth Indicators Optimized at Different Growth Stages Using Unmanned Aerial Vehicle Digital Imagery. *Remote Sensing.* **2020**, *12(19)*, 3228, doi:10.3390/rs12193228.
38. Kondhia, A.; Tabien, R.E.; Ibrahim, A. Evaluation and Selection of High Biomass Rice (*Oryza Sativa L.*) for Drought Tolerance. *American Journal of Plant Science.* **2015**, *6(12)*, 1962, doi:10.4236/ajps.2015.612197.
39. Mansaray, L.R.; Kanu, A.S.; Yang, L.; Huang, J.; Wang, F. Evaluation of Machine Learning Models for Rice Dry Biomass Estimation and Mapping Using Quad-Source Optical Imagery. *GIScience & Remote Sensing.* **2020**, *57(6)*, 785–796, doi:10.1080/15481603.2020.1799546.
40. Jiang, Q.; Fang, S.; Peng, Y.; Gong, Y.; Zhu, R.; Wu, X.; Ma, Y.; Duan, B.; Liu, J. UAV-Based Biomass Estimation for Rice-Combining Spectral, TIN-Based Structural and Meteorological Features. *Remote Sensing.* **2019**, *11(7)*, 890, doi:10.3390/rs11070890.
41. Zheng, H.; Cheng, T.; Zhou, M.; Li, D.; Yao, X.; Tian, Y.; Cao, W.; Zhu, Y. Improved Estimation of Rice Aboveground Biomass Combining Textural and Spectral Analysis of UAV Imagery. *Precision Agriculture.* **2019**, *20*, 611–629, doi:10.1007/s11119-018-9600-7.
42. Gnyp, M.L.; Miao, Y.; Yuan, F.; Ustin, S.L.; Yu, K.; Yao, Y.; Huang, S.; Bareth, G. Hyperspectral Canopy Sensing of Paddy Rice Aboveground Biomass at Different Growth Stages. *Field Crops Research.* **2014**, *155*, 42–55, doi:10.1016/j.fcr.2013.09.023.
43. Jimenez-Sierra, D.A.; Correa, E.S.; Benítez-Restrepo, H.D.; Calderon, F.C.; Mondragon, I.F.; Colorado, J.D. Novel Feature-Extraction Methods for the Estimation of Above-Ground Biomass in Rice Crops. *Sensors.* **2021**, *21(13)*, 4369, doi:10.3390/s21134369.
44. Peprah, C.O.; Yamashita, M.; Yamaguchi, T.; Sekino, R.; Takano, K.; Katsura, K. Spatio-Temporal Estimation of Biomass Growth in Rice Using Canopy Surface Model from Unmanned Aerial Vehicle Images. *Remote Sens.* **2021**, *13(12)*, 2388, doi:10.3390/rs13122388.
45. Cheng, T.; Song, R.; Li, D.; Zhou, K.; Zheng, H.; Yao, X.; Tian, Y.; Cao, W.; Zhu, Y. Spectroscopic Estimation of Biomass in Canopy Components of Paddy Rice Using Dry Matter and Chlorophyll Indices. *Remote Sens.* **2017**, *9*, 319, doi:10.3390/rs9040319.
46. Xu, T.; Wang, F.; Xie, L.; Yao, X.; Zheng, J.; Li, J.; Chen, S. Integrating the Textural and Spectral Information of UAV Hyperspectral Images for the Improved Estimation of Rice Aboveground Biomass. *Remote Sensing.* **2022**, *14(11)*, 2534, doi:10.3390/rs14112534.
47. Butterfield, H.S.; Malmström, C.M. The Effects of Phenology on Indirect Measures of Aboveground Biomass in Annual Grasses. *International Journal of Remote Sensing.* **2009**, *30(12)*, 3133–3146, doi:10.1080/01431160802558774.
48. Zhang, K.; Ge, X.; Shen, P.; Li, W.; Liu, X.; Cao, Q.; Zhu, Y.; Cao, W.; Tian, Y. Predicting Rice Grain Yield Based on Dynamic Changes in Vegetation Indexes during Early to Mid-Growth Stages. *Remote Sensing.* **2019**, *11(4)*, 387, doi:10.3390/rs11040387.
49. Hashimoto, N.; Saito, Y.; Yamamoto, S.; Ishibashi, T.; Ito, R.; Maki, M.; Homma, K. Feasibility of Yield Estimation Based on Leaf Area Dynamics Measurements in Rice Paddy Fields of Farmers. *Field Crops Research.* **2022**, *286*, 108609, doi:10.1016/j.fcr.2022.108609.
50. Wang, H.; Zhu, Y.; Li, W.; Cao, W.; Tian, Y. Integrating Remotely Sensed Leaf Area Index and Leaf Nitrogen Accumulation with RiceGrow Model Based on Particle Swarm Optimization

Algorithm for Rice Grain Yield Assessment. *Journal of Applied Remote Sensing.* **2014**, *8(1)*, 083674, doi:10.1117/1.JRS.8.083674.

51. Aboelghar, M.; Arafat, S.; Abo Yousef, M.; El-Shirbeny, M.; Naeem, S.; Massoud, A.; Saleh, N. Using SPOT Data and Leaf Area Index for Rice Yield Estimation in Egyptian Nile Delta. *The Egyptian Journal of Remote Sensing and Space Science.* **2011**, *14(2)*, 81–89, doi:10.1016/j.ejrs.2011.09.002.

Chapter II: Combining Spectral and Texture Features of UAV-Derived Multispectral Images to Estimate Rice LAI

Abstract: The use of UAV-derived multispectral images can provide LAI monitoring and estimation. This study examined the effects of texture features and their combination with spectral features derived from UAV multispectral images on rice LAI estimation. Multispectral images and ground-truth LAI were collected from the field trials between 2020 and 2021. The spectral and texture features used in the LAI estimation were the vegetation indices (VIs) and two types of texture indices derived from the gray-level co-occurrence matrix (GLCM). Feature selection methods Exhaustive Feature Selection (EFS), Variance Threshold, and Variance Inflation Factor (VIF) were employed for each of the machine learning methods, Multiple Linear Regression (MLR), Support Vector Regression (SVR), Random Forest (RF), and Ridge regression. The results suggest that random forest can give reasonable LAI estimates (R^2 = 0.60 to 0.65, RMSE = 0.68 to 0.73), with feature selection having little effect on the model performance. Type I texture index also improved LAI estimation compared to Vis Combining spectral (RVI, GRVI) and texture (DTI(NIR, R), RTI(NIR, G)) can further improve LAI estimation, with all five rice cultivars showing good LAI estimation results ranging from 0.68 to 0.82.

---

1. Introduction

The leaf area index is an essential indicator of crop productivity. It is the estimated amount of foliage relative to the ground when considering a plane. It can be used to characterize field conditions such as the amount of potential evapotranspiration in the area and light attenuation in the canopy, potentially estimating the amount of photosynthetic or biomass accumulation of the crop. Leaf area index estimation has undergone significant developments through the years, from the traditional ruler method to the plant canopy analyzer that allows non-destructive estimation of LAI. LAI measurement has been a part of rice breeding strategies, as the role of LAI in crop productivity has been acknowledged [1]. Recently, high throughput phenotyping has become even more possible with UAVs. Early research showed a linear relationship between rice LAI and NDVI [2]. Moreover, vegetation index (VI), such as the narrowband DVI and SR generated from red-edge and near-infrared band

pairs, were optimal for the whole rice growth period and each growth stage [3]. However, a study from [4] showed a weak relationship between rice LAI and VI thought the growth period.

The accuracy of rice LAI estimation depends on the type of VIs and the growth stage used. Transformed forms of VIs, such as the first derivative, showed a better estimate of LAI than the original VI [3,5]. Other research found that the original VI method is more suited for use at the vegetative stage than using the first derivative of VI [3]. On the other hand, the first derivative of VI employed in Random Forest for the whole growth period can estimate LAI at each growth stage [3]. Other research tried to estimate LAI by combining the VI with its raw reflectance values, such as in the case of [6]. Earlier research also showed that LAI had a high correlation with difference index (DI), ratio index (RI), and normalized index (NI) [7].

Research on rice LAI estimation using hyperspectral data and involving different nutrient management showed that Machine learning (ML) algorithms like Random Forest (RF) and Support Vector Machine (SVM) have shown to have better prediction performance than Multiple Linear Regression (MLR) and Partial Least Square Regression (PSLR) [3,8]. Another study showed that the Deep Learning (DL) with RGB Images resulted in similar LAI estimation performance compared to the ML mentioned above algorithms with MS images [4]. This implies that RGB images are enough to estimate LAI instead of using sensors with more bands. However, DL requires a much higher dataset for the training process than ML algorithms. ML algorithm was also observed to reduce overfitting issues of LAI estimation of three different rice cultivars [6].

Another improvement in the rice LAI estimation model focused on reducing the hysteresis effect of the growth stage on rice LAI estimation by combining VIs with other variables such as texture index. The most common texture analysis used is the Gray-level co-occurrence matrix, where texture indices can also be derived. The estimation of rice LAI was improved by combining VARI (3 visible bands) with NDTI from the Mean texture feature of Red and Green bands using Random Forest [9]. The variance texture feature also improved rice LAI estimation using an exponential regression model [10, 11]

Texture indices can be generated in two ways. The first is by calculating texture indices using two bands with similar GLCM parameters (statistical texture feature, window size, and direction). The

second is calculating texture indices using two statistical texture features with different optimum GLCM parameters, and optimum parameters were based on their correlation with LAI.

When LAI is estimated using VIs, a pixel's different spectral reflectance values are considered independent of the neighboring pixels. The average spectral values of all the ROI pixels are considered the representative estimate of the target surface, rice LAI. It is assumed that transforming the reflectance values in a combination will highlight the target surface, and the interaction of light scattering properties of each component in the ROI is reduced. This is where the texture image of an image can be of interest.

Determining texture as fineness or coarseness of an image is a method to identify distinct objects by segmenting the image into a homogeneous texture using the texture gradient created in the image based on a defined window size [12].

In this study, we aimed (1) to determine the relationship between LAI and the UAV-related variables such as VIs, GLCM-based textures, and Texture Indices, and (2) to determine the best combination of UAV-related variables that can estimate LAI using different machine learning algorithm, and (3) determine if there are differences in the performance of LAI estimation models of different rice cultivars.

2. Materials and Method

2.1. Experimental site

The study site is at the Togo Field, Field Science Research Center of Nagoya University in Hatajiri, Morowa District, Togo, Aichi Prefecture, Japan. Aichi Prefecture belongs to a humid subtropical climate zone. The average sunshine hours are 2141.0. The mean annual temperature is 16.2 °C. The average rainfall is 1578.9 mm. During the growing season, the average monthly total sunshine duration is 165.38 hours, the average monthly total precipitation is 223.35, and the average daily temperature is 25.7 °C during the growing season. The average rainfall is 1578.9 mm [13]. The primary soil type is ultisols.

2.2. UAV-Based Image Acquisition and LAI Measurements

The study utilized a UAV system: Matrice 210 RTK v2 with a Zenmuse X7 50 mm camera (DJI, Shenzhen, Guangdong, China) and Micasense RedEdge-MX sensors. The multispectral bands used in this study were the following: blue (475 ±32 nm), green (560 ± 27 nm), red (668 ±14 nm), red edge (717 ± 12 nm), and near-IR (842 ± 57 nm). The flight altitude was 20.0 m, with a forward overlap of 80% and a side overlap of 75%. The shooting mode was hovering with a flight speed of 1.2 m/s. The approximate resolution was 0.20 cm/pix.

For each UAV flight, the sensors were calibrated using a Calibrate Reflectance Panel (CRP) provided by the sensor manufacturer according to their instructions. UAV flights were conducted between 10:00 am and 4:00 pm under windless and clear-sky conditions once a week until the heading stage.

Table 1. Summary of field experiments

Rice season	UAV Flight Date	LAI Sample	Growth Stage
2020	15 July[4], 21 July[2], 29 July[135]	144,48,48	Tillering Stage
	29 July[4], 5 August[35], 11 August[12]	144,96,48	Stem Elongation
	17 August[145], 23 August[32]	144,96	Booting
2021	22 July[4], 28 July[35], 31 July[1], 5 August[2]	48,96,48,48	Tillering Stage
	5 August[4], 11 August[35], 18 August[12]	48,96,96	Stem Elongation
	20 August[4], 25 August[15], 31 August[23]	48,96,96	Booting

[1]Aichinokaori [2]Asahi [3]Hatsushimo [4]Nakate Shinsenbon [5]Nikomaru
The number indicates which variety was the spectral data extracted for a given UAV flight date.

The acquired images were ortho-mosaicked using the Pix4D mapper software (Pix4D SA, Prilly, Switzerland) to generate the spectral reflectance images of the experimental plots and georeferenced using ground control points.

LAI was sampled for each variety during the critical growth stages for tillering, stem elongation and booting stages. For spectral data collection, sampling was conducted after the UAV flight (Table 1). The spectral data for each variety at a given growth stage were extracted from different UAV flight date. Four adjacent hills of rice plants were sampled in each plot at three different growth stages (tillering, stem elongation, booting stages). The number of tillers per sampled hill was counted and separated into leaves and stems. The detached leaves were used to determine the LAI using a leaf area meter, AAM-9 (Hayashi Denko co ltd., Tokyo, Japan). After measuring the leaf area, the separate plant parts were oven-dried at 70 °C for 48 h until a constant weight was attained and weighed.

2.3. Vegetation Index (VI) Calculation

Nine vegetation indices were calculated using the formulas given in Table 2. These were the common VIs used in the estimation of different crop parameters.

Table 2. List of Vegetation Indices used in the study.

Vegetation Index	Formula	Reference
Difference Vegetation Index (DVI)	NIR – R	[14]
Green Difference Vegetation Index (GDVI)	NIR – G	[15]
Red Edge Difference Vegetation Index (REDVI)	NIR – RE	[16]
Normalized Difference Vegetation Index (NDVI)	(NIR − R) / (NIR + R)	[17]
Green Normalized Difference Vegetation Index (GNDVI)	(NIR − G) / (NIR + G)	[18]
Normalized Difference Red-Edge (NDRE)	(NIR − RE) / (NIR + RE)	[19]
Ratio Vegetation Index (RVI)	NIR / R	[14]
Green Ratio Vegetation Index (GRVI)	NIR / G	[20]
Red Edge Ratio Vegetation Index (RERVI)	NIR / RE	[21]

R = red reflectance; G = green reflectance; B = blue reflectance; NIR = near infrared reflectance; RE = red-edge reflectance.

2.4. Texture Analysis

The gray-level co-occurrence matrix (GLCM) method was used to extract the texture features of the UAV multi-temporal images. It is called the gray level co-occurrence matrix because the square matrix contains the counts of a number of the co-occurrence of neighboring gray levels in the image. In the GLCM method, the GLCM is generated by dividing the whole grayscale image into sliding window sizes. We used a 9 x 9 window size for this study's raw reflectance maps. The type of neighboring gray levels was based on the following angles: (1) 0^o, (2) 90^o, and (3) one-rotation invariant (combination of 0 degree, 45^o,90^o,135^o). The angle is determined by using a reference pixel where the angle direction between two gray levels is based.

Once the GLCM is produced, different statistical metrics are computed. The GLCM features are statistical metrics that can quantitatively describe the texture features of the image. These were Contrast (CON), Dissimilarity (DIS), Entropy (ENT), Homogeneity (HOM), Mean (MEA), Second Moment (SEM), and Variance (VAR). The texture features for each plot were then extracted using the ROI shapefile using the 'raster' package in R. The texture features were calculated using the 'raster' and 'glam' packages in R. The statistical metrics were calculated to generate texture maps using the 'glcm' package in R with a sliding window size of 9 x 9 pixels with varying angles (0 °, 90^o, and one-rotation invariant (combination of 0^o, 45^o,90^o,135^o). The texture features in each plot were extracted using the ROI shapefile using the 'raster' package in R [22].

Texture indices were also calculated by transforming the GLCM-based features calculated from each band. The texture indices were generated using two types of calculation: (1) Type I: texture indices derived from the transformation of the optimized bands, and (2) Type II: texture indices derived

from the transformation of texture metrics with each metric optimized according to band and angle. Both types used the following equations,

Ratio texture index (T2 / T1); (B2 / B1), Eq'n (1)

Normalized texture index (T2 - T1)/ (T2 + T1); (B2 - B1)/ (B2 + B1) Eq'n (2)

Difference texture index (T2 - T1); (B2 - B1) Eq'n (3)

where T1 and T2 represent two different GLCM-based texture features while B1 and B2 represent two different bands.

2.5. Feature Selection Methods

Exhaustive Feature Selection is simply the combination of all the features specified in the model. The number of features to be selected is determined by a particular performance measure such as Akaike Information Criterion (AIC) or MSE. It is computed using the 'ExhaustiveSearch' package in R. In this study, and we used the AIC score as the performance measure. The model variables with the lowest AIC score were the feature variables selected.

Variance Thresholding is a baseline feature selection method to remove features with zero or low variance. It is assumed that high variance will provide more information to predict the target variable. It is computed using the 'caret' package in R [23]. In this study, we set the variance threshold at 0.10.

Variance Inflation Factor (VIF) is a score corresponding feature selection method to the level of multicollinearity. Multicollinearity is the collinearity between feature variables which can result in instability of a model result. This is because the correlated feature variable indirectly influences the effect of one feature variable on the target variable. A value of more than 5.0 was considered multicollinearity and removed from our model. It was calculated using the 'car' package in R [24].

2.6. Modeling Methods

Linear regression (LR), Ridge Regression (RR) Support Vector Machine (SVR) and Random Forest (RF) were used to establish the LAI estimation models using VI, GLCM-based textures, and texture indices as predictor variables.

Linear regression model is a least-squares approach that defines the linear relationship between two or more variables. It can be represented using the universal set containing a simple or multiple regression as follows:

$$Y = a + \sum_{i=1}^{k} bi\, X\mathrm{i} + \mathrm{u}$$

where Y is the dependent variable, X1, X2...Xk are the independent variables, *a* and *b*i are the regression coefficients representing the model's parameter in a sample population and u is the random error term. The simple linear regression has a fixed Xi and random Y, while multiple linear regression has both random Xi and Y.

Ridge regression is a parameter estimation method used to solve a model's collinearity problem. In multivariate regression models, variable elimination is seen as the solution to counter the effect of multicollinearity in the model. In ridge regression, the variables are penalized due to the model's complexity but not removed from the model. The variables with less effect will have coefficients that are close to zero. It is, in effect, a method for feature selection, resulting in a variable whose coefficients can predict better and has lower squared errors than the simple least-square method.

A support vector machine is a machine learning algorithm that searches for a hyperplane with the maximum distance from the data points. It is a decision boundary whose either side represents classified data points. Classifiers are maximized by the influence of support vectors, points near the hyperplane, and influences the position of the hyperplane.

Random Forest is a non-parametric estimation method that creates randomized regression trees. A subset of observations from the training dataset is drawn for each tree. Then, each tree is split depending on the number of variables a split in each tree must have. The split of a tree is stopped when the number of observations is below the node size points. A prediction is made for each tree, then the predictions are averaged to get the final prediction.

2.7. Statistical Methods

A workflow chart is shown in Figure 2 to illustrate the steps to estimate LAI using different statistical methods, including feature selection methods and machine learning algorithms. Datasets from the 2020 and 2021 rice seasons were combined and split into 70 % training data (252 observations) and 30% test data (108 observations). Training data was used for model establishment and cross-validation, while test data was used for model evaluation. The test data is the independent

dataset that was not used during model establishment and is used to determine the generalization capacity of the developed estimation model.

Feature variables such as GLMC-based features and texture indices were selected using their Pearson's Correlation Coefficient with rice LAI. After the correlated texture-related variables were selected, these variables, together with the calculated VIs, were used to develop LAI estimation models using SLR, MLR, Ridge, SVR, RF, and XGBoost algorithms. Different feature selection methods were performed before model training for the LAI estimation models with multiple explanatory variables. LAI estimation models were developed for each machine learning algorithm in each set of variables derived from a feature selection method.

The training dataset was employed to train the model using a 10-fold cross-validation method, and the model performance was evaluated using R^2 and RMSE.

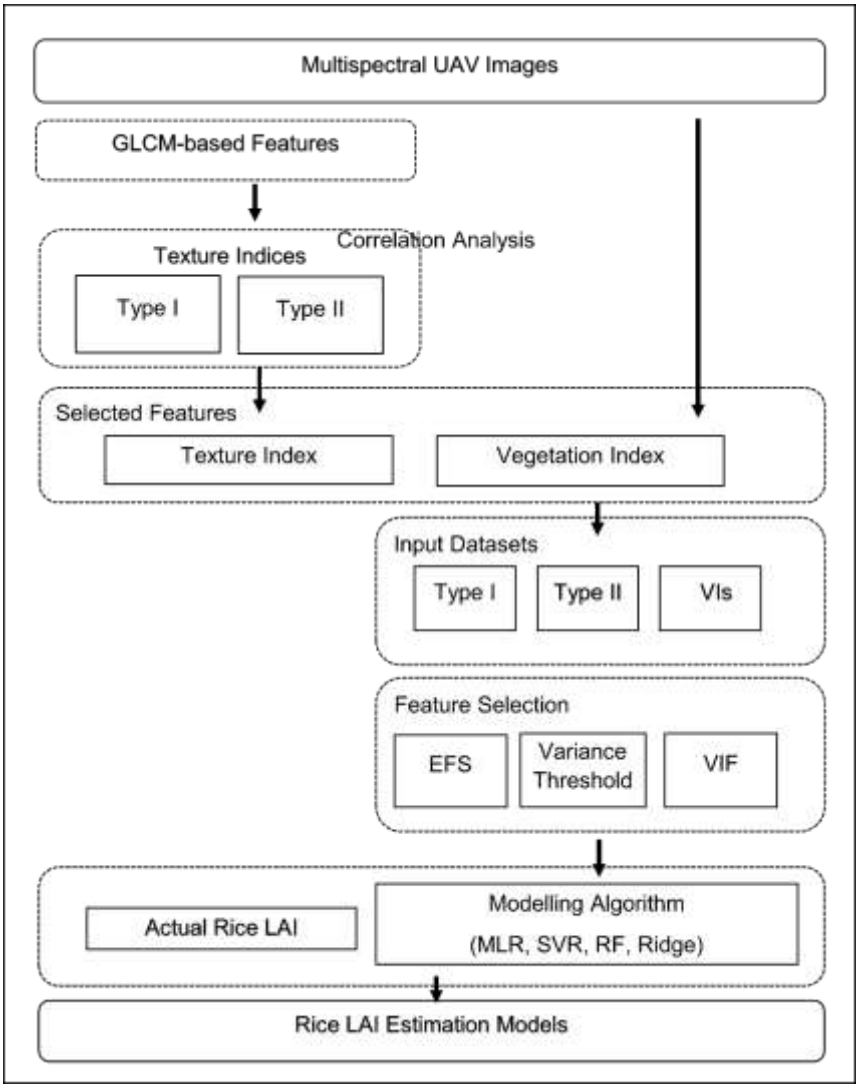

Figure 1 Workflow of the Rice LAI Estimation Model

2.7.1. Correlation Analysis

Correlation analysis is a method used to identify the relationship between two variables. For a pair of both numerical variables, the Pearson Product Moment Coefficient is used. Pearson's correlation coefficient is a unitless measure of the linearity between two numerical variables.

2.7.2. Validation of the Regression Models

The developed models were validated using the test dataset after data splitting. The performance metrics R^2 and RMSE were computed to evaluate model performance.

3. Results

3.1. Correlation Analysis of UAV Image-derived Features and Actual LAI Data

The linear relationships between LAI and different VIs were assessed and summarized in Table 3. To better understand the relationship of LAI with VI, the VIs were divided into three (3) groups: (1) Difference vegetation index (DVI, GDVI, REDVI), (2) Normalized difference vegetation index (NDVI), and Ratio vegetation index (RVI). The correlation between LAI and DVI differed from the correlations between LAI and GDVI and LAI and REDVI. NDVI correlation with LAI was similar to NDRE correlation with NDRE. GRVI and RERVI had a similar correlation with LAI and differed from RVI. On average, ratio vegetation indices had the highest correlation with LAI compared with difference vegetation indices and normalized difference vegetation indices.

Table 3. Correlation coefficient between LAI and Vegetation Index (VI)

VI	DVI	GDVI	REDVI	NDVI	GNDVI	NDRE	RVI	GRVI	RERVI
R	0.52	0.54	0.57	0.54	0.65	0.55	0.71	0.61	0.61

The GLCM-based texture features used in the study were calculated based on the gray level co-occurrence matrix generated for each raw reflectance map. The texture of each raw reflectance map was calculated using the different directions between two neighboring gray levels. An optimum combination of band and direction was determined for each texture feature by using its correlation with LAI as a criterion. The optimum combinations are presented in Table 4. The NIR band was the optimum for textures CON, MEA, and VAR, while the red band was for textures DIS, ENT, HOM, and SEM. The angle 90º was the optimum direction for textures DIS, ENT, HOM, and SEM, while at 0º angle, textures CON and VAR were at optimum correlation with LAI. The one-rotation invariant was the optimum direction for MEA texture. Texture MEA and VAR had a good correlation with LAI, while the other textures had moderately weak correlations with LAI.

Table 4. Optimal parameters for each texture feature for Type II texture index and its correlation with rice LAI.

Texture	CON	DIS	ENT	HOM	MEA	SEM	VAR
Band	NIR	R	R	R	NIR	R	NIR
Direction	0	90	90	90	Invariant	90	0
R	0.23	-0.26	-0.29	0.27	0.55	0.30	0.56

Table 5 shows the optimum combination of texture features and direction for each band according to its correlation with LAI. It means that the texture of each band is represented by only one texture feature. The representing texture feature for each band and each growth stage was established to ensure a relationship between texture and LAI.

At the tillering stage, MEA with 0° angle was the optimum texture parameter for blue and green bands, while MEA with 90° angle was the optimum texture parameter for red and NIR bands. The texture feature of the red edge band was optimum in HOM texture. Different optimum combinations were observed between bands at the stem elongation stage. It is noted that only the red band maintained the same optimum texture parameters for the 1st two growth stages. MEA was the optimum texture feature for all bands at the booting stage. The optimum texture parameters for the blue, green, and NIR bands were similar for the tillering and booting stages.

Table 5. Optimum parameters for the texture of each band for Type I texture index computation and its correlation with LAI.

Band	Tillering		Stem Elongation		Booting	
	Texture, Direction	r	Texture, Direction	r	Texture, Direction	r
Blue	MEA, 0°	-0.52	SEM, 0°	-0.39	MEA, 0°	-0.29
Green	MEA, 0°	-0.36	CON, 90°	-0.44	MEA, 0°	-0.22
Red	MEA, 90°	-0.54	MEA, 90°	-0.33	MEA, Invariant	-0.49
Red Edge	HOM, 0°	-0.12	CON, Invariant	-0.39	MEA, Invariant	-0.17
NIR	MEA, 90°	0.61	MEA, Invariant	0.51	MEA, 90°	0.57

There were two types of texture indexes created in this study. The optimum parameters summarized in Tables 4 and 5 were used to calculate the Type II and Type I texture indices, respectively, whose formulas are indicated in Equations 1 to 3.

Nine (9) Type I texture indices were calculated in this study and divided into three groups (RTI, NDTI, and DTI). In each group, three texture indices were generated. Three combinations of texture parameters were used for each band comprising a texture index, and each combination referred to each growth stage.

Similarly, Type II texture indices were divided into three groups, as shown in Figures 2a-c. In total, 42 texture feature combinations were produced for each group. However, redundant texture indices were not shown in the correlation matrix. A redundant texture index refers to the texture index

whose texture combination is the exact opposite of another texture index. The two texture indices had a similar absolute correlation with LAI. The texture index chosen between the two related texture indices was based on the alphabetical order, with the chosen texture index coming first in the alphabetical order. Limiting the relationship between LAI and Type II texture indices based on Figures 1a-c, it was observed that Type II texture indices were moderate to weakly correlated with LAI.

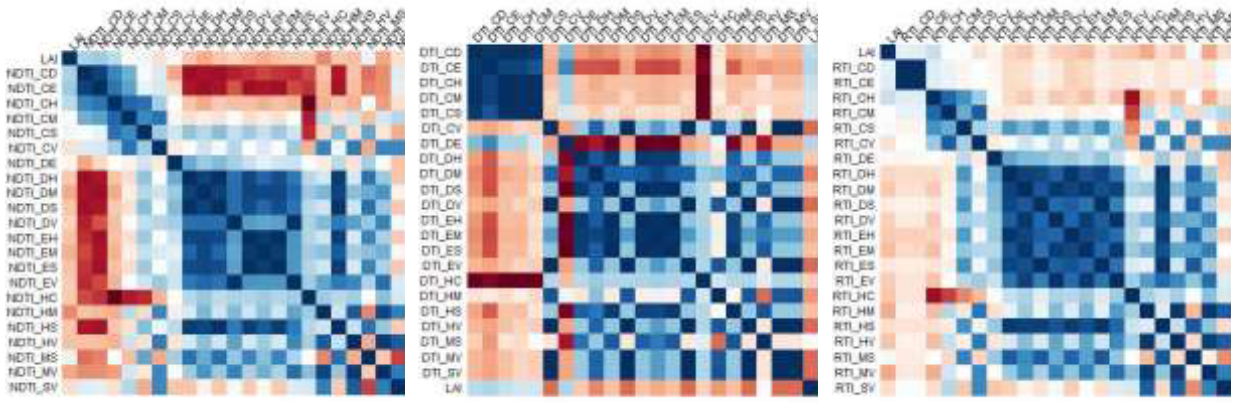

(a) (b) (c)

Figure 2. Correlation matrix between LAI and Texture Indices Type II given as following: (a) NDTI, (b) DTI, and (c) RTI.

3.2. Rice LAI Estimation Model Based on Single Features

The rice LAI estimation model employed the spectral and textural features derived from the UAV images taken across rice growth stages, from tillering to booting. A linear regression model was developed for each feature to determine the merit of using a UAV-derived feature in the LAI estimation model. However, the number of texture features was reduced according to the optimization (Tables 4 and 5) done prior to regression modeling.

After establishing a linear model using the 10-fold cross-validation method, an independent test dataset (30 % of the whole dataset) was used to evaluate the generalization of the LAI estimation model. The summary of these model evaluations is shown in Tables 6, 7, and 8. Among the VIs tested (Table 6) in this study, only RVI had a good model performance (R^2 = 0.50), while NDVI performed the worst (R^2 = 0.29).

The same model training process was performed for LAI estimation using Type I texture indices. Table 7 shows the model performance with DTI (NIR, R) as the relatively best LAI predictor

using Type I texture indices while DTI (NIR, G), DTI (NIR, RE), and NDTI (NIR, G) as features with the least prediction power. On the other hand, the LAI estimation using Type II texture indices results in poor prediction performance, as shown in Table 8.

Table 6. Model evaluation of the LAI estimation using VIs using the independent test data.

Feature	DVI	GDVI	REDVI	NDVI	GNDVI	NDRE	RVI	GRVI	RERVI
R^2	0.30	0.33	0.36	0.29	0.43	0.33	0.50	0.34	0.41
RMSE	0.96	0.94	0.92	0.97	0.87	0.94	0.81	0.93	0.89

Table 7. Model evaluation of the LAI estimation using Type I texture indices using the independent test data.

Feature	DTI (NIR, R)	DTI (NIR, G)	DTI (NIR, RE)	NDTI (NIR, R)	NDTI (NIR, G)	NDTI (NIR, RE)	RTI (NIR, R)	RTI (NIR, G)	RTI (NIR, RE)
R^2	0.53	0.14	0.14	0.40	0.14	0.29	0.48	0.19	0.34
RMSE	0.79	1.07	1.07	0.90	1.07	0.97	0.83	1.04	0.94

Table 8. Model evaluation of the LAI estimation using Type II texture indices using the independent test data.

Feature	NDTI (HM)	NDTI (CE)	NDTI (DM)	DTI (EV)	DTI (DV)	DTI (MV)	RTI (VH)	RTI (VM)	RTI (MH)
R^2	0.20	0.15	0.15	0.28	0.28	0.28	0.27	0.25	0.22
RMSE	1.07	1.10	1.10	1.01	1.01	1.01	1.02	1.03	1.05

3.3. Rice LAI Estimation using Machine Learning Methods

Adding more feature variables can improve the LAI estimation model, and the addition of features may include a similar type of a variable or a combination of different types of variables. In this study, it was determined which type of UAV-derived variable can best estimate rice LAI. Moreover, it was examined if adding UAV-derived variables in a model can further improve LAI estimation compared to the LAI estimation model using the relatively best Type of UAV-derived variable.

Thus, feature selection was needed to accomplish these two tasks. Numerous feature variables can be incorporated into an estimation model. However, not all features will bring significant value to the model. It removes features that are considered redundant and will not bring significant effects to the model. In this study, three feature selection methods were performed for each type of feature variable. These were exhaustive feature selection (EFS), variance threshold (VT), and variance inflation factor (VIF). After feature selection, the LAI estimation model was developed using different machine learning methods. The study set the number of feature variables in each estimation model to five (5) feature variables. This allowed 100 observations for each feature variable since the total training data was 502 (70% of the whole dataset). The results from the feature selection methods are summarized in Table 9. The most frequently selected UAV-derived variables from the different feature selection methods were GRVI, RVI, and NDVI for VIs, DTI (NIR, R), RTI (NIR, G), NDTI(NIR, R) for type I texture index, and RTI_DS for Type II texture index.

Table 9. The selected UAV-derived variables using three (3) different types of feature selection methods.

Feature	Set of Features	Most selected
VIs		
EFS	DVI, NDVI, RVI, GRVI, RERVI	GRVI, RVI,NDVI
VT	RVI, GVI, RERVI, NDVI, GNDVI	
VIF	GRVI, RVI, NDVI, NDRE, GNDVI	
Type I texture index		
EFS	$NDTI_{(NIR,R)}$, $DTI_{(NIR,R)}$, $DTI_{(NIR,G)}$, $RTI_{(NIR,G)}$, $RETI_{(NIR, RE)}$	$DTI_{(NIR,R)}$, $RTI_{(NIR,G)}$
VT	$RTI_{(NIR,R)}$, $NDTI_{(NIR,R)}$, $DTI_{(NIR,R)}$, $RTI_{(NIR,G)}$, $NDTI_{(NIR,G)}$	$NDTI_{(NIR,R)}$
VIF	$NDTI_{(NIR,R)}$, $RTI_{(NIR,R)}$, $RTI_{(NIR,G)}$, $DTI_{(NIR,R)}$, $DTI_{(NIR,RE)}$	
Type II texture index		
EFS	RTI_CD, RTI_DS, RTI_MC, RTI_SC, RTI_VS	RTI_DS
VT	RTI_EM, RTI_CE, RTI_EC, RTI_DS, RTI_CH	
VIF	RTI_CD, RTI_ED, RTI_DS, RTI_SV, RTI_VS	

After cross-validation of all LAI estimation models, the models were evaluated using an independent test dataset (30% of the whole dataset). Results show that the Type I texture index was the best performing feature variable for all the ML methods compared to VIs and Type II texture index. Type I texture index was also observed to perform best for estimation models developed using features that were selected using the extractive feature search method (Table 10) and variance threshold (Table 11). Random forest had the best estimation performance among the four (4) ML methods tested in this study. MLR and Ridge regression resulted in similar model performance, indicating that regularization in the Ridge regression did not improve the model. SVR was the least-performing ML method. Type I and II texture indices did not estimate LAI well when variable inflation factor was used as the feature selection method (Table 12).

Table 10. Model evaluation of the different LAI estimation models using selected features from exhaustive feature selection method (EFS)

	VIs		**Type I TI**		**Type II TI**	
	R^2	**RMSE**	**R^2**	**RMSE**	**R^2**	**RMSE**
MLR	0.535	0.785	0.612	0.717	0.149	0.968
RF	0.633	0.697	0.633	0.697	0.337	0.855
SVR	0.529	0.790	0.598	0.729	0.132	0.978
Ridge	0.535	0.785	0.612	0.717	0.141	0.973

Table 11. Model evaluation of the different LAI estimation models using Variance Threshold as feature selection method.

	VIs		Type I TI		Type II TI	
	R^2	RMSE	R^2	RMSE	R^2	RMSE
MLR	0.535	0.785	0.617	0.712	0.132	0.990
RF	0.605	0.724	0.648	0.683	0.271	0.908
SVR	0.521	0.797	0.615	0.714	0.125	0.994
Ridge	0.535	0.785	0.617	0.712	0.128	0.992

Table 12. Model evaluation of the different LAI estimation models using Variance Inflation Factor as feature selection method.

	VIs		Type I TI		Type II TI	
	R^2	RMSE	R^2	RMSE	R^2	RMSE
MLR	0.539	0.782	0.601	0.727	0.114	1.000
RF	0.601	0.727	0.640	0.691	0.239	0.927
SVR	0.533	0.787	0.578	0.748	0.114	1.000
Ridge	0.539	0.782	0.601	0.727	0.114	1.000

The prediction performance of the LAI estimation model using the combination of different UAV-derived variables was also examined. Two sets of LAI estimation models were developed using (1) most frequently and (2) least selected feature variables from each feature selection method. Five (5) feature variables were selected according to the result of the exhaustive feature search. Table 13 shows the result of the model evaluation. The result shows that Random Forest can give reasonable LAI estimates even if the feature variables were derived from only one feature selection. However, a decrease in model performance can be observed in MLR, SVR, and Ridge when the feature variable was not selected from two or more feature selection methods.

Table 13. Model evaluation of the different LAI estimation models using the five common feature variables from different feature selection methods.

	I		II	
	R^2	RMSE	R^2	RMSE
MLR	0.676	0.677	0.465	0.870
RF	0.751	0.594	0.731	0.617
SVR	0.654	0.700	0.430	0.898
Ridge	0.676	0.677	0.465	0.870

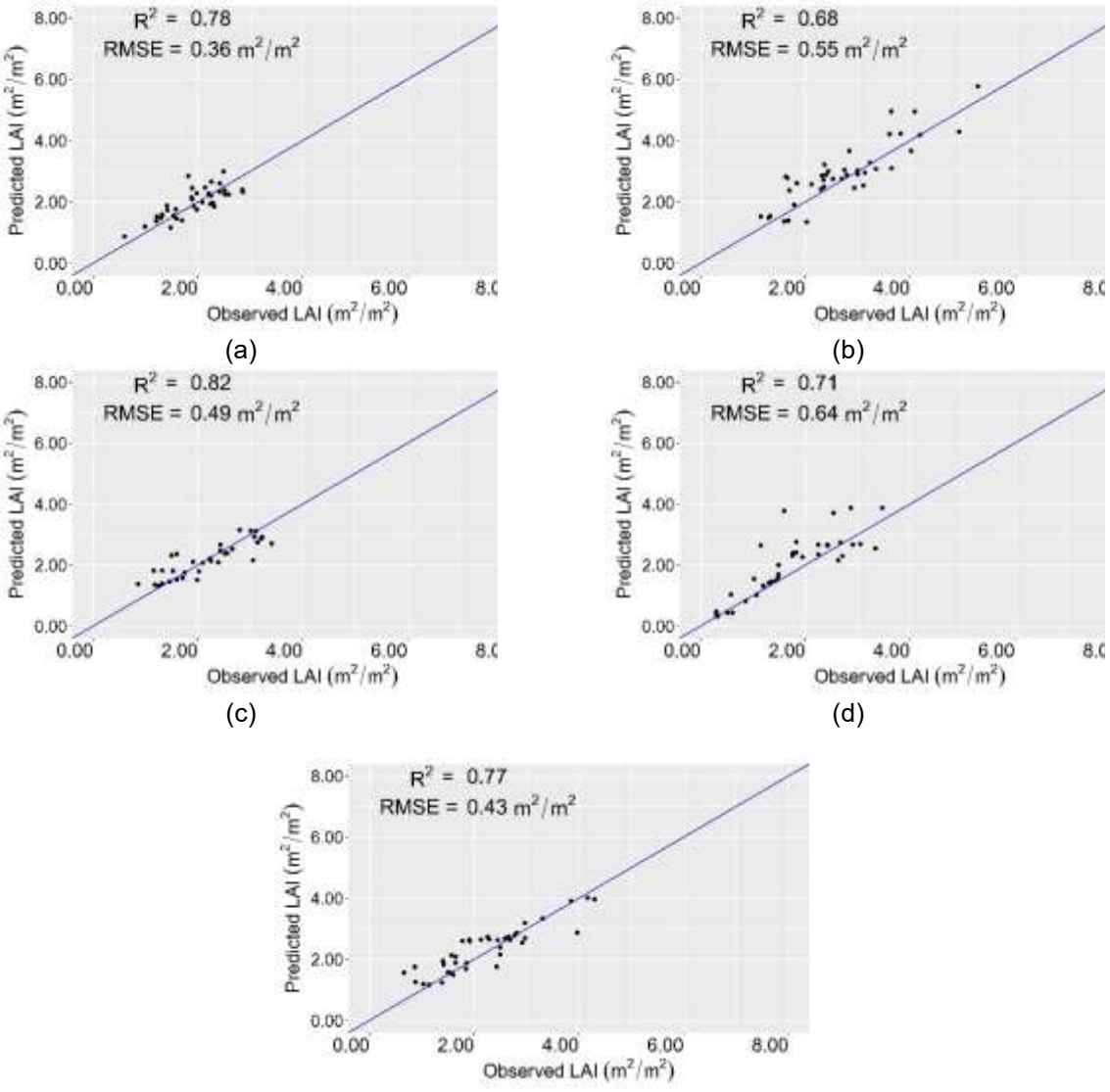

Figure 3. Model evaluation of the LAI estimation model for varieties (a) Aichinokaori, (b) Asahi, (c) Hatsushimo, (d) Nakate Shinsenbon, and (e) Nikomaru.

The LAI estimation model using Random Forest and feature variables NDVI, RVI, GVI, DTI(NIR, R), and RTI(NIR, G) was developed for each of the five (5) rice cultivars. An independent test dataset was used to evaluate the model performance and is summarized in Figures 3a-e. LAI estimation model had good prediction performance using the independent test dataset. The RMSE ranged from 0.36 to 0.64 m^2/m^2.

4. Discussion

4.1. Effect of Spectral and Texture Features on Rice LAI Estimation

The relatively fast and easy calculation of VIs made it a standard feature for LAI estimation. The predictive power of VIs in estimating LAI depends on the range of data utilized to train the model. According to [25], the power relation of ratio vegetation index of NIR to green band with LAI estimation is improved when different growth stages and nitrogen levels in the field trial were used to provide LAI variation in the model. In this study, LAI variations were provided by the fertilizer levels and varieties. Linear regression models using VIs were evaluated using an independent dataset (Table 6) instead of power regression. Even with the difference in the function, ratio vegetation index performed best in estimating LAI, with the ratio vegetation index of NIR to the red band showing the highest R^2. Individually, the growth stage affected the LAI estimation performance. Good LAI estimation of RVI was best achieved at the stem elongation stage (R^2 = 0.71). At this stage, the fraction of rice canopy relative to paddy soil for a defined ROI (one hill in the field) is high. Thus, the reflectance observed in the ROI had a higher probability of being as leaves. Depending on the leaf canopy architecture of the rice cultivars, the soil background is visible at tillering stage. Wet paddy soil has a lower reflectance at the visible and NIR spectrums than vegetation. Moreover, the scattering mechanism of light in rice may include the transmittance of light from the leaf canopy to the soil. And also, the reflectance from the soil to the leaf canopy [26]. In this case, the vegetation index may be underestimated depending on the soil fraction cover in the ROI. A lower RVI value for a pixel containing soil is expected as NIR and red reflectance have closer values than the NIR and red reflectance from vegetation pixels. Thus, ROI with boundaries concentrated on the canopy is beneficial for more accurate LAI estimation of VIs at tillering stage.

For the booting stage, the clumping of leaves may have contributed to overestimating rice LAI per ROI. The booting stage in rice can be characterized by horizontally and diagonally aligned flag leaves, especially at the late booting stage, thereby resulting in the leaves of one plant being captured in the ROI of another plant. In this study, the 9 x 9 window size was used in mapping the texture of the multi-temporal five single-band images. This is to equalize the computation time and complexity between GLCM-based textures and VIs. This is higher than the window size applied, which was 3 x 3 in [9]. Other research opted to apply different window sizes and took the average texture measures

to regulate the effect of window sizes on the image's texture [27]. Small window size is advised in a homogenous field but is considered to produce unstable GLCM measurements [28].

The orientation between neighboring pixels is also considered a factor in texture analysis. According to [28], the orientation of GLCM analysis did not affect the estimation of forest LAI. However, the study hypothesized that orientation between neighboring pixels affects the LAI estimation. It also tested if the effect can be regulated by using the texture values for all the orientations. In evaluating the appropriate GLCM parameters, its high correlation with LAI is considered the optimum GLCM parameter. The results showed that the LAI correlation varied in a window size of 9 x 9. At tillering and booting stages, the MEA texture was relatively more correlated with LAI in most bands with varying optimum orientations. This was probably due to the large window size used in this study. Differing orientation would have little effect on small window size. It should be noted that the result at the stem elongation stage showed different optimum texture measures and orientation, but on average, LAI was best estimated at this stage. The MEA texture feature was the best for image segmentation analysis [29], suggesting that differing orientation and window size may have little effect on GLCM-base texture.

Comparing the results in Table 7 with the results of [9], both showed that high LAI estimation gains at middle to later growth stages of rice could be achieved, but on the average of the growth stages, LAI estimation using texture can result in R^2 ranging from 0.2 to 0.5. With these results, it is reasonable to use 9 x 9 as the window size for the additional computation time needed for a smaller window size would not likely result in a significant difference from the texture values computed at a higher window size of 9 x 9. As shown in Table 8, low prediction performance was observed for all Type II texture indices. It is perhaps due to the lack of optimization of Type II texture indices at each growth stage compared to Type I texture indices and the combination of two similar reflectance bands, which will result in a lack of vegetation emphasis generated from the transformation of different reflectance bands. In this study, the optimum band for each statistical texture metric was either Red or NIR bands only.

4.2. Comparison of Different Machine Learning Methods

Adding feature variables in a regression model can increase prediction performance and the probability of overfitting. However, the improvement of a model depends on the kinds of feature variables added to the model. Thus, feature selection is an essential task in any prediction model. Three (3) feature selection methods were assessed in this study. Each of these feature selection methods influences the LAI estimation model. Exhaustive feature selection (EFS) is simply finding the combination of feature variables that can best predict the data. In this study, AIC was used as the performance metric. In AIC, the best combination of features has the best data variation with the smallest combination of feature variables. It is an estimator of prediction error, and the high value of AIC indicates that the model is less fit to predict the target.

Setting a variance threshold is a baseline method used in most prediction models. In this study, a high variance threshold of 0.10 was used. It is assumed that data with high variation will provide helpful information for prediction. On the other hand, variance inflation factor (VIF) is a method used to detect multicollinearity in a model. Multicollinearity is the correlation between predictor variables in a model. It may not be a problem in large dataset sizes. However, this study's dataset size cannot be considered large relative to other prediction models. Thus, VIF as a feature selection was considered. Results from the feature selection methods (Table 9) show that a feature variable can be selected from all the different feature selection methods. This may indicate either of the two reasons: (1) the three feature selection methods were similar in the selection process, which tends to be a variance of the data in the model, or (2) the feature variable selected in all the feature selection methods is robust. Variance threshold is an unsupervised feature selection with no need for the target output, while EFS and VIF methods use performance metrics of the regression model with the target variable (LAI) to select feature variables.

Random forest was evaluated to be the best regression method in estimating LAI (Table 10-12), regardless of the feature selection method employed in the study. An estimation model for grassland LAI developed by [30] was found to perform well using the RF algorithm. However, their feature selection method resulted in different RF results [29]. A multi-year experiment on rice LAI using VIs derived from hyperspectral reflectance showed that RF optimally predicted LAI when the feature variable was 10 with RMSE values below 0.80 [5]. In this study, RMSE values of less than

0.80 (0.697 to 0.797) were achieved at five (5) feature variables (VIs and Type I texture index, but RMSE values of more than 0.80 was observed when Type II texture index was used.

The results of multiple regression models (Table 10-12) suggest that the Type I texture index improved rice LAI estimation. The improvement from using VIs was consistent for all regression models and feature selection methods. The improvement can be attributed to the optimization of GLCM parameters per growth stage before the texture index generation. However, a 10% improvement in the R^2 and a 0.10 decrease in RMSE values may not be too high considering the additional computation time required to generate GLCM-based texture indices. LAI estimation using VIs can achieve the same level of performance if additional VIs are added to the model if the additional VI will provide variation in the model and is not highly correlated with another VI.

A more apparent difference was observed between the two types of texture index. However, it may be inaccurate to conclude that the Type I texture index was better than the Type II texture index. The optimization procedure for the calculation of the two types of texture index was not the same. The disparity in their performances can be remedied by two approaches (1) optimizing Type I texture index across growth stages and (2) optimizing Type II texture index for each growth stage. The Type II texture index could achieve a similar prediction performance if optimization of the GLCM parameters were done for each growth stage. Nevertheless, the results suggest that the texture index derived from multispectral images can improve rice LAI estimation.

After determining the most frequently selected features for each Type of UAV-derived variable, these were combined to develop another LAI estimation model. A separate LAI estimation model was developed to determine the feature variable's robustness, and this model consisted of feature variables least selected from the feature selection method. Table 13 shows that employing feature variables most selected from all feature selection methods results in a better LAI estimation model, but RF was not affected by this. This is because the RF predicts the target in a non-parametric way, so the variance and multicollinearity level of the features did not affect the estimation performance of the RF.

The LAI estimation model using the combined VIs and texture indices showed that good estimation could be obtained for all rice cultivars used in the study. Model evaluation using the independent dataset showed that a combination of spectral and texture features of multi-temporal

UAV-derived images could explain 68 to 82% of the LAI variation among the five rice cultivars. This proposes that LAI estimation for different rice cultivars can be improved by combining spectral and texture features of multispectral images.

5. Conclusion

This study evaluated the effect of combining the texture and spectral features of UAV-derived multispectral images using different feature selections and machine learning methods in rice LAI estimation. Two types of texture indices were developed from the GLCM-based texture metrics. These were 1). Type I: texture indices derived from the transformation of the optimized bands, and 2). Type II: texture indices derived from the transformation of texture metrics with each metric optimized according to band and angle. Feature selection methods such as EFS, variance threshold, and VIF were utilized to reduce the redundant features in the model.

Moreover, MLR, SVR, Ridge, and RF were used to develop rice LAI estimation. Results have shown that combining texture and the spectral index could improve LAI estimation when the Type I texture index is used. However, the Type II texture index was a poor LAI estimator. All the feature selection methods did not significantly influence the estimation performance.

This study provides information on the effect of texture features on rice LAI estimation. Future research work can consider the optimization of GLCM parameters, the robustness of the machine learning model, and the insignificance of feature selection methods in improving rice LAI estimation. Optimization of Type II texture index by growth stage needs to be examined.

6. References

1. Khan, M.H.; Dar, Z.A.; Dar, S.A. Breeding Strategies for Improving Rice Yield—A Review. *Agricultural Sciences.* **2015**, *6(5)*, 467, doi:10.4236/as.2015.65046.
2. Xiao, X.; He, L.; Salas, W.; Li, C.; Moore, B.; Zhao, R.; Frolking, S.; Boles, S. Quantitative Relationships between Field-Measured Leaf Area Index and Vegetation Index Derived from VEGETATION Images for Paddy Rice Fields. *International Journal of Remote Sensing.* **2002**, *23(18)*, 3595–3604, doi:10.1080/01431160110115799.
3. Wang, L.; Chang, Q.; Li, F.; Yan, L.; Huang, Y.; Wang, Q.; Luo, L. Effects of Growth Stage Development on Paddy Rice Leaf Area Index Prediction Models. *Remote Sensing.* **2019**, *11(3)*, 361, doi:10.3390/rs11030361.
4. Gong, Y.; Yang, K.; Lin, Z.; Fang, S.; Wu, X.; Zhu, R.; Peng, Y. Remote Estimation of Leaf Area Index (LAI) with Unmanned Aerial Vehicle (UAV) Imaging for Different Rice Cultivars throughout the Entire Growing Season. *Plant Methods* **2021**, *17*, 88, doi:10.1186/s13007-021-00789-4.
5. Wang, L.; Chang, Q.; Yang, J.; Zhang, X.; Li, F. Estimation of Paddy Rice Leaf Area Index Using Machine Learning Methods Based on Hyperspectral Data from Multi-Year Experiments. *PloS one.* **2018**, *13(12)*, e0207624, doi:10.1371/journal.pone.0207624.
6. Liu, S.; Zeng, W.; Wu, L.; Lei, G.; Chen, H.; Gaiser, T.; Srivastava, A.K. Simulating the Leaf Area Index of Rice from Multispectral Images. *Remote Sensing.* **2021**, *13(18)*, 3663, doi:10.3390/rs13183663.
7. Xiao, X.; He, L.; Salas, W.; Li, C.; Moore, B.; Zhao, R.; Frolking, S.; Boles, S. Quantitative Relationships between Field-Measured Leaf Area Index and Vegetation Index Derived from VEGETATION Images for Paddy Rice Fields. *International Journal of Remote Sensing.* **2002**, 23(18), 3595–3604, doi:10.1080/01431160110115799.
8. Wang, F.; Huang, J.; Lou, Z. A Comparison of Three Methods for Estimating Leaf Area Index of Paddy Rice from Optimal Hyperspectral Bands. *Precision Agriculture.* **2011**, *12*, 439–447, doi:10.1007/s11119-010-9185-2.
9. Li, S.; Yuan, F.; Ata-UI-Karim, S.T.; Zheng, H.; Cheng, T.; Liu, X.; Tian, Y.; Zhu, Y.; Cao, W.; Cao, Q. Combining Color Indices and Textures of UAV-Based Digital Imagery for Rice LAI Estimation. *Remote Sensing.* **2019**, *11(15)*, 1763, doi:10.3390/rs11151763.
10. Yang, K.; Gong, Y.; Fang, S.; Duan, B.; Yuan, N.; Peng, Y.; Wu, X.; Zhu, R. Combining Spectral and Texture Features of UAV Images for the Remote Estimation of Rice LAI throughout the Entire Growing Season. *Remote Sens.* **2021**, *13(15)*, 3001, doi:10.3390/rs13153001.
11. Zhang, X.; Zhang, K.; Sun, Y.; Zhao, Y.; Zhuang, H.; Ban, W.; Chen, Y.; Fu, E.; Chen, S.; Liu, J.; et al. Combining Spectral and Texture Features of UAS-Based Multispectral Images for Maize Leaf Area Index Estimation. *Remote Sensing.* **2022**, *14(2)*, 331, doi:10.3390/rs14020331.
12. Karu, K.; Jain, A.K.; Bolle, R.M. Is There Any Texture in the Image? *Pattern Recognition*. **1996**, 29(9), 1437–1446, doi:10.1016/0031-3203(96)00004-0.
13. Japan Meteorological Agency | Tables of Climatological Normals (1991–2020) Accessed on 27 May 2022. https://www.data.jma.go.jp/stats/data/en/normal/normal.html.
14. Zhou, X.; Zheng, H.B.; Xu, X.Q.; He, J.Y.; Ge, X.K.; Yao, X.; Cheng, T.; Zhu, Y.; Cao, W.X.; Tian, Y.C. Predicting Grain Yield in Rice Using Multi-Temporal Vegetation Indices from UAV-Based Multispectral and Digital Imagery. *ISPRS Journal of Photogrammetry and Remote Sensing.* **2017**, *130*, 246–255, doi:10.1016/j.isprsjprs.2017.05.003.
15. Kang, Y.; Nam, J.; Kim, Y.; Lee, S.; Seong, D.; Jang, S.; Ryu, C. Assessment of Regression Models for Predicting Rice Yield and Protein Content Using Unmanned Aerial Vehicle-Based Multispectral Imagery. *Remote Sens.* **2021**, *13(8)*, 1508, doi:10.3390/rs13081508.
16. Zha, H.; Miao, Y.; Wang, T.; Li, Y.; Zhang, J.; Sun, W.; Feng, Z.; Kusnierek, K. Improving Unmanned Aerial Vehicle Remote Sensing-Based Rice Nitrogen Nutrition Index Prediction with Machine Learning. *Remote Sens.* **2020**, *12(2)*, 215, doi:10.3390/rs12020215.
17. Wang, F.; Huang, J.; Tang, Y.-L.; Wang, X. New Vegetation Index and Its Application in Estimating Leaf Area Index of Rice. *Rice Sci.* **2007**, *14(3)*, 195–203, doi:10.1016/S1672-6308(07)60027-4.

18. Teal, R.K.; Tubana, B.; Girma, K.; Freeman, K.W.; Arnall, D.B.; Walsh, O.; Raun, W.R. In-Season Prediction of Corn Grain Yield Potential Using Normalized Difference Vegetation Index. *Agron. J.* **2006**, *98(6)*, 1488–1494, doi:10.2134/agronj2006.0103.
19. Tian, Y.C.; Yao, X.; Yang, J.; Cao, W.X.; Hannaway, D.B.; Zhu, Y. Assessing Newly Developed and Published Vegetation Indices for Estimating Rice Leaf Nitrogen Concentration with Ground- and Space-Based Hyperspectral Reflectance. *Field Crops Research.* **2011**, 120(2), 299-310, https://doi.org/10.1016/j.fcr.2010.11.002.
20. The Potential of Small-Unmanned Aircraft Systems for the Rapid Detection of Threatened Unimproved Grassland Communities Using an Enhanced Normalized Difference Vegetation Index. *PloS one.* **2017**, *12(10)*, e0186193, doi:10.1371/journal.pone.0186193.
21. Li, S.; Ding, X.; Kuang, Q.; Ata-UI-Karim, S.T.; Cheng, T.; Liu, X.; Tian, Y.; Zhu, Y.; Cao, W.; Cao, Q. Potential of UAV-Based Active Sensing for Monitoring Rice Leaf Nitrogen Status. *Frontiers in Plant Science.* **2018**, *9*, 1834, https://doi.org/10.3389/fpls.2018.01834.
22. Hijmas, R.J. raster: Geographic Data Analysis and Modeling. R package version. 3.5-15. 2022, Accessed on 25 June 2022. https://CRAN.R-project.org/package=raster.
23. Kuhn, M. Building Predictive Models in R Using the Caret Package. J. Stat. Softw. **2008**, 28, 1–26, doi:10.18637/jss.v028.i05.
24. John Fox and Sanford Weisberg An {R} Companion to Applied Regression, Third Edition. **2019**.Thousand Oaks CA: Sage. https://socialsciences.mcmaster.ca/jfox/Books/Companion/
25. Li-Hong, X.U.E.; Wei-Xing, C. a. O.; Wei-Hong, L.U.O.; Shao-Hua, W. Relationship Between Spectral Vegetation Indices and LAI in Rice. *Chinese Journal of Plant Ecology.* **2004**, *28(1)*, 47-52, doi:10.17521/cjpe.2004.0007.
26. Erten, E.; Rossi, C.; Yüzügüllü, O.; Hajnsek, I. Phenological growth stages of paddy rice according to the BBCH scale and SAR images. In 2014 IEEE Geoscience and Remote Sensing Symposium. Quebec City, QC, Canada. **2014,** 1017-1020, doi: 10.1109/IGARSS.2014.6946600.
27. Xu, T.; Wang, F.; Xie, L.; Yao, X.; Zheng, J.; Li, J.; Chen, S. Integrating the Textural and Spectral Information of UAV Hyperspectral Images for the Improved Estimation of Rice Aboveground Biomass. *Remote Sensing.* **2022**, *14(11)*, 2534, doi:10.3390/rs14112534.
28. Zhou, J.; Yan Guo, R.; Sun, M.; Di, T.T.; Wang, S.; Zhai, J.; Zhao, Z. The Effects of GLCM Parameters on LAI Estimation Using Texture Values from Quickbird Satellite Imagery. *Sci. Rep.* **2017**, *7*, 7366, doi:10.1038/s41598-017-07951-w.
29. Mridula, J.; Kumar, K.; Patra, D. Combining GLCM Features and Markov Random Field Model for Colour Textured Image Segmentation. In Proceedings of the 2011 International Conference on Devices and Communications (ICDeCom). Mesra, India. **2011**, 1-5, doi: 10.1109/ICDECOM.2011.5738494
30. Li, Z.; Xin, X.; Tang, H.; Yang, F.; Chen, B.; Zhang, B. Estimating Grassland LAI Using the Random Forests Approach and Landsat Imagery in the Meadow Steppe of Hulunber, China. *Journal of Integative Agriculture.* **2017**, *16(2)*, 286–297, doi:10.1016/S2095-3119(15)61303-X.

Chapter III: Estimating rice AGB using UAV-derived multispectral images

Abstract: Rice aboveground biomass (AGB) is an important indicator of crop productivity. The accuracy of AGB estimation using vegetation index is usually affected by the non-plant area. Thus, vegetation extraction is critical in improving AGB estimation. The study aimed to confirm the robustness of select vegetation indices and the effect of vegetation fraction cover (VF) derived from the threshold-based segmentation of UAV images when combined with the vegetation index and to determine the best feature selection and machine learning method that can estimate rice AGB. Feature selection methods, RFE, M-statistic, and z-test were calculated before training the model. Random forest was observed to perform good prediction of AGB (R^2 = 0.62 to 0.73) compared to other machine learning algorithms, SVR (R^2 = 0.39 – 0.54) and XGBoost (R^2 = 0.60 to 0.71). VF slightly improved AGB estimation. Results show that RF-RFE is the best estimation model for AGB estimation. AGB estimation model using RFE and z-test selected feature variables performed better than M-statistic selected features. Likewise, RF and XGBoost showed comparable performance in estimating AGB, while SVR had poor estimation performance regardless of the feature selection method.

---

1. Introduction

Estimating in-season aboveground biomass (AGB) is vital in evaluating the effectiveness of cultural and nutrient management practices in rice. This is because AGB is an effective indicator of crop productivity, which these crop management practices try to increase. When rice AGB is estimated at a particular growth stage and compared to a target AGB estimate, necessary calibration can be made for implementing any cultural or nutrient management [1]. However, actual AGB estimation is labor-intensive and time-consuming. Thus, the use of remote sensing poses to be a cost-efficient evaluation method for field crop intervention.

The introduction of UAVs has seen an increase in the use of remote sensing to estimate AGB. The most common remote sensing approach to estimate AGB is the use of raw reflectance values and vegetation indices derived from RGB, multispectral (MS) [2], or hyperspectral sensors [3].

Generating vegetation indices from hyperspectral images can identify the optimal multiple narrow-band reflectance that correlates with AGB [4]. Earlier research also showed that 560 nm and 728 nm were the optimal wavelengths for biomass estimation at individual rice plant levels [3]. On the other hand, using MS sensors can bring marginal improvement when compared to RGB sensors with advanced imaging techniques [5]. This is supported by most research results wherein RGB-based indices can perform better in prediction models than MS-derived VIs [6].

Aside from the spectral information, other quantitative image analyses were conducted to increase the accuracy of extracting the vegetation cover in the UAV images. Previous research showed that AGB estimation could be done by estimating vegetation cover using thresholding image segmentation methods such as ExG-ExR [7]. However, this type of vegetation cover extraction is affected by illumination, and the illumination variation can be treated by using local thresholding or considering the soil NDVI [8].

Another approach to estimate AGB in rice is to use canopy height derived from LiDAR point cloud [9] and RGB sensors by generating a digital surface model and digital terrain model to estimate canopy height [5,10]. Other research separately estimated plant height from aboveground biomass using high-resolution stereo images derived from UAVs [11], or texture features were used to improve AGB estimation [12]. A combination of spectral, structural, and meteorological features was attempted to estimate rice AGB with observed improvement from using the combination compared to the VI approach alone [13]. Other types of plant growth index were also considered in estimating AGB, such as the chlorophyll content index calculated from CCM [14].

Feature engineering was also done to improve AGB estimation. The most prevalent was using raw reflectance values' first and second derivatives and calculating VIs. However, this data augmentation did not accurately estimate AGB beyond the stem elongation stage [4]. Another approach is to combine spectral and structural information. Structural information that deals with variation in structure and volume is suited for non-perennial vegetation such as rice [7,10].

Modifying the raw RGB images before VI generations and feature extraction was also done to improve AGB estimation. The algorithm to smooth the pixel information in an image to create a binary output could distinguish the vegetation foreground from the ground background [15].

The sampling size of the ROI also varies with research. The standard feature extraction method is the use of quadrat or block shape as the ROI, such as one square meter as sampling area [2], while others used individual plants as ROIs [3].

However, most of this remote sensing research on agriculture uses remote sensing to estimate aboveground at any growth stage in the crop growth cycle. For example, a multiple linear regression model using different multi-temporal VIs [16] was used to estimate the aboveground biomass of rice varieties. This is an applicable prediction model since the VIs were measured simultaneously at defined points in a field trial. However, these are multi-level field trials [5,16] involving treatments such as fertilizer application and variety which can have interaction effects with the Vis. It could affect the prediction performance using regression models that do not consider categorical variables in the prediction process, such as the multiple linear regression model. In this case, a prediction model that can account for the effect of a categorical variable in the prediction should be considered. An AGB estimation model improved significantly when a categorical growth-stage dependent variable was included in the model [17].

On the other hand, other AGB estimation models evaluated the effect of the categorical variable on the continuous independent variable. A separate model for each categorical variable is considered when the slopes are not the same between the categorical variable [18]. One of the determining factors affecting remote sensing data in the field was the effect of the growth stages [6].

The aims of the study were (1) to confirm the robustness of select vegetation indices and the effect of vegetation fraction derived from the binarization of UAV images when combined with the vegetation index and (2) to determine the best feature selection and machine learning method that can estimate rice AGB.

2. Materials and Methods

2.1. Experimental Area and Design

The description for the study site is similar to the one described in Chapter 2. Two experimental trials, no fertilizer trial and with fertilizer trial, were conducted in 2020 and 2021, involving five Japonica rice varieties, Aichinokaori, Asahi, Hatsushimo, Nakate Shinsenbon, and Nikomaru. Basal fertilization was applied according to local practices for the fertilizer trial, and top-dressing was not performed for both trials. The plot size for both years was 1.68 m x 5.52 m with 24 cm plant spacing. The experiments were laid out in a randomized complete block design with three replications. Randomization for the two trials was the same in both years.

2.2. Field Data Collection

Aboveground biomass was sampled for each variety during the critical growth stages for tillering, stem elongation, booting, heading, and ripening. Sampling was done after the UAV flight for spectral data collection. Four adjacent hills of rice plants were selected in each plot. The number of tillers per sampled hill was counted, and the roots were removed. The sampled AGB was then oven-dried at 70oC for 48 hours until a constant weight was determined.

2.3. UAV Image Acquisition and Preprocessing

The study utilized a UAV system: Matrice 210 RTK v2 (DJI, Shenzhen, Guangdong, China) with Micasense RedEdge-MX sensors onboard. Details of the UAV flights are described in Table 1. For each UAV flight, the sensors were calibrated for their reflectance using a calibration panel, Calibrate Reflectance Panel (CRP), provided by the sensor manufacturer. The image of the calibration panel was taken before and after the UAV flight to acquire existing light conditions during the flight. UAV flights were conducted between 10:00 to 4:00 pm under windless and clear-sky conditions. The UAV flight and sampling dates are listed in Table 2.

After the UAV flight, the acquired images were ortho-mosaicked using the Pix4D mapper software (Pix4D SA, Prilly, Switzerland) to generate the spectral reflectance image of the experimental plots. The generated images from all UAV flight missions were georeferenced, and UAV flights were conducted once a week until the heading stage.

Five hundred twenty spectral reflectance images were obtained from the 2020 and 2021 trials. An ortho-mosaicked true (RGB) image was used to create a Region of Interest (ROI). A shapefile consisting of circular polygons with a 10 cm radius overlapping the georeferenced reflectance images served as the ROI. One circular polygon corresponds to one hill of rice plant. The reflectance images were then rasterized using R's 'raster' package [19]. The whole ortho-mosaicked reflectance images were first clipped into smaller raster images that covered the experimental plot. The images were then clipped using the ROI shapefile for individual hills, and the mean values of reflectance from the clipped hill images were computed. These mean reflectance values were used to compute vegetation indices.

2.4. Vegetation Fraction

The vegetation fraction was estimated using the mean reflectance values generated from the rasterized images. The color index ExG-ExR from the color indices, Excess Green (ExG) and ExR (Excess Red) was used to estimate the vegetation fraction of the rice crop in the field. First, the ExG and ExR maps were generated for each UAV flight date. Below is the given formula for ExG and ExR. Then, the difference of ExG from ExR values per pixel was generated. The difference served as the threshold value for the image binarization between plant and non-plant pixels. In this study, a difference of more than -0.06 was considered a plant component.

$$ExG = (2*G - R - B)/(G + R + B) \quad \text{Eq'n 1}$$

$$ExR = (1.4 * R - G)/(G + R + B) \quad \text{Eq'n 2}$$

where R, G, and B were red, green, and blue raw reflectance generated from the UAV-derived sensors.

2.5. Vegetation Indices

A total of 14 vegetation indices (Table A1) were computed using different combinations of the five spectral bands.

2.6. Feature Selection Methods

Recursive feature elimination (RFE) is a type of backward feature selection. It uses a subset of the dataset to train a model by using all the features specified in the model. Then the weakest element is eliminated in every iteration until the best set of features is identified. The lowest feature

is determined by calculating each feature's coefficients and ranking the feature variables' importance. It was calculated using the 'caret' package [20] in R.

The m-statistic method is a statistical filter type of feature selection. M-statistical value is calculated for vegetation index taken from distinct experimental factors such as fertility level, and the formula is written below. An M-statistical value of less than 1.0 indicates that VI has poor separability between two treatment factors, no fertilizer and with fertilizer trials.

$$M = \frac{uf - unf}{\sigma f - \sigma nf} \qquad \text{Eq'n 3}$$

where uf and unf are the mean VIs of the fertilizer and no fertilizer trials, respectively, while σf and σnf are the standard deviations of the VIs.

Z-test after the Correlation Analysis is a statistical test to determine the significant difference between two correlation pairs. A reference correlation analysis was established first to serve as the comparison for all the other correlation pairings. It was calculated using R's 'cocor' package [21].

2.7. Machine Learning Methods

A support vector machine is a machine learning algorithm that searches for a hyperplane with the maximum distance from the data points. It is a decision boundary whose either side represents classified data points. Classifiers are maximized by the influence of support vectors, points near the hyperplane, and influences the position of the hyperplane.

Random Forest is a non-parametric estimation method that creates randomized regression trees. A subset of observations from the training dataset is drawn for each tree. Then, each tree is split depending on the number of variables a split in each tree must have. The split of a tree is stopped when the number of observations is below the node size points. A prediction is made for each tree, then the predictions are averaged to get the final prediction.

Extreme gradient boosting or XGBoost is a gradient-boosted decision tree with a regularizing framework. It predicts by selecting a set of weak learners and training the model iteratively by considering the errors of the previous decision tree. The predictions for each iteration are combined to make a final prediction. It was calculated using R's 'xgboost' package [22].

2.8. Data Analysis

AGB data in 2020 and 2021 were pulled together to comprise the whole dataset for the study. Remote sensing variables, vegetation fraction, and vegetation index were used to estimate aboveground biomass.

The workflow of the study (Figure 1) to develop the AGB estimation model consisted of the following: (1) data collection of multispectral UAV images, (2) calculation of vegetation index and vegetation fraction, (3) feature selection method such as correlation analysis, use of M-statistic and recursive feature elimination method, (4) integration of vegetation fraction with the VI selected from the different feature selection method, (5) training of the estimation model and (6) validation and selection of the optimum estimation models.

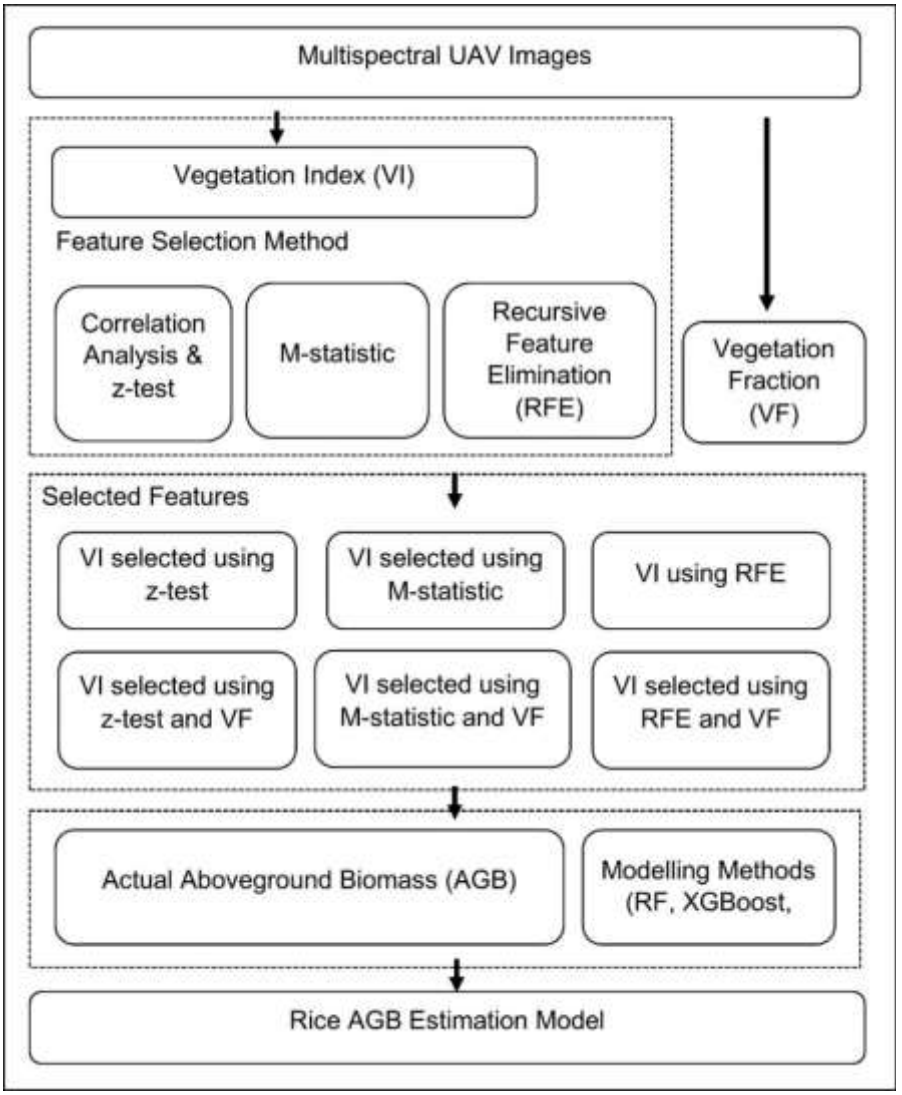

Figure 1. Workflow of the AGB Estimation Model

3. Results and Discussion

3.1. Selection of Vegetation Index using Correlation Analysis and z-test

Estimating rice AGB is essential in assessing crop status and predicting grain yield. The relationship between the AGB and VIs used in this study was first established between VIs of similar types (Figure 2). The types of V.I. used were (1) difference VI, (2) normalized, (3) soil-insensitive VI, (4) atmosphere-insensitive VI, (5) soil-and atmosphere-insensitive VI, and (6) four-band normalized VI. Figures 2 a-d show the correlation between AGB across growth stages and the different types of VI. The Pearson correlation analysis shows that regardless of the type of VI, AGB was positively correlated with VI.

Moreover, the range of correlation values was closer among AGB vs. VI pairings, thereby increasing the number of VIs that can be utilized for AGB estimation models. Nevertheless, GBNDVI shows to be the VI most correlated with AGB based on absolute r values. However, multicollinearity between these VIs is also apparent, indicating that using all these VIs in one estimation model may affect the estimation performance. Thus, knowing which set of these VIs can be combined for optimum estimation is needed.

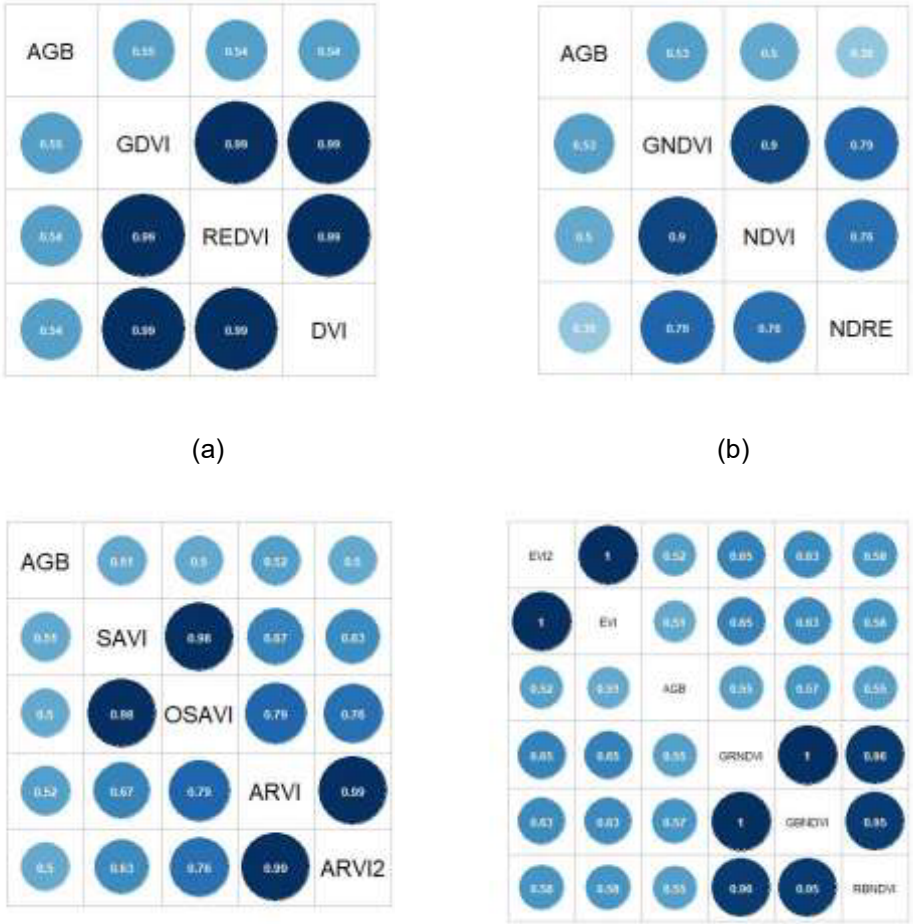

Figure 2. Pearson correlation matrix between aboveground biomass and select vegetation indices such as (a) difference VI, (b) normalized VI, (c) soil-insensitive VI and atmosphere-insensitive VI and (d) soil-and atmosphere-insensitive VI, and four-band normalized VI.

A comparison between different AGB vs. VI pairings was determined in the study using the z-test (Table 1). As mentioned previously, GBNDVI is the most correlated VI with AGB. As such, each z-test was compared to the AGB vs. GBNDVI relationship. The VI in Table 1 was listed in its descending order of correlation with AGB, with RBNDVI being the second VI most correlated with AGB, next to GBNDVI. Based on the z-test result, GBNDVI correlation with AGB was significantly different from the correlation of AGB with VIs, GRNDVI, ARVI, OSAVI, ARVI2, NDVI, and NDRE. This indicates that soil and atmospheric-insensitive VIs and normalized VIs have different performances in possibly estimating AGB.

The z-test also measured the correlation between the VIs in a particular comparison. The VIs mentioned above were also correlated with GBNDVI, with values ranging from 0.76 to 0.99, thus

indicating multicollinearity. However, instead of choosing the VIs with related correlations of less than 0.75 and non-significant correlation pairings, the study selected the VIs whose correlation with AGB was significantly different from GBNDVI. This is to capture the differential association of VIs to AGB. Thus, the AGB estimation model in this study selected GBNDVI, GRNDVI, ARVI, OSAVI, ARVI2, NDVI, and NDRE for AGB estimation models.

Table 1. Comparison of the Pearson correlation (r) of AGB vs. GBNDVI with the other AGB vs. VI correlations using the z-test.

	Difference	Related Correlation	z statistic	Significance level (p-value)	95% CI
RBNDVI	0.02	0.95	1.13	0.26	-0.02 - 0.08
GRNDVI	0.02	0.99	4.59	0.00	0.02 - 0.05
GDVI	0.04	0.61	0.95	0.34	-0.07 - 0.19
REDVI	0.05	0.64	1.07	0.28	-0.06 - 0.19
DVI	0.05	0.59	1.10	0.27	-0.06 - 0.21
ARVI	0.04	0.95	2.36	0.02	0.01 - 0.11
EVI2	0.06	0.64	1.42	0.15	-0.03 - 0.21
SAVI	0.07	0.67	1.69	0.09	-0.02 - 0.22
EVI	0.08	0.64	1.69	0.09	-0.02 - 0.23
OSAVI	0.08	0.76	2.16	0.03	0.01 - 0.21
ARVI2	0.07	0.94	3.49	0.00	0.04 - 0.15
NDVI	0.07	0.94	3.49	0.00	0.04 - 0.15
NDRE	0.19	0.79	5.13	0.00	0.15 - 0.34

The VIs were listed in descending order of Related Correlation value.

3.2. Selection of Vegetation Index using M-statistic

M-statistic values represent the level of separability that a VI can show in estimating a parameter of interest when measured in different conditions or treatments. When VI is used as a proxy for actual vegetation, the ability of the VI to distinguish between different types and densities of foliage is essential, given that external factors such as soil and atmosphere can affect the reflectance being transferred into the sensors. In M-statistic, a value of more than 1.0 indicates good separability, and a VI with good separability for a particular series of treatments has a histogram with no overlapping frequencies. Table 2 shows the M-statistic value of different VI at different growth stages between two fertility trials, with no fertilizer and with fertilizer. The higher the M-statistic value, the better the VI distinguishes vegetation of the two trials.

Results show that the separability of a VI varies with the growth stage. In particular, VIs such as DVI, EVI, EVI2, GBNDVI, and GRNDVI have good separability in only one growth stage. Other VIs such as GDVI, SAVI, and RBNDVI have good separability in two consecutive growth stages. NDVI,

REDVI, and ARVI2, on the other hand, showed to have good separability in three growth stages, while NDRE showed to have bad separability in all growth stages. Separability of VI appeared less at the booting stage, with fewer VIs having M-statistic values of more than 1.0. Better VI separability was observed at tillering stage.

The dynamics of the VI should also be noted. GDVI had an increasing separability index until the booting stage. Soil-insensitive VIs, OSAVI, and SAVI had the same increasing trend in separability. Normalized VIs decreased as the crop reached full canopy but slightly improved at the heading stage. Atmospheric effect-insensitive VIs had high separability at early and late growth stages. Soil and atmospheric effect-insensitive VIs had a decreasing trend in separability with a peak value at tillering stage. However, EVI2 had a drastic reduction in its separability at later growth stages than EVI.

Given these dynamics, a VI with good separability in at least two growth stages was selected as an AGB estimator. These were GDVI, REDVI, SAVI, NDVI, ARVI, ARVI2, and RBNDVI.

Table 2. Comparison of M-Statistics values obtained from different vegetation indices at different crop growth stages of two fertility trials.

	Tillering Stage	Stem Elongation Stage	Booting Stage	Heading Stage
DVI	-0.63	**1.40**	-3.20	- 0.35
GDVI	-3.66	0.39	**8.28**	**1.54**
REDVI	**3.51**	**2.92**	-8.57	**1.01**
SAVI	-0.26	**1.42**	**6.19**	0.76
OSAVI	0.20	-0.11	0.84	**1.58**
NDVI	**1.37**	**1.04**	0.62	**5.37**
GNDVI	**1.45**	0.60	-0.75	0.18
NDRE	-0.40	-0.54	-0.85	0.45
ARVI	**6.03**	-1.72	0.34	**1.69**
ARVI2	**1.37**	**1.04**	0.62	**5.37**
EVI	-1.55	**1.59**	-1.39	-1.77
EVI2	**1.59**	0.61	-6.87	-4.55
RBNDVI	-0.59	-4.79	**1.01**	**2.51**
GBNDVI	0.83	0.05	**4.04**	-0.04
GRNDVI	0.46	**2.12**	0.32	0.70

The numbers in bold font are VIs with good separability (M-statistic value > 1.0)

3.3. Selection of Vegetation Index using Recursive Feature Elimination

A recursive feature elimination (RFE) was used to identify the best possible estimator for AGB. Unlike the Correlation Analysis and M-statistics method, RFE employs all the features in a model and removes the weakest features in each iteration until the most desired set of features is achieved. Cross-validation techniques were applied to get the representative score of a feature as the basis for elimination. Table 3 shows the cross-validated result of the RFE for the AGB estimation model. The method searched for the best predictors among the 16 features included in the model. The number of predictors is determined by the number of variables that resulted in the lowest RMSE.

According to the result, six (6) were the optimum number of predictors to estimate AGB, and the R^2 and RMSE were at the peak and lowest values, respectively. At seven (7) up to the total number of features (16), R^2 values had an accumulated 0.02 decrease in value while RMSE had an accumulated 0.40 increase when ten more variables were added from the optimum six (6) variables. This indicates that estimating AGB in this study using more than six VI features will not result in a substantial model improvement.

The selected VIs were NDRE, REDVI, GBNDVI, RBNDVI, GDVI, and GNDVI. NDRE and REDVI are both spectral transformations of NIR and Red Edge bands, while GDVI and GNDVI are spectral transformations of NIR and green bands. GBNDVI and RBNDVI are normalized VIs from the transformation of four bands, with NIR and blue bands in common.

Table 3. Cross-validated result of the recursive feature elimination (RFE) method

Variable	R^2	RMSE
1	0.14	2.67
2	0.50	1.90
3	0.67	1.53
4	0.72	1.42
5	0.73	1.40
6	**0.74**	**1.37**
7	0.73	1.39
16	0.73	1.41

The number in bold font indicates the optimum number of variables that will give the lowest RMSE.

3.4. Vegetation Fraction derived from Threshold-based Segmentation Method

Vegetation fraction (VF) or fractional vegetation cover was estimated in this study using the threshold-based segmentation method using the ExG-ExR formula. One threshold value was used

for all the ExG-ExR feature maps created to determine the plant and the non-plant area component per pixel in the image at a given spatial extent. VF represents the area the vegetation covers relative to the ground reference area. Thereby, VF represents the vegetation growth trend and the changes in vegetation density. Figure 3 shows the VF at different growth stages of rice varieties grown in two different fertilizer trials. The VF of Asahi and Aichinokaori reached 100% at the stem elongation stage, while the VF of Nakate Shinsenbon and Hatsushimo reached 100% at the heading stage and Nikomaru did not reach 100% VF at the heading stage.

VF was not consistently higher in crops in the fertilizer trial, depending on the variety. In particular, similar VFs were observed for Hatsushimo in both fertilizer trials. The low VF observed in Nakate Shinsenbon was also apparent. It represented the low growth density of Nakate Shinenbon in the fertilizer trial, whose plot was characterized by shallow, sandy soil relative to other plots in the trial. VF decrease of Aichinokaori at the heading stage from 100% to 95% can be attributed to the limitation of the spectral reflectances involved in ExG and ExR. The repeated measure of hills was done in the VF calculation throughout the growth stages. As such, the previously identified plant area became a non-plant area. This is possibly due to different reasons. First, the illumination in the field at the heading stage might be less uniform due to the presence of panicles, changing the scattering of reflected light. This may result in different threshold values for plant areas in a vegetation map. The bending of the foliage at the late booting to the heading stage might also contribute to the presence of non-plant areas inside the dominant foliage area determined from the spatial extent given by the shapefile for raster extraction. Nevertheless, the variation in the VF of different rice varieties was integrated into VI to determine if it could improve the AGB-VI estimation model.

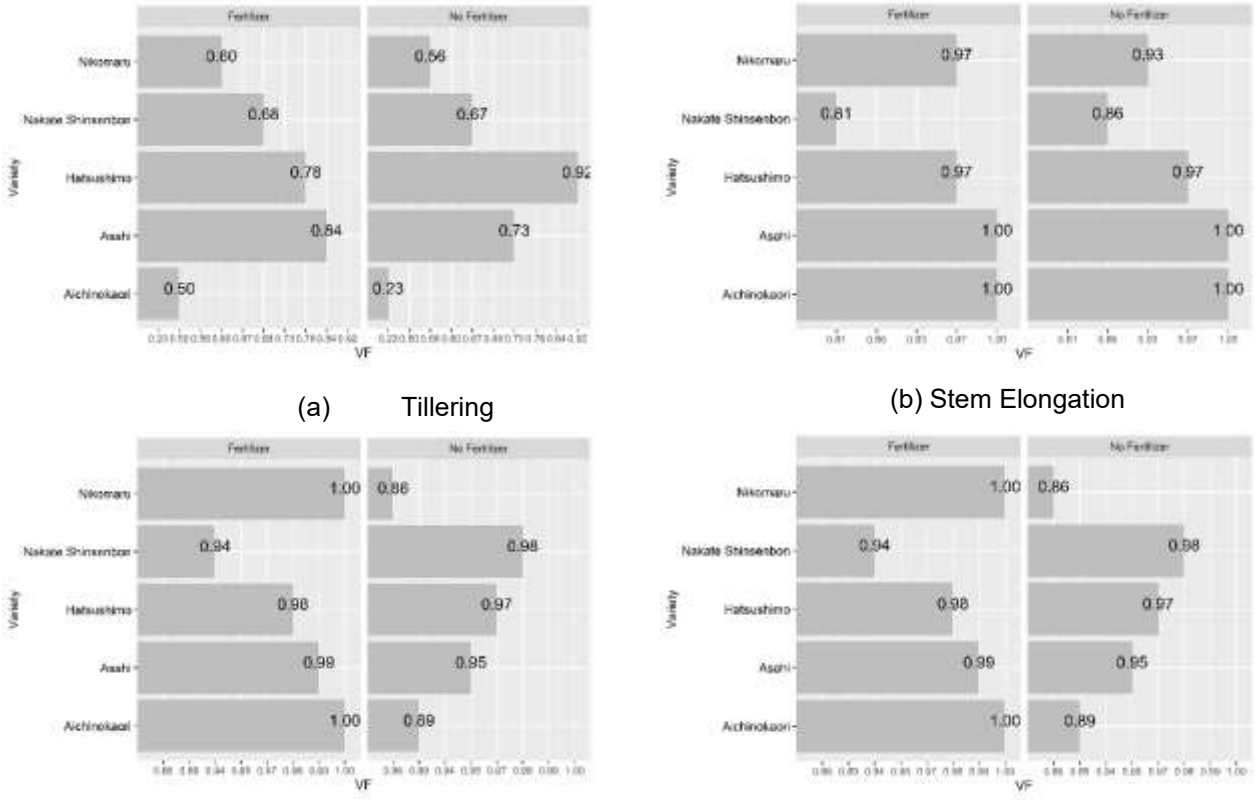

(a) Tillering (b) Stem Elongation

(c) Booting (d) Heading

Figure 3. Vegetation fraction of five rice varieties in two fertility trials at different growth stage; (a) tillering, (b) stem elongation, (c) booting (d) heading stage.

3.5. AGB Estimation using Vegetation Index selected using Correlation Analysis and z-test

Three (3) machine learning (ML) algorithms were employed to estimate AGB using the VI selected from the VI and VI*VF. Repeated cross-validation of the models showed that AGB estimation models could explain 53 to 70% variation in AGB (Table 4). Validating the models using an independent dataset showed no overfitting issues for all the ML used (Figure 4). However, comparing the results between models, SVR was lower compared to RF and XGBoost, both in the training and testing phases. The VI features in these models were derived from a correlation matrix with high related correlation values, resulting in the multicollinearity of these features. The two ML algorithms, RF and XGBoost, used a decision tree to train the regressor for estimation, while SVR used a linear estimator to train the model. Multicollinearity affects the linear-based model, making the regressor unstable as the weight of each variable changes quickly with the change in the data.

Integration of VF into the AGB-VI model also did not improve the performance of SVR compared to RF and XGBoost. Regardless of the ML algorithm, AGB estimation slightly improved when VF was integrated with VI.

Table 4. Model evaluation results of estimation models using VI selected using Correlation Analysis.

	Cross-validation		Independent Test Dataset	
	R^2	RMSE	R^2	RMSE
		VI		
RF	0.70	1.51	0.72	1.35
SVR	0.53	1.90	0.56	1.70
XGBoost	0.69	1.54	0.69	1.42
		VI * VF		
RF	0.74	1.39	0.73	1.32
SVR	0.58	1.80	0.60	1.62
XGBoost	0.71	1.48	0.71	1.39

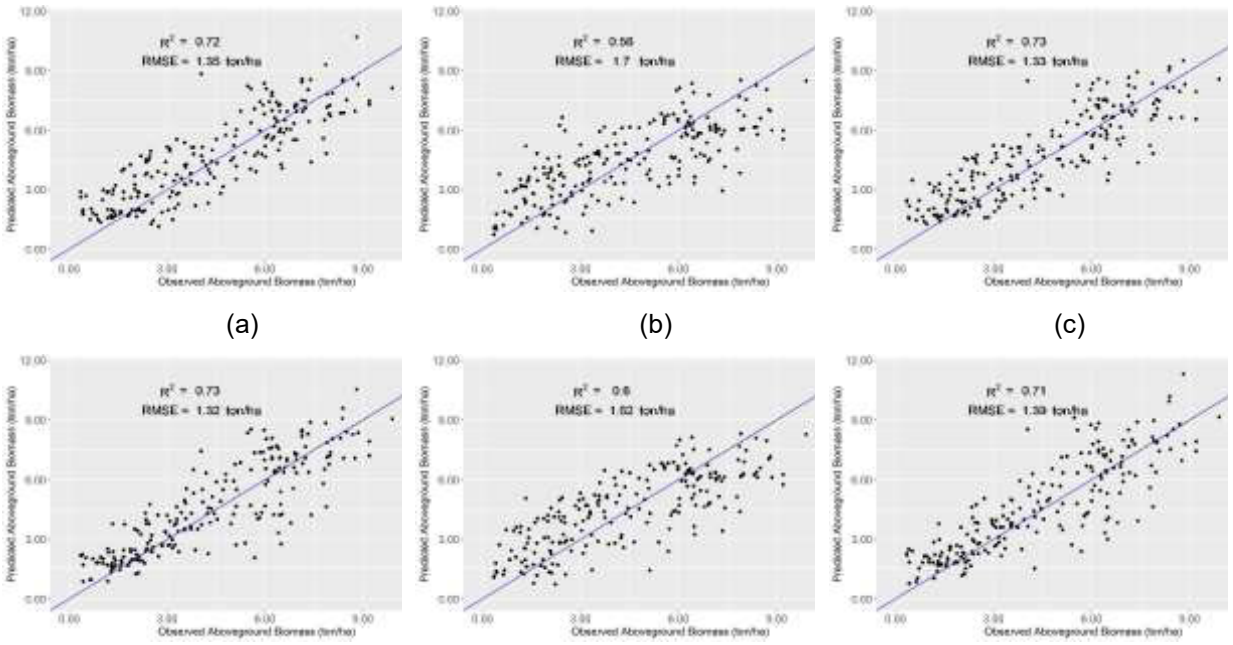

Figure 4. Validation result of AGB estimation model using VI selected using *Z-test.* The AGB was estimated using VIs and VI*VF with 3 ML methods, (a,d) RF, (b,e,) SVR, (c,f) XGBoost, respectively.

3.6. AGB Estimation using Vegetation Index selected using M-statistic

The cross-validated result of the AGB estimation model using VI with good separability as estimators are shown in Table 5. The similar performances between RF and XGBoost might be due to the non-parametric voting involved in the decision tree performed in the training process. The subset of the dataset in the RF and XGBoost model may have consisted of VIs with similar separability, resulting in a similar decision in each stem node, constricting the model to decrease in complexity, which the XGBoost might have employed its regularization function that the RF lacks. Thus, a marginal difference between XGBoost and RF was observed.

Relative to the 60 to 70% explained variation by RF and XGBoost (Figure 5), SVR resulted in underfitting. In SVR, a decision boundary is created to define the data into different regressors, aiding in the learning process of the model. In VI with good M-statistic, the treatments were distinguishable from each other through VIs. The decision boundary was probably a wiggly curve rather than an optimal hyperplane, generating a narrow margin between regressors., thereby resulting in higher residual values between the predicted and the observed AGB values as the far-away data points were not considered in the training process. Also, the actual AGB values between the two fertilizer trials were possibly not as distinguishable from each other as the M-statistic values of the VI imply.

AGB estimation model using RF and XGBoost improved when interaction with VF was added to the model. However, the integration of VF into the selected VIs did not improve the AGB-VI estimation model using SVR. This possibly further weakened the model's generalization ability, resulting in higher residuals in the model validation process.

Table 5. Model evaluation results of estimation models using VI selected using M-statistic.

	Cross-validation		Independent Test Dataset	
	R^2	RMSE	R^2	RMSE
		VI		
RF	0.67	1.58	0.68	1.45
SVR	0.52	1.91	0.59	1.63
XGBoost	0.64	1.65	0.61	1.60
		VI*VF		
RF	0.71	1.47	0.70	1.39
SVR	0.52	1.92	0.53	1.74
XGBoost	0.68	1.57	0.67	1.46

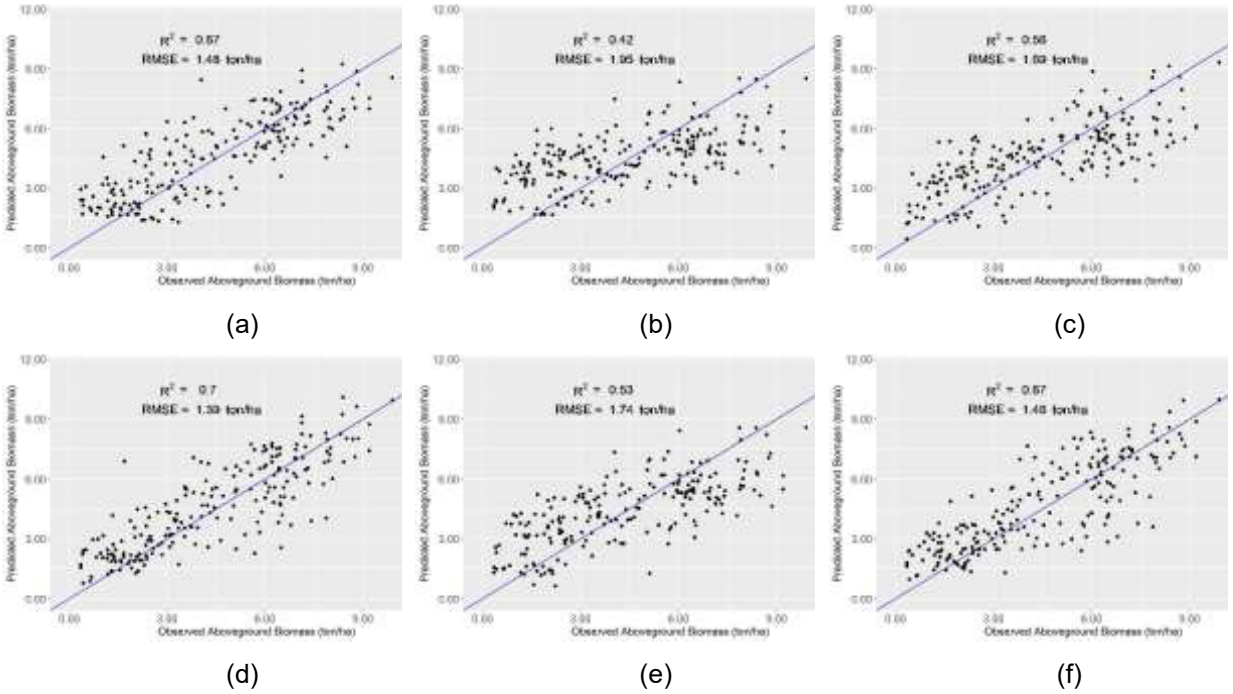

Figure 5. Validation results of AGB estimation model using VI selected using M-statistic. The AGB was estimated using VIs and VI*VF with 3 ML methods, (a,d) RF, (b,e,) SVR, (c,f) XGBoost, respectively.

3.7. AGB Estimation using Vegetation Index selected using Recursive Feature Elimination

The performance of AGB estimation models using VI selected using the RFE method is shown in Table 6. SVR appeared to have a relatively poorer performance than RF and XGBoost (Figure 6). A difference of R^2 = 0.20 was observed between SVR, RF, and XGBoost. The selected VIs were highly correlated with each other, thus resulting in lower performance of SVR. In RFE, the features are divided into a subset and evaluated the number of features that can result in optimum model performance.

Table 6. Cross-validation results of estimation models using VI selected using RFE.

	Cross-validation		Independent Test Dataset	
	R^2	RMSE	R^2	RMSE
		VI		
RF	0.73	1.44	0.73	1.33
SVR	0.54	1.88	0.56	1.69
XGBoost	0.71	1.49	0.73	1.32
		VI * VF		
RF	0.75	1.39	0.75	1.28
SVR	0.57	1.82	0.56	1.69
XGBoost	0.71	1.49	0.72	1.35

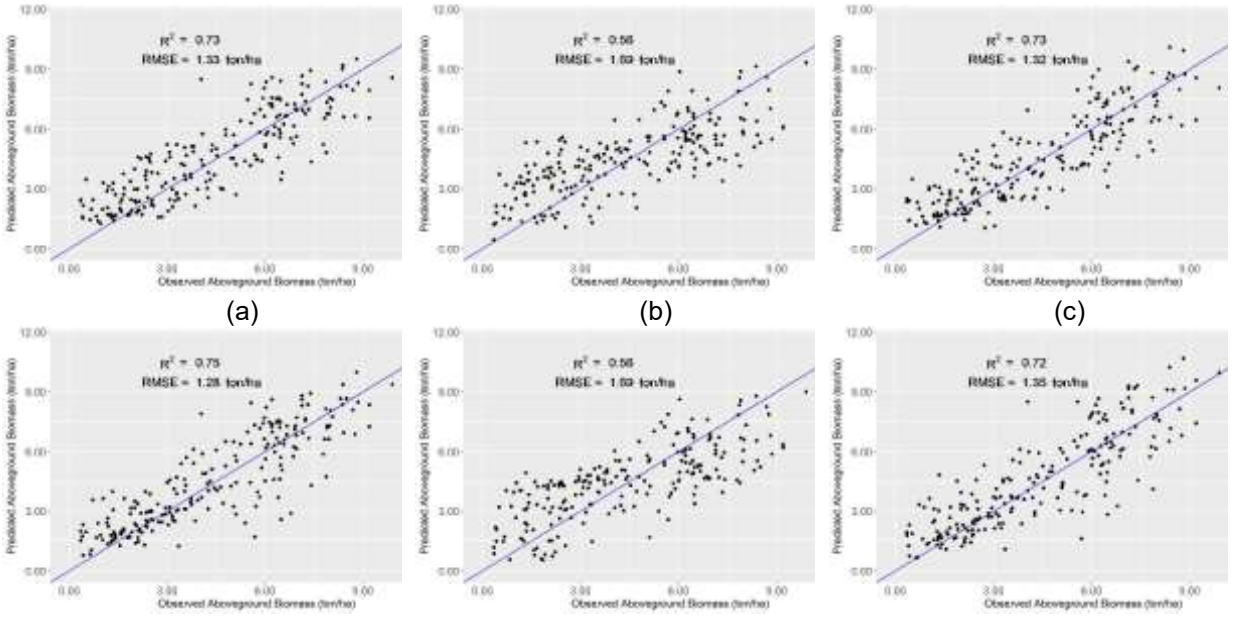

(a) (b) (c)

(d) (e) (f)

Figure 6. Validation results of AGB estimation model with feature selected using RFE. The AGB was estimated using VIs and VI*VF with 3 ML methods, (a,d) RF, (b,e,) SVR, (c,f) XGBoost, respectively.

3.8. Model Selection using Descriptive Statistics of the Resampling Data

Figure 7 shows the mean of the R^2 and MAE of the different estimation models using VIs selected using different feature selection methods. The highest R^2 was observed in RF using VIs selected using the RFE method, while the lowest R^2 was observed in SVM using VI selected using M-statistic. Regardless of the ML algorithm, VI selected using M-statistic as the filter criterion had the poorest estimation performance. Likewise, regardless of the feature selection method, SVR had the poorest performance. RF and XGBoost had similar estimation performances. When used by the same ML algorithm, VIs selected using Correlation Analysis and RFE also had similar estimation performance.

A similar trend in reverse was observed in the MAE score of the estimation models. A higher MAE score was observed in SVM- M statistic model, while the lowest MAE score was observed in RF – RFE estimation model. RF using VIs selected using RFE is the best estimation model scheme in this regard.

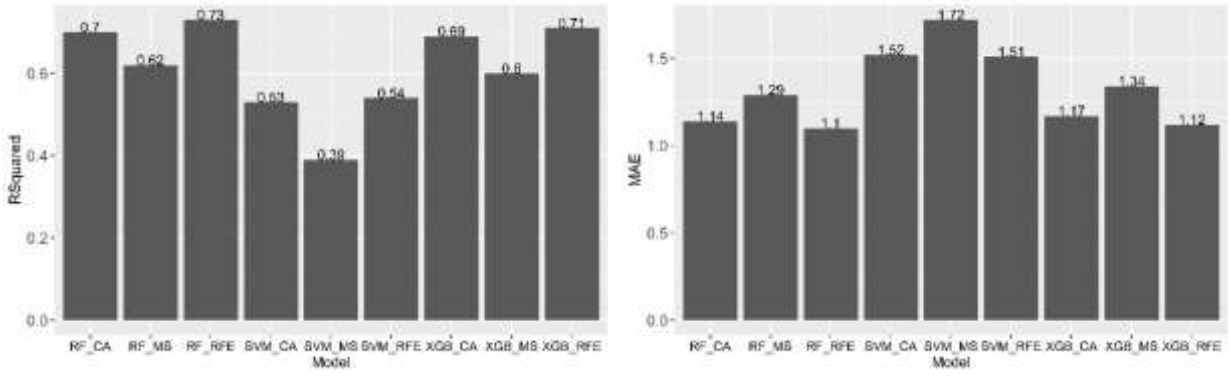

(a) (b)

Figure 7. Average (a) R^2 and (b) MAE using the resampled training data of the different AGB estimation model.

The AGB estimation models developed in this study followed an ensemble-like method of a prediction model. First, a correlation analysis that established the relationship between AGB and VI was computed. Due to closer r values, an appropriate evaluation test was applied to the correlated dataset to determine the significance of each r value between two paired correlation groups. Results from the z-test showed that VIs of the same type had a relative association level with AGB, such as the difference in reflectance between NIR vs. Green, NIR vs. Red, and NIR vs. RE. On the other hand, improved versions of a VI did not guarantee a better level of association with the AGB measured in this study, as seen in Table 1. This may indicate that the adjustment parameter included in the improved VI version was not the correct value suitable for the field conditions where the AGB was sampled. A separate optimization test to determine the adjustment factor would likely improve the correlation between AGB and VIs.

AGB estimation models consisting of a single VI did not explain the variation of AGB for more than 50%, regardless of the type of VI. This indicates that spectral information alone was not enough to estimate AGB accurately. Due to this, an additional source of variation was added to the model. The addition of VF into the model was introduced by multiplying VF with the VIs. Results showed that

adding another variable into the model could increase the coefficient of determination. However, when the additional variable was added, it did not result in a VI being better than the other VIs. It is because the effect of the additional variable on the model was the same for all VIs, resulting in a similar result trend compared to AGB-VI models. This can be a strategy to improve the estimation model without the need for increasing the dimension of the model all at once, resulting in a lower modeling process or avoiding dimensional reduction techniques, which are sometimes black-box and will not provide interpretable information as to the classification and selection processes.

The usefulness of a model can be tested by its capacity to predict from an independent test dataset, representing the general behavior of the target variable, thereby assessing the parsimony of the model. This study's validation of the AGB-VI estimation model (AGB-VF*VI model) showed that a general AGB estimation model could not estimate AGB of any given growth stage with similar accuracies. In this study, AGB seemed best estimated at the booting stage. In this stage, the canopy density of the crop has reached its peak. This resulted in higher reflectance values recorded by the sensors for vegetation estimation at the booting stage relative to other growth stages. However, the coefficient of determination is still low at the booting stage. The VI tested in this study is saturated at high canopy levels, thus resulting in higher residuals and lowering the coefficient of determination.
Due to VI limitations brought upon by soil and atmospheric effects, the VIs were adjusted to account for these effects. These adjustments were expected to increase AGB estimation accuracy. Thus, estimation models using improved VIs were compared with estimation models using difference and normalized difference types of VIs. Results showed that improved VIs did not improve correlation with AGB substantially (Figure 2). However, a comparison of correlation pairings between AGB and VI showed that atmospheric and soil-insensitive VIs had significantly different AGB correlations. Model evaluation results show RF and XGBoost had comparable estimation performance, while the M-statistic method showed poor performance compared with the z-test and RFE.

4. Conclusion

Improvement of rice AGB estimation using Vegetation Fraction Cover (VF) was evaluated in the study. The performance of AGB estimation models using different feature selection methods and machine learning was also assessed. The VF derived from a threshold-based segmentation method slightly improved the AGB estimate compared to VI alone. AGB estimation model using RFE and z-test selected feature variables performed better than M-statistic selected features. Likewise, RF and XGBoost showed comparable performance in estimating AGB, while SVR had poor estimation performance regardless of the feature selection method.

5. Appendix

Table A1. List of vegetation indices used in the study.

Vegetation Index	Formula	References
Atmospherically Resistant Vegetation Index (ARVI)	(NIR - (2 *R) + B)/ (NIR + (2 * R) + B),	[23]
Atmospherically Resistant Vegetation Index 2 (ARVI2)	−0.18 + 1.17[(NIR − R) / (NIR + R)]	[24]
Difference Vegetation Index (DVI)	NIR – R	[25]
Enhanced Vegetation Index (EVI)	2.5[(NIR − R) / ((NIR + 6R−7.5B) + 1)]	[26]
Enhanced Vegetation Index 2 (EVI2)	2.4[(NIR − R) / (NIR + R + 1)]	[27]
Green-Blue Normalized Difference Vegetation Index (GBNDVI)	[NIR − (G + B)] / [NIR + (G + B)]	[28]
Green Difference Vegetation Index (GDVI)	NIR – G	[29]
Green Normalized Difference Vegetation Index (GNDVI)	(NIR − G) / (NIR + G)	[30]
Green-Red Normalized Difference Vegetation Index (GRNDVI)	[NIR − (G + R)] / [NIR + (G + R)]	[29]
Normalized Difference Red-Edge (NDRE)	(NIR − RE) / (NIR + RE)	[31]
Normalized Difference Vegetation Index (NDVI)	(NIR − R) / (NIR + R)	[32]
Red-Blue Normalized Difference Vegetation Index (RBNDVI)	[NIR − (R + B)] / [NIR + (R + B)]	[33]
Red Edge Difference Vegetation Index (REDVI)	NIR – RE	[34]
Soil Adjusted Vegetation Index (SAVI)	(NIR – R)/(NIR + R + 0.5)	[23]
Optimized Soil Adjusted Vegetation Index (OSAVI)	(1+ 0.16) ((NIR – R)/(NIR + R + 0.16))	[23]

R = red reflectance; G = green reflectance; B = blue reflectance; NIR = near-infrared reflectance; RE = red-edge reflectance.

6. References

1. Buresh, R.J.; Castillo, R.L.; Dela Torre, J.C.; Laureles, E.V.; Samson, M.I.; Sinohin, P.J.; Guerra, M. Site-Specific Nutrient Management for Rice in the Philippines: Calculation of Field-Specific Fertilizer Requirements by Rice Crop Manager. *Field Crops Research.* **2019**, *239*, 56–70, doi:10.1016/j.fcr.2019.05.013.
2. Deusing, C.A.; Rojas, J.P.; Petro, E.; Martinez, C.; Mondragon, I.F.; Patino, D.; Rebolledo, M.C.; Colorado, J. High-Throughput Biomass Estimation in Rice Crops Using UAV Multispectral Imagery. *Journal of Inteligent & Robotic System.* **2019**, *96*, 573–589, doi:10.1007/s10846-019-01001-5.
3. Feng, H.; Jiang, N.; Huang, C.; Fang, W.; Yang, W.; Chen, G.; Xiong, L.; Liu, Q. A Hyperspectral Imaging System for an Accurate Prediction of the Above-Ground Biomass of Individual Rice Plants. *Review of Science Instruments.* **2013**, *84(9)*, 095107, doi:10.1063/1.4818918.
4. Gnyp, M.L.; Miao, Y.; Yuan, F.; Ustin, S.L.; Yu, K.; Yao, Y.; Huang, S.; Bareth, G. Hyperspectral Canopy Sensing of Paddy Rice Aboveground Biomass at Different Growth Stages. *Field Crops Research.* **2014**, *155*, 42–55, doi:10.1016/j.fcr.2013.09.023.
5. Adeluyi, O.; Harris, A.; Foster, T.; Clay, G.D. Exploiting Centimetre Resolution of Drone-Mounted Sensors for Estimating Mid-Late Season above Ground Biomass in Rice. *European Journal of Agronomy.* **2022**, *132*, 126411, doi:10.1016/j.eja.2021.126411.
6. G. Poley, L.; J. McDermid, G. A Systematic Review of the Factors Influencing the Estimation of Vegetation Aboveground Biomass Using Unmanned Aerial Systems. *Remote Sensing.* **2020**, *12(7)*, 1052, doi:10.3390/rs12071052.
7. Zhang, D.; Mansaray, L.R.; Jin, H.; Sun, H.; Kuang, Z.; Huang, J. A Universal Estimation Model of Fractional Vegetation Cover for Different Crops Based on Time Series Digital Photographs. *Computers and Electronics in Agriculture.* **2018**, *151*, 93–103, doi:10.1016/j.compag.2018.05.030.
8. Montandon, L. M., & Small, E. E. The impact of soil reflectance on the quantification of the green vegetation fraction from NDVI. *Remote Sensing of Environment*. **2008.** *112*(4), 1835-1845.
9. Zhang, G.; Ganguly, S.; Nemani, R.R.; White, M.A.; Milesi, C.; Hashimoto, H.; Wang, W.; Saatchi, S.; Yu, Y.; Myneni, R.B. Estimation of Forest Aboveground Biomass in California Using Canopy Height and Leaf Area Index Estimated from Satellite Data. *Remote Sensing of Environment.* **2014**, *151*, 44–56, doi:10.1016/j.rse.2014.01.025.
10. Peprah, C.O.; Yamashita, M.; Yamaguchi, T.; Sekino, R.; Takano, K.; Katsura, K. Spatio-Temporal Estimation of Biomass Growth in Rice Using Canopy Surface Model from Unmanned Aerial Vehicle Images. *Remote Sensing.* **2021**, *13(12)*, 2388, doi:10.3390/rs13122388.
11. Li, W.; Niu, Z.; Chen, H.; Li, D.; Wu, M.; Zhao, W. Remote Estimation of Canopy Height and Aboveground Biomass of Maize Using High-Resolution Stereo Images from a Low-Cost Unmanned Aerial Vehicle System. *Ecological Indicators.* **2016**, *67*, 637–648, doi:10.1016/j.ecolind.2016.03.036.
12. Zheng, H.; Cheng, T.; Zhou, M.; Li, D.; Yao, X.; Tian, Y.; Cao, W.; Zhu, Y. Improved Estimation of Rice Aboveground Biomass Combining Textural and Spectral Analysis of UAV Imagery. *Precision Agriculture.* **2019**, *20*, 611–629, doi:10.1007/s11119-018-9600-7.
13. Jiang, Q.; Fang, S.; Peng, Y.; Gong, Y.; Zhu, R.; Wu, X.; Ma, Y.; Duan, B.; Liu, J. UAV-Based Biomass Estimation for Rice-Combining Spectral, TIN-Based Structural and Meteorological Features. *Remote Sensing.* **2019**, *11(7)*, 890, doi:10.3390/rs11070890.
14. Liu, C.; Liu, Y.; Lu, Y.; Liao, Y.; Nie, J.; Yuan, X.; Chen, F. Use of a Leaf Chlorophyll Content Index to Improve the Prediction of Above-Ground Biomass and Productivity. *PeerJ.* **2019**, *6*, e6240, doi:10.7717/peerj.6240.
15. Colorado, J.D.; Calderon, F.; Mendez, D.; Petro, E.; Rojas, J.P.; Correa, E.S.; Mondragon, I.F.; Rebolledo, M.C.; Jaramillo-Botero, A. A Novel NIR-Image Segmentation Method for the Precise Estimation of above-Ground Biomass in Rice Crops. *PloS one* **2020**, *15(10)*, e0239591, doi:10.1371/journal.pone.0239591.
16. Xu, T.; Wang, F.; Xie, L.; Yao, X.; Zheng, J.; Li, J.; Chen, S. Integrating the Textural and Spectral Information of UAV Hyperspectral Images for the Improved Estimation of Rice Aboveground Biomass. *Remote Sens.* **2022**, *14(11)*, 2534, doi:10.3390/rs14112534.
17. Vaesen, K.; Gilliams, S.; Nackaerts, K.; Coppin, P. Ground-Measured Spectral Signatures as Indicators of Ground Cover and Leaf Area Index: The Case of Paddy Rice. *Field Crops Research.* **2001**, *69(1)*, 13–25, doi:10.1016/S0378-4290(00)00129-5.

18. Lee, K.-J.; Lee, B.W. Estimation of Rice Growth and Nitrogen Nutrition Status Using Color Digital Camera Image Analysis. *European Journal of Agronomy.* **2013**, *48*, 57–65, doi:10.1016/j.eja.2013.02.011.
19. Hijmas, R.J. raster: Geographic Data Analysis and Modeling. R package version. 3.5-15. **2022**. Accessed on 25 June 2022. https://CRAN.R-project.org/package=raster.
20. Kuhn, M. Building Predictive Models in R Using the Caret Package. *Journal of Statistical Sofware*. **2008**, 28, 1–26, doi:10.18637/jss.v028.i05
21. Diedenhofen, B.; Musch, J. cocor: A Comprehensive Solution for the Statistical Comparison of Correlations. *PloS one*. **2015**, 10(4), e0121945, http://dx.doi.org/10.1371/journal.pone.0121945
22. Chen, T.; He, H.T.; Benesty, M.; Khotilovich, V.; Tang, Y.; Cho, H.; Chen, K.; Mitchell, R.; Cano, I.; Zhou, T.; Li, M.; Xie, J.; Lin, M.; Geng, Y.; Li, Y.; Yuan, J. xgboost: Extreme Gradient Boosting. R package version 1.6.0.1. **2022**, Accessed on 25 June 2022. https://CRAN.R-project.org/package=xgboost.
23. Binte Mostafiz, R., Noguchi, R., & Ahamed, T. Agricultural land suitability assessment using satellite remote sensing-derived soil-vegetation indices. *Land*. **2021**. *10(2)*, 223, https://doi.org/10.3390/land10020223.
24. Kaufman, Y. J., & Tanre, D. Atmospherically resistant vegetation index (ARVI) for EOS-MODIS. *IEEE transactions on Geoscience and Remote Sensing*. **1992**. *30*(2), 261-270, https://ieeexplore.ieee.org/document/134076.
25. Zhou, X.; Zheng, H.B.; Xu, X.Q.; He, J.Y.; Ge, X.K.; Yao, X.; Cheng, T.; Zhu, Y.; Cao, W.X.; Tian, Y.C. Predicting Grain Yield in Rice Using Multi-Temporal Vegetation Indices from UAV-Based Multispectral and Digital Imagery. *ISPRS J. Photogramm. Remote Sens.* **2017**, *130*, 246–255, doi:10.1016/j.isprsjprs.2017.05.003.
26. Xiao, X.; Boles, S.; Liu, J.; Zhuang, D.; Frolking, S.; Li, C.; Salas, W.; Moore, B. Mapping Paddy Rice Agriculture in Southern China Using Multi-Temporal MODIS Images. *Remote Sens. Environ.* **2005**.*95(4),* 480-492. doi:10.1016/j.rse.2004.12.009.
27. Qiu, B.; Li, W.; Tang, Z.; Chen, C.; Qi, W. Mapping Paddy Rice Areas Based on Vegetation Phenology and Surface Moisture Conditions. *Ecol. Indic.* **2015**, *56*, 79–86, doi:10.1016/j.ecolind.2015.03.039.
28. Qiu, C.; Liao, G.; Tang, H.; Liu, F.; Liao, X.; Zhang, R.; Zhao, Z. Derivative Parameters of Hyperspectral NDVI and Its Application in the Inversion of Rapeseed Leaf Area Index. *Appl. Sci.* **2018**, *8*, 1300.
29. Kang, Y.; Nam, J.; Kim, Y.; Lee, S.; Seong, D.; Jang, S.; Ryu, C. Assessment of Regression Models for Predicting Rice Yield and Protein Content Using Unmanned Aerial Vehicle-Based Multispectral Imagery. *Remote Sens.* **2021**, *13*, 1508, doi:10.3390/rs13081508.
30. Teal, R.K.; Tubana, B.; Girma, K.; Freeman, K.W.; Arnall, D.B.; Walsh, O.; Raun, W.R. In-Season Prediction of Corn Grain Yield Potential Using Normalized Difference Vegetation Index. *Agron. J.* **2006**, *98*, 1488–1494, doi:10.2134/agronj2006.0103.
31. Tian, Y.C.; Yao, X.; Yang, J.; Cao, W.X.; Hannaway, D.B.; Zhu, Y. Assessing Newly Developed and Published Vegetation Indices for Estimating Rice Leaf Nitrogen Concentration with Ground- and Space-Based Hyperspectral Reflectance. *Field Crops Res.* **2011**.*120(2)*, 299-310.
32. Wang, F.; Huang, J.; Tang, Y.-L.; Wang, X. New Vegetation Index and Its Application in Estimating Leaf Area Index of Rice. *Rice Sci.* **2007**, *14*, 195–203, doi:10.1016/S1672-6308(07)60027-4.
33. Tanaka, S.; Goto, S.; Maki, M.; Akiyama, T.; Muramoto, Y.; Yoshida, K. Estimation of leaf chlorophyll concentration in winter wheat [*Triticum aestivum*] before maturing stage by a newly developed vegetation index- rbNDVI. *J. Jpn. Agric. Syst. Soc. Jpn.* **2007** *4,* 297-303.
34. Zha, H.; Miao, Y.; Wang, T.; Li, Y.; Zhang, J.; Sun, W.; Feng, Z.; Kusnierek, K. Improving Unmanned Aerial Vehicle Remote Sensing-Based Rice Nitrogen Nutrition Index Prediction with Machine Learning. *Remote Sens.* **2020**, *12*, 215, doi:10.3390/rs12020215.

Chapter IV: Rice grain yield prediction using UAV-based multispectral images

Abstract: Rice grain yield prediction is important in evaluating crop management strategies applied in the field. Remote sensing using UAV is a potential method in predicting grain yield. Thus, the accuracy of predicting grain yield using UAV-derived variables must be evaluated. The study aimed to determine the relationship between grain yield and VIs taken at different growth stage and the effect of VI variables on the grain yield prediction. Multitemporal VI were calculated from the spectral reflectances measured at tillering, stem elongation, booting, and heading stages. Correlation between VIs and grain yield were low across growth stages (r = 0.07 to 0.99). Thus, multivariate regression model was used to improve the grain yield prediction. Random forest (RF) was observed to perform best among the regression model used in the study such as Support Vector Regression (SVR), Multiple Linear Regression (MLR), and Ridge regression. Grain yield prediction of RF with five selected VIs resulted in R^2 = 0.35 and RMSE = 0.78 ton/ha. The five selected VIs were CVI, GARI, GRNDVI, NDRE and REWDRVI, indicating the suitability of red edge based normalized VIs in predicting grain yield by providing optimal variation in the model. Transformation of VIs by adding the VIs taken at booting and heading stages did not substantially improve grain yield prediction (R^2 = 0.39, RMSE = 0.75 ton/ha). When the prediction model was developed for each cultivar, a better performance was observed for cultivars Hatsushimo (R^2 = 0.50, RMSE 0.84 ton/ha) and Nikomaru (R^2 = 0.50, RMSE = 0.53 ton/ha).

---

1. Introduction

Total rice production in an area is an important concern for agricultural policymakers and local rice producers. In a supply and demand-driven economy with rice consumption having a more constant rate, total rice supply is an indicator of the prevailing farmgate price and will be the basis for the next season's area for production. Experimental yield trial for a new agricultural product such as fertilizer or new rice cultivar is often the benchmark method in evaluating the effectiveness of the testing product. In the private sector, this is highly important and must be accomplished with accuracy

and considerable speed. On the other hand, the government sector gathers rice yield estimates all over the country to monitor the strength of the rice industry and can be used as the basis for possible repeal or changes in rice production policies. Thus, a fast and reliable grain yield estimation is encouraged to be part of an agricultural improvement program.

One of the most recognized methods in grain yield estimation is remote sensing data. UAV-derived multispectral images transformed as Vegetation Indices (VIs) were usually coupled with machine learning methods to estimate rice grain yield. A study by [1] used VIs and phenological data in a Random Forest model to estimate the grain yield of different rice cultivars. Deep learning methods were also applied to estimate grain yield to improve the low correlation between VIs and grain yield at the ripening stage [2]

Rice grain yield estimation using VIs is usually derived from satellites [3] and active sensors such as Green Seekers [4]. Both remote sensing approaches showed that grain yield can be optimally estimated at the early growth stage but had contrasting evaluations on weather variables to improve grain yield estimation using VIs. UAV-aided field crop monitoring has allowed measuring VIs at higher temporal and spectral resolutions. Although this does not mean that VIs derived from UAVs were better grain yield predictors. A comparison of sensors between UAVs and Green Seekers showed that there were VIs that performed better when calculated from active sensors than from sensors-mounted UAVs [5].

The findings of UAV-related research have provided more evidence of the applicability of VIs in estimating grain yield. Including UAV flights from different growth, stages can better estimate grain yield [6]. Other research has shown that variables of multi-temporal VIs enhance yield estimation [7,8]. One type is the derivation of VIs at the parcel level, wherein the relative VIs value is based on a reference parcel [9]. This method is primarily a change detection map and relies on the saturation of the VIs and the level of homogeneity of the different parcels of the whole experimental site.

Optimization of vegetation index using fluorescence spectral information resulted in high grain yield estimation (R^2 = 0.869) [10]. The texture of remotely sensed images also improved yield estimation [11]. Spectral mixture analysis of multispectral images was found to estimate rice grain yield with an error of less than 10% [12,13]. Another image segmentation method using K-mean clustering to detect the grain area in an image was also examined to estimate rice grain yield [14].

However, grain yield estimation at the early growth stage is much preferred, given its usefulness in evaluating agricultural interventions. Such preference points to determining and optimizing VIs that can estimate grain yield at the early growth stage.

Previous research has shown that VIs' correlation with grain yield varies with the growth stage. TNDVI is an effective predictor at the milky stage [15]. NDVI taken at the booting and heading stage and VARI at the jointing and booting stages performed well in rice yield prediction [8]. Color index NDYI effectively predicted grain yield at the heading stage [7]. Other VIs can be explored for grain yield estimation.

In this study, we aimed to (1) determine the relationship between VIs and grain yield at different growth stages, (2) the effect of the variables of vegetative indices on the grain yield estimation, and (3) determine what machine learning algorithms can best predict grain yield of different rice cultivars using VIs.

2. Materials and Method

2.1 Experimental design

The study site is located at the Togo Field, Field Science Research Center of the Nagoya University in Hatajiri, Morowa District, Togo, Aichi Prefecture, Japan (35°06'37.1"N 137°04'59.4"E). Two field trials, No Fertilizer and With Fertilizer, were established in rice seasons 2020 and 2021. The experimental design was a randomized complete block design (RCBD) with three replications and five cultivars (1) Aichinokaori, (2) Asahi, (3) Hatsushimo, (4) Nakate Shinsenbon, and (5) Nikomaru.

2.2. Field Data Collection

For each rice cultivar, eight (8) hills per plot was harvested at physiological maturity. The grains were cleaned, weighed, and converted to ton/ha.

2.3. UAV image acquisition and processing

The study utilized a UAV system. The UAV system and flight details were written in Chapter 2.

2.4. Image processing

The acquired images were ortho-mosaicked using the Pix4D mapper software (Pix4D SA, Prilly, Switzerland) to generate the spectral reflectance images of the experimental plots and georeferenced using ground control points.

An ortho-mosaicked true (RGB) image was used to create a region of interest (ROI). A shapefile consisting of circular polygons with a 10 cm radius corresponding to each hill of rice plants served as the ROI.

The reflectance images were then rasterized using the ‘raster’ [16] package in R. The ortho-mosaicked reflectance images were clipped into smaller raster images covering the experimental plot and cut for individual hills using the ROI shapefile. The mean values of reflectance from the clipped hill images were calculated. A total of 24 vegetation indices (Table A1) were calculated using different combinations of the mean values of the five spectral reflectance images.

2.5. Data Analysis

Data from rice seasons (2020 and 2021) were combined to comprise the whole dataset for the study. Correlation analyses between VI and grain yield for each rice cultivar and growth stage were established using the 'corrplot' package in R[17]. For each VIs, a linear regression model was developed. Variables of the multi-temporal vegetation indices were calculated to determine if these variables can improve grain yield estimation. Below are formulas for computing these variables. A hill-based relative vegetation index was generated by computing the difference between the VI taken from the Fertilizer level and VI taken from the No Fertilizer level.

$$VI_{dv1} = SUM(VI) = X_{ts} + X_{ss} + X_{bs} + X_{hs} \quad \text{Eq'n (1)}$$

$$VI_{dv2} = SUM(VI) = X_{ss} + X_{bs} \quad \text{Eq'n (2)}$$

$$VI_{dv3} = SUM(VI) = X_{bs} + X_{hs} \quad \text{Eq'n (3)}$$

$$VI_{dv4} = DIFF(VI) = X_{hs} - X_{ts} \quad \text{Eq'n (4)}$$

where X_{ts}, X_{ss}, X_{bs}, and X_{hs} represent VI values at tillering, stem elongation, booting, and heading stages. VI_{dv} refers to the variable of VI.

Recursive feature elimination was used to reduce dimension of the model and was performed using the 'caret' package in R [18]. Multivariate regression model such as Random Forest (RF), Support Vector Regression (SVR), Multiple Linear Regression (MLR), and Ridge regression were used to predict grain yield using the 'caret' package in R [18].

3. Results

3.1. Relationship between Grain Yield and Vegetation Index across Growth Stage

Table A2 shows the correlation analysis between different VIs and grain yield. The VIs had varying levels of correlation with grain yield at different growth stages. On average, higher correlations were observed at the stem elongation and booting stages. To reduce the multicollinearity effect in the model, recursive feature elimination (RFE) was done. RFE determines the number of features that will give the lowest RMSE value. Figures 1a-e show that different growth stages have different feature variables that will result in the lowest RMSE value.

Feature elimination results show that the stem elongation stage requires the lowest number of feature variables compared to other growth stages. Estimating grain yield using VIs taken at the heading stage required all 24 feature variables. Tillering and booting stages require 14 feature variables were needed to achieve the lowest RMSE. Stem elongation requires 8 feature variables, while across growth stages requires 14 feature variables.

Among the feature variables selected across growth stages, the most frequently selected features were REWDRVI, CVI, DVIMSS, BWDRVI, and GARI. However, in this study, we selected the top 5 feature variables selected at the heading stage, CVI, GARI, GRNDVI, NDRE, and REWDRVI.

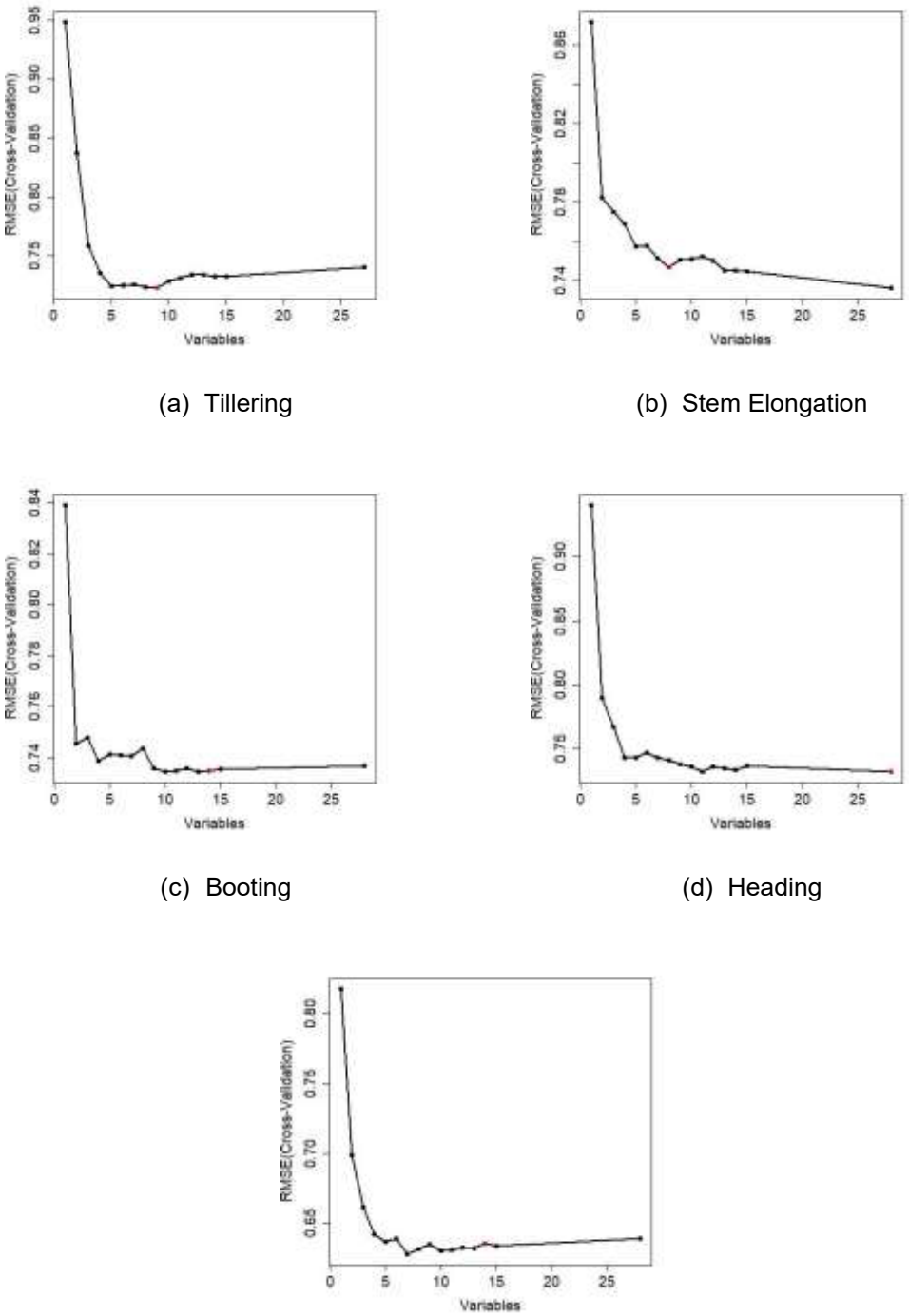

Figure 1. RMSE result of the cross-validation of the Recursive Feature Elimination Using VIs taken at different growth stages, (a). tillering, (b) stem elongation, (c) booting, (d) heading, and (e) all growth stages.

Table 1 shows the correlation of the top five (5) feature variables at each growth stage with rice grain yield. The highest correlation was observed at the heading stage for VIs GARI, REWDRVI, and GRNDVI. The lowest correlations were mainly observed at the tillering stage. The correlations of

different VIs with rice grain yield were low across growth stages. Predicting grain yield using VIs had a lower probability of good prediction performance. Table 2 shows the result of the linear regression model using the top five (5) feature variables. All the VIs poorly predicted the grain yield (R^2 = 0.0 – 0.04).

Table 1. Correlation analysis between vegetation index and grain yield.

	GARI	NDRE	REWDRVI	GRNDVI	CVI
Tillering	0.09	0.17	0.09	0.13	0.04
Stem Elongation	0.20	0.30	0.19	0.25	0.13
Booting	0.09	0.13	0.29	0.31	0.30
Heading	0.26	0.14	0.32	0.31	0.17

3.2. Effect of Variables of Vegetation Index in Grain Yield Prediction

According to other research, using multi-temporal VIs can improve grain yield prediction. Thus, variables of each of the selected VIs were examined to determine if these can improve grain yield estimation. Table 2 also shows the cross-validation result of these variables employed with the multiple linear regression model. The summation of a VI value taken at all growth stages did not improve grain yield prediction considerably, and the highest R^2 was 0.13. Likewise, adding VI values taken at only two growth stages, either VI values at stem elongation and booting stage or VI values at booting stage and heading stage, did not improve grain yield prediction. The difference in the VI values between the heading and tillering stages also did not improve grain yield prediction.

Table 2. Cross-validation result of grain yield estimation model using different variables of the multi-temporal VIs.

	VI	VI_{dv1}	VI_{dv2}	VI_{dv3}	VI_{dv4}
VIs	R^2	R^2	R^2	R^2	R^2
CVI	0.02	0.02	0.04	0.04	0.01
GARI	0.04	0.08	0.08	0.05	0.01
GRNDVI	0.02	0.13	0.12	0.14	0.01
NDRE	0.02	0.09	0.10	0.05	0.01
REWRDVI	0.00	0.06	0.04	0.18	0.04

3.3. Effect of Machine Learning in Grain Yield Prediction

Most of the VIs examined in this study had a low correlation with grain yield, indicating a non-linearity of the relationship between grain yield and VIs. Thus, machine learning (ML) methods were adopted to determine data patterns that a simple linear regression cannot identify. Using the top five

(5) VIs as predictors, the study evaluated four ML methods and selected the ML method that best predicted grain yield. Results show that Random Forest (RF) was the best performing model among the ML methods tested (Table 3). However, low prediction performance was observed, despite increasing the dimension of the model to add variance to the model.

This is perhaps due to the model's lower number of feature variables. Following the number of feature variables identified in RFE across the growth stage (14 variables), another set of grain yield prediction models was explored. Figure 2 shows the model evaluation result using an independent test dataset. The prediction model using five feature variables (RF, R^2 = 0.35) was comparable to prediction model using 14 feature variables (RF, VI, R^2 = 0.34; RF, VIdv1, R^2 = 0.31; RF, VIdv2, R^2 = 0.34; RF, DIFF(VI), R^2 = 0.32). Only the prediction model using the difference in VIs taken at the heading and tillering stages showed better prediction (RF, VIdv3, R^2 = 0.41). The slight improvement in the grain yield prediction from 5 feature variables to 14 feature variables shows that five (5) feature variables are the optimum number of VIs to predict grain yield.

Table 3. Cross validation result of different machine learning model using the top five (5) feature variables selected from the RFE method.

Metrics	MLR	RF	SVR	Ridge
R^2	0.059	0.346	0.060	0.059
RMSE	0.938	0.782	0.937	0.938

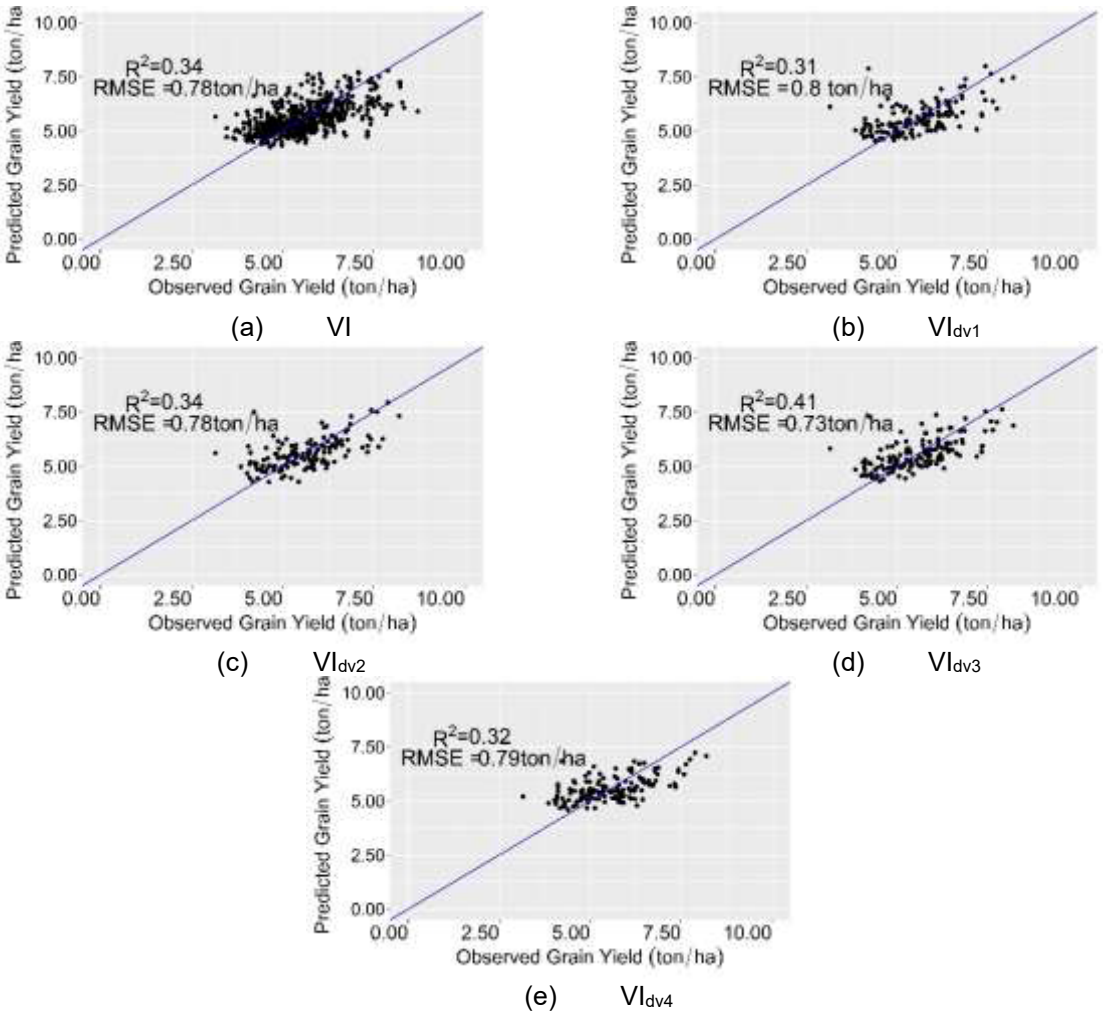

Figure 2. Model evaluation of grain yield prediction model using RF with (a) 14 VIs selected from RFE method. The VIs values were transformed as (b) sum of VI values taken at tillering (ts), stem elongation (ss), booting (bs), and heading (hs) stages, (c) sum of VI values taken at ss and bs, (d) sum of VI values taken at bs and hs, (e) difference of VI value taken at hs from VI value taken at ts.

3.4. Effect of Multivariate Vegetation Index in Grain Yield Prediction

The top five (5) feature variables identified from the RFE were used to predict grain yield using RF. Figure 3 shows that relatively, grain yield can be predicted using the sum of each of the VI values taken at booting and heading stages. Prediction of grain yield by using the addition of VIs value taken at booting and heading stages were examined for each variety. Results show that rice grain yield prediction model of cultivars Aichinokaori, Hatsushimo, and Nikomaru had good prediction performance while Asahi and Nakate Shinsenbon had moderately weak grain yield prediction model (Figure 4).

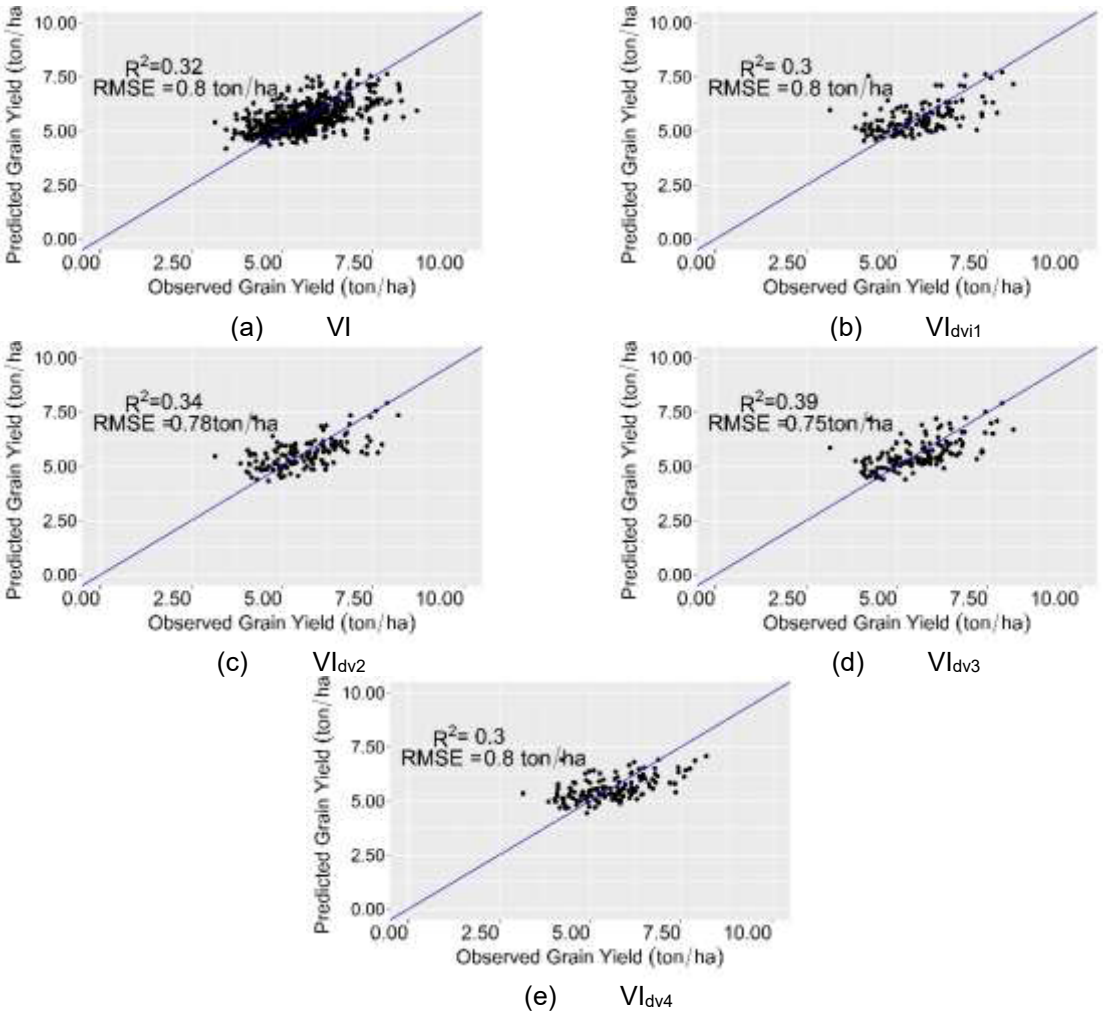

Figure 3. Model evaluation of grain yield prediction model using RF with (a) five VIs selected from RFE method. The VIs values were transformed as (b) sum of VI values taken at tillering (ts), stem elongation (ss), booting (bs), and heading (hs) stages, (c) sum of VI values taken at ss and bs, (d) sum of VI values taken at bs and hs, (e) difference of VI value taken at hs from VI value taken at ts.

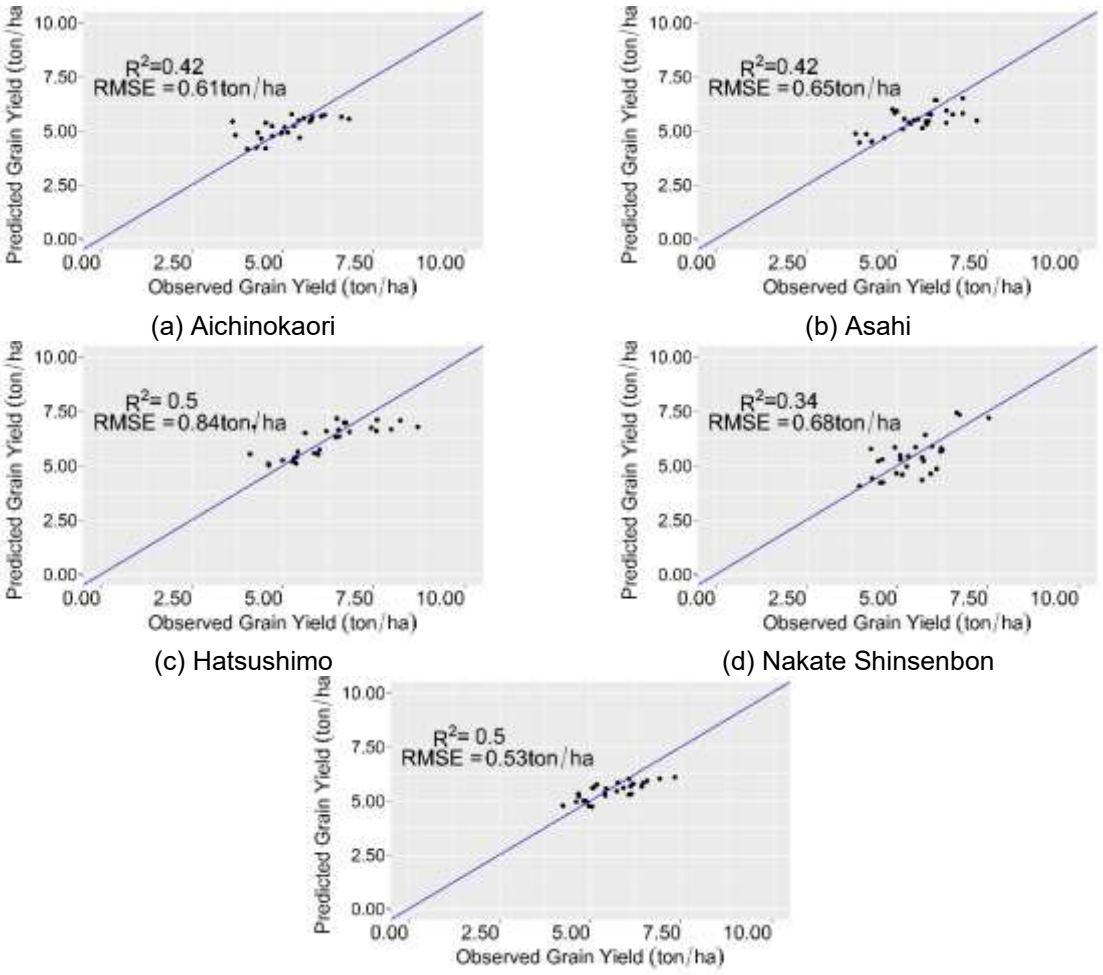

(a) Aichinokaori (b) Asahi

(c) Hatsushimo (d) Nakate Shinsenbon

(e) Nikomaru

Figure 4. Model evaluation of grain yield prediction model using RF with five VIs selected from RFE method of cultivars (a) Aichinokaori, (b) Asahi, (c) Hatsushimo, (d) Nakate Shinsenbon, and (e) Nikomaru.

4. Discussion

A grain yield prediction model using multi-temporal VIs was examined in the study. Correlation analysis between VIs and grain yield was established first, and the correlation between grain yield and VIs was moderately weak. Then, a feature selection method called Recursive Feature Elimination (RFE) was applied to the dataset. A set of VIs was selected for each growth stage. Results show that grain yield prediction varies with the multi-temporal VIs used in the model, and the heading stage needs numerous VIs to have the lowest RMSE value. Using 14 feature variables to predict grain yield was observed to have comparable performance with the prediction model using only five (5) feature variables.

The top 5 feature variables were GARI, CVI, NDRE, REWDRVI, and GRNDVI. Individually, these VIs had a low correlation with grain yield. RFE method selects a combination of features that can result in the lowest prediction error. In an evaluation of VIs conducted by [19], it was concluded that red-edge-based normalized VIs such as NDRE and REWDRVI provide the optimum variations in VI values by normalizing the NIR and red-edge values while unaffected by the saturation observed in red bands. Thus, red edge-based normalized VIs performed better than NDVI, which is affected by the saturation at the red band, resulting from narrowing VI values at the growth stage where canopy variations could be more observed. Moreover, the ratio-based VIs have a broader variation in values compared to normalized VIs, resulting in more noise in the model. This also explains why GRNDVI was one of the selected VIs. The narrow values in NDVI were adjusted in the GRNDVI by providing reflectance values from the green band, resulting in the less narrow VI values. Moreover, the red/green ratio in the CVI delineates reflectance between soil and vegetation, where the red/green ratio of soil and vegetation are > 1.0 and < 1.0, respectively. The formulas for these VIs can be observed in Table A1.

Other research on the use of UAV-based vegetation index in crop prediction showed that the five RFE-selected VIs in this study significantly affected the grain yield prediction of various crops. GARI has been found to predict corn at the tasseling stage [20]. Conversely, CVI is insensitive to the difference in canopy LAI before canopy closure [21]. NDRE can estimate N nutrition in rice, predicting grain yield at the early to mid-growth stages [22]. REWDRVI, on the other hand, can estimate rice

plant traits such as plant height, biomass, and foliar N content [23]. GRNDVI has been found to estimate rice protein content [24].

The VI transformation generated in the study consisted of a summation of the VIs taken at different growth stages and the difference in VI values at two growth stages. These VI variables did not significantly improve the grain yield prediction from the grain yield prediction model using the actual VI values. However, when the grain yield prediction model was trained on a single cultivar, the grain yield prediction of some cultivars, such as Hatsushimo, and Nakate Shinsenbon, the R^2 improved by 0.10 while the other cultivars had a prediction performance of R^2 less than 0.50, similar to the grain yield prediction model using all the five cultivars. In research done by [7], the grain yield of one rice cultivar was optimally predicted at the initial heading stage using UAV-based RGB and multispectral images. In this study, the VIs taken at booting at heading stages relatively had a better prediction performance than the prediction model that considers the VI values taken at all growth stages. This indicates that the variation observed at the tillering stage was noise contributing to the overfitting in the model. This is apparent in the lack of correlation between VIs and grain yield at the tillering stage (Table 1).

The differences in prediction performance between varieties may be due to the inability of some VIs to capture the canopy characteristics of some cultivars. In this study, grain yield predictions of Asahi and Nakate Shinsenbon were moderately weak.

5. Conclusion

Grain yield prediction using VIs was evaluated in this study. VIs were calculated from tillering to heading stages. Multitemporal VIs were used in a Random Forest to predict grain yield, and the correlation between VIs and grain yield was low. A feature selection method, RFE, was employed to select a combination of VIs that can predict grain yield. The number of selected VIs from the feature selection method varied between growth stages, with the heading stage having the highest number of VIs required to achieve the lowest RMSE, while the stem elongation stage had the lowest number of VIs required. However, grain yield prediction using the top five (5) VIs selected from the multitemporal VIs had a comparable performance with the prediction model that used 14 VIs. VI transformation, such as the addition of VI values at all growth stages and two growth stages (stem elongation + booting stage; booting stage + heading stage) and the difference between VIs taken at heading and tillering stages did not substantially improve grain yield prediction from $R^2 = 0.35$ to $R^2 = 0.39$.

Nevertheless, the prediction model using VIs taken at booting and heading stages had the relatively best performance. When this prediction model was developed for each cultivar, some cultivars had good prediction performance, with cultivars Hatsushimo and Nikomaru having an $R^2 = 0.50$. On the other hand, grain yields of cultivars Aichinokaori, Asahi, and Nakate Shinsenbon cannot be predicted with good performance using VIs having an R^2 of less than 0.45.

6. Appendix

Table A1. Vegetation indexes used in the prediction model.

Vegetation Index	Formula	References
Green Atmospherically Resistant Vegetation Index (GARI)	(NIR – (G – (B – R)) / (NIR + (G – (B – R))	[20]
Chlorophyll Vegetation Index (CVI)	NIR × (R/G²)	[21]
Green-red Normalized Difference Vegetation Index (GRNDVI)	(NIR – (R + G)) /(NIR + (R + G))	[24]
Normalized Difference Red-Edge (NDRE)	(NIR – RE) / (NIR + RE)	[22]
Red Edge Wide Dynamic Range Vegetation Index (REWDRVI)	(a × NIR – RE) / (a × NIR + RE) (a = 0.12)	[23]

Table A2. The Pearson correlation coefficient between Vegetation Index taken at different growth stages and grain yield.

VI	Tillering	Stem Elongation	Booting	Heading
ARVI2	0.087	0.252	0.205	0.271
ATSAVI	0.163	0.309	0.059	0.007
AVI	0.256	0.348	0.076	0.063
BWDRVI	0.183	0.323	0.329	0.257
CVI	0.041	0.126	0.302	0.170
DVI	0.249	0.357	0.086	0.072
DVIMSS	0.127	0.181	- 0.072	- 0.065
EVI	0.223	0.337	0.070	0.048
EVI2	0.224	0.340	0.069	0.045
EVI2.2	0.228	0.341	0.077	0.051
GARI	0.017	0.202	0.092	0.263
GBNDVI	0.135	0.255	0.338	0.295
GDVI	0.273	0.354	0.121	0.095
GLI	0.146	0.014	- 0.164	- 0.072
GNDVI	0.127	0.227	0.325	0.284
GOSAVI	0.205	0.291	0.150	0.088
GRNDVI	0.131	0.255	0.306	0.314
GSAVI	0.239	0.317	0.124	0.076
NDRE	0.165	0.301	0.133	0.135
NDVI	0.087	0.252	0.205	0.271
PNDVI	0.144	0.272	0.316	0.312
RBNDVI	0.112	0.268	0.246	0.265
REDVI	0.277	0.370	0.144	0.132
REOSAVI	0.209	0.320	0.127	0.107
RESAVI	0.239	0.338	0.131	0.111
REWDRVI	0.093	0.193	0.285	0.321
RVI	0.302	0.399	0.318	0.361
WDRVI	0.075	0.140	0.368	0.363

7. References

1. Ge, H.; Ma, F.; Li, Z.; Du, C. Grain Yield Estimation in Rice Breeding Using Phenological Data and Vegetation Indices Derived from UAV Images. *Agronomy* **2021**, *11(12)*, 2439, doi:10.3390/agronomy11122439.
2. Yang, Q.; Shi, L.; Han, J.; Zha, Y.; Zhu, P. Deep Convolutional Neural Networks for Rice Grain Yield Estimation at the Ripening Stage Using UAV-Based Remotely Sensed Images. *Field Crops Res.* **2019**, *235*, 142–153, doi:10.1016/j.fcr.2019.02.022.
3. Jeong, S.; Ko, J.; Yeom, J.-M. Predicting Rice Yield at Pixel Scale through Synthetic Use of Crop and Deep Learning Models with Satellite Data in South and North Korea. *Science of the Total Environment.* **2022**, *802*, 149726, doi:10.1016/j.scitotenv.2021.149726.
4. Harrell, D.L.; Tubaña, B.S.; Walker, T.W.; Phillips, S.B. Estimating Rice Grain Yield Potential Using Normalized Difference Vegetation Index. *Agron. J.* **2011**, *103(6)*, 1717–1723, doi:10.2134/agronj2011.0202.
5. Rehman, T.H.; Lundy, M.E.; Linquist, B.A. Comparative Sensitivity of Vegetation Indices Measured via Proximal and Aerial Sensors for Assessing N Status and Predicting Grain Yield in Rice Cropping Systems. *Remote Sens.* **2022**, *14(12)*, 2770, doi:10.3390/rs14122770.
6. Perros, N.; Kalivas, D.; Giovos, R. Spatial Analysis of Agronomic Data and UAV Imagery for Rice Yield Estimation. *Agriculture* **2021**, *11(9)*, 809, doi:10.3390/agriculture11090809.
7. Wan, L.; Cen, H.; Zhu, J.; Zhang, J.; Zhu, Y.; Sun, D.; Du, X.; Zhai, L.; Weng, H.; Li, Y.; et al. Grain Yield Prediction of Rice Using Multi-Temporal UAV-Based RGB and Multispectral Images and Model Transfer – a Case Study of Small Farmlands in the South of China. *Agricultural and Forest Meteorology.* **2020**, *291*, 108096, doi:10.1016/j.agrformet.2020.108096.
8. Zhou, X.; Zheng, H.B.; Xu, X.Q.; He, J.Y.; Ge, X.K.; Yao, X.; Cheng, T.; Zhu, Y.; Cao, W.X.; Tian, Y.C. Predicting Grain Yield in Rice Using Multi-Temporal Vegetation Indices from UAV-Based Multispectral and Digital Imagery. *ISPRS Journal of Photogrammetry and Remote Sensing.* **2017**, *130*, 246–255, doi:10.1016/j.isprsjprs.2017.05.003.
9. Wang, F.; Wang, F.; Zhang, Y.; Hu, J.; Huang, J.; Xie, J. Rice yield estimation using parcel-level relative spectral variables from UAV-based hyperspectral imagery. *Frontiers in plant science*. **2019**. 10, 453, https://doi.org/10.3389/fpls.2019.00453.
10. Wang, F.; Yao, X.; Xie, L.; Zheng, J.; Xu, T. Rice Yield Estimation Based on Vegetation Index and Florescence Spectral Information from UAV Hyperspectral Remote Sensing. *Remote Sensing.* **2021**, *13(17)*, 3390, doi:10.3390/rs13173390.
11. Wang, F.; Yi, Q.; Hu, J.; Xie, L.; Yao, X.; Xu, T.; Zheng, J. Combining Spectral and Textural Information in UAV Hyperspectral Images to Estimate Rice Grain Yield. *Internation Journal of Applied Earth Observation and Geoinformation.* **2021**, *102*, 102397, doi:10.1016/j.jag.2021.102397.
12. Yuan, N.; Gong, Y.; Fang, S.; Liu, Y.; Duan, B.; Yang, K.; Wu, X.; Zhu, R. UAV Remote Sensing Estimation of Rice Yield Based on Adaptive Spectral Endmembers and Bilinear Mixing Model. *Remote Sensing.* **2021**, *13(11)*, 2190, doi:10.3390/rs13112190.
13. Duan, B., Fang, S., Zhu, R., Wu, X., Wang, S., Gong, Y., & Peng, Y. Remote estimation of rice yield with unmanned aerial vehicle (UAV) data and spectral mixture analysis. *Frontiers in Plant Science*, **2019.** 10, 204, https://doi.org/10.3389/fpls.2019.00204.
14. Reza, M.N.; Na, I.S.; Baek, S.W.; Lee, K.-H. Rice Yield Estimation Based on K-Means Clustering with Graph-Cut Segmentation Using Low-Altitude UAV Images. *Biosyst. Eng.* **2019**, *177*, 109–121, doi:10.1016/j.biosystemseng.2018.09.014.
15. Goswami, S.; Choudhary, S.S.; Chatterjee, C.; Mailapalli, D.R.; Mishra, A.; Raghuwanshi, N.S. Estimation of Nitrogen Status and Yield of Rice Crop Using Unmanned Aerial Vehicle Equipped with Multispectral Camera. *Journal of Applied Remote Sensing.* **2021**, *15(4)*, 042407, doi:10.1117/1.JRS.15.042407.
16. Hijmas, R.J. raster: Geographic Data Analysis and Modeling. R package version. 3.5-15. **2022**. https://CRAN.R-project.org/package=raster17.
17. Wei, T.; Simko, V.; Levy, M.; Xie, Y.; Jin, Y.; Zemla, J. Package 'Corrplot'. *Statistician* **2017**, *56(316)*, e24, https://peerj.com/articles/9945/Supplemental_Data_S10.pdf.
18. Kuhn, M. Building Predictive Models in R Using the Caret Package. *Journal of Statistical Software.* **2008**, *28*, 1–26, doi:10.18637/jss.v028.i05.
19. Kanke, Y.; Tubana, B.; Dalen, M.; Harrell, D. Evaluation of Red and Red-Edge Reflectance-Based Vegetation Indices for Rice Biomass and Grain Yield Prediction Models in Paddy Fields. *Precision Agriculture.* **2016**. *17*, doi:10.1007/s11119-016-9433-1.

20. Barzin, R.; Pathak, R.; Lotfi, H.; Varco, J.; Bora, G.C. Use of UAS Multispectral Imagery at Different Physiological Stages for Yield Prediction and Input Resource Optimization in Corn. *Remote Sensing.* **2020**, *12(15)*, 2392, doi:10.3390/rs12152392.
21. Vincini, M.; Frazzi, E.; D'Alessio, P. A Broad-Band Leaf Chlorophyll Vegetation Index at the Canopy Scale. *Precision Agriculture.* **2008**, *9*, 303–319, doi:10.1007/s11119-008-9075-z.
22. Zhang, K.; Ge, X.; Shen, P.; Li, W.; Liu, X.; Cao, Q.; Zhu, Y.; Cao, W.; Tian, Y. Predicting Rice Grain Yield Based on Dynamic Changes in Vegetation Indexes during Early to Mid-Growth Stages. *Remote Sensing.* **2019**, *11(4)*, 387, doi:10.3390/rs11040387.
23. Muharam, F.M.; Nurulhuda, K.; Zulkafli, Z.; Tarmizi, M.A.; Abdullah, A.N.H.; Che Hashim, M.F.; Mohd Zad, S.N.; Radhwane, D.; Ismail, M.R. UAV- and Random-Forest-AdaBoost (RFA)-Based Estimation of Rice Plant Traits. *Agronomy.* **2021**, *11(5)*, 915, doi:10.3390/agronomy11050915.
24. Kang, Y.; Nam, J.; Kim, Y.; Lee, S.; Seong, D.; Jang, S.; Ryu, C. Assessment of Regression Models for Predicting Rice Yield and Protein Content Using Unmanned Aerial Vehicle-Based Multispectral Imagery. *Remote Sensing.* **2021**, *13(8)*, 1508, doi:10.3390/rs13081508.

Chapter V: Estimating Yield-Related Traits Using UAV-Derived Multispectral Images to Improve Rice Grain Yield Prediction

Abstract: Rice grain yield prediction with UAV-driven multispectral images is a re-emerging interest in precision agriculture, and optimal sensing time is an essential factor. This study aimed to predict rice grain yield by using the estimated aboveground biomass (AGB) and leaf area index (LAI) from vegetation indices (VIs) and determine the optimal sensing time in estimating AGB and LAI using VIs for grain yield prediction. An experimental trial was conducted in 2020 and 2021, involving two fertility conditions and five japonica rice cultivars (Aichinokaori, Asahi, Hatsushimo, Nakate Shinsenbon, and Nikomaru). Multi-temporal VIs were used to estimate AGB and LAI throughout the growth period with the extreme gradient boosting model and Gompertz model. The optimum time windows for predicting yield for each cultivar were determined using a single-day linear regression model. The results show that AGB and LAI could be estimated from VIs (R^2: 0.56 – 0.83 and 0.57 – 0.73), and the optimum time window for UAV flights differed between cultivars, ranging from 4 to 31 days between the tillering stage and the initial heading stage. These findings help researchers to save resources and time for numerous UAV flights to predict rice grain yield.

---

1. Introduction

Precision agriculture involves real-time crop monitoring to aid in necessary field management intervention to ensure a good harvest. This is made possible by the innovation of using unmanned aerial vehicles (UAVs) in the field. The images taken from the UAV serve as an alternative parameter to actual plant traits such as plant height [1–3], leaf area index (LAI) [4–6], and aboveground biomass (AGB) [7–9]. In recent years, this type of remote sensing has also been applied in creating prediction models using machine learning algorithms [10–12].

Rice grain yield prediction presents several benefits. With the market demand, the basis for the import and export inventories in a district is the grain yield estimates [13]. Yield forecast, to some extent, can be a strategy for crop insurance providers in evaluating if a farm is entitled to an indemnity due to low production. Local agricultural officers can use grain yield prediction to determine if the

current crop management program in the area is bridging the yield gap, with normal year-to-year variation in consideration. Inter-annual variations in rice grain yield can be attributed to year-to-year climate variability such as anomalous weather. The increase in nighttime temperature and longer hot days are expected to affect rice productivity The presence of cloud cover, reducing solar radiation and change in fertility application can influence grain yield variation between years [14, 15].

These situations require reliable results yet with a short-term process. The use of UAVs presents an advantage as it provides higher spatial–temporal resolution than the use of satellites, allowing for more precise crop monitoring than the situations mentioned above require.

However, rice grain yield prediction models using UAVs are not without difficulty. The need to acquire data during certain rice growth stages, which are important for yield determination, and differences in observed phenotype trends due to differences in plant architecture among rice cultivars are inevitable problems in yield prediction by remote sensing.

Previous research has shown that the use of vegetation indices (VIs) to predict grain yield resulted in a good coefficient of determination (R^2) when yield—VI models were incorporated with other variables such as phenological data [16,17] and other plant parameters such as days to maturity, plant height [9], and ground coverage [18,19]. Better results were also observed when different VIs [20,21] and multi-temporal VIs [22,23] were incorporated into the model. These prediction models work on the hypothesis that grain yield can be predicted using plant parameters and weather data that indicate the plant's physiological efficiency during grain filling. Additionally, increasing the predictors may improve the determination efficiency to a certain number of terms. Combining VIs with texture indices measured at the booting stage had comparable results to VIs measured at the booting and heading stages [24, 25].

However, incorporating these parameters did not always result in better prediction. In particular, the inclusion of growing degree-days did not improve the model compared to using the NDVI alone [26] Rice prediction models use a generalized optimal sensing time and multi-temporal VIs to predict grain yield and their performances depend on the accuracy of monitoring certain rice growth stages that are known to be important in grain yield determination such as panicle initiation and flowering stages. Sensing beyond panicle differentiation resulted in a lower rice grain yield prediction than during the interval between panicle initiation and differentiation [22, 26].

Other research has also shown that the prediction method is more important than the sample size, with the random forest model being the best method in most cases. The sample size can influence the performance of cross-validated prediction models, and a small sample size is used in a high number of k-fold cross-validations, where a high R^2 in the test dataset can be observed, resulting in a biased result [9, 17, 27].

The target cultivar used in the prediction is also crucial. The importance of VIs is often evaluated on a case-to-case basis using correlation analyses and variable importance plots, meaning that a particular VI may show a linear relationship in one study but not in another study. Using VIs that can represent the morphological differences among cultivars can improve the variability aspect of the prediction model [28]. Grain yield prediction models for different cultivars have attempted to avoid high variance in prediction model research [29].

The results of the above experiments indicate that the current UAV-based grain yield prediction model consists of multi-temporal VIs, other image-derived variables, and the selection of the best prediction model. Little attention has been paid to estimated plant parameters using UAVs and these estimates to predict rice grain yield.

Our study hypothesized that reasonable estimates of individual rice plant AGB and LAI throughout the growth period from UAV-derived data could predict grain yield without incorporating the actual plant parameters measured manually. The extreme gradient boosting algorithm (XGBoost), a robust ensemble machine learning algorithm, was chosen to estimate AGB and LAI. Previous research has shown that XGBoost outperformed other machine learning algorithms in the yield forecasting of several crops [30, 31]. It can also determine trends in crop-yield-related parameters such as rainfall and temperature [32]. XGBoost uses a gradient boosting method wherein the model learns from the weak learners and corrects the mistake in the prediction while regularizing the model due to complexity. Compared to the simple random forest and ridge regression, XGBoost has both strengths of regularization (ridge) and decision trees (random forest). The grain yield prediction using the estimated AGB and LAI depends on the estimation accuracy of AGB and LAI first. Using predicted values to predict another variable poses an inherent prediction error but can be mitigated using a model that can bode well.

Once the AGB and LAI are estimated using VIs, the AGB and LAI dynamics throughout the growth duration can be calculated using the developed estimation models and the Gompertz growth curve. A sigmoid curve such as the Gomperz growth curve is often used to describe the plant weight and LAI as a function of time [33, 34]. The Gompertz curve has also been applied in determining a relationship between plant dry matter and vegetation cover derived from computer vision techniques [35].

When the dynamics have been estimated, the optimum time for UAV flights can be determined. This is to optimize the UAV data acquisition by avoiding unnecessary and redundant UAV flights for AGB and LAI estimation that can be used for grain yield prediction. The proposed prediction method was developed for each of the cultivars tested in the study. This study attempted to build a two-step grain yield prediction model by estimating the in-season AGB and LAI using correlated VIs and then utilizing these estimated parameters to predict grain yield. This study also aimed to determine the optimum time window for UAV flights.

2. Materials and Methods

The workflow of the study consisted of the following: (1) data collection and processing of AGB, LAI, grain yield, and UAV spectral data for the years 2020 and 2021, (2) establishment of baseline grain yield prediction, and (3) estimation models for AGB and LAI to be used as predictors for the GY prediction model. The details are described in Figure 1.

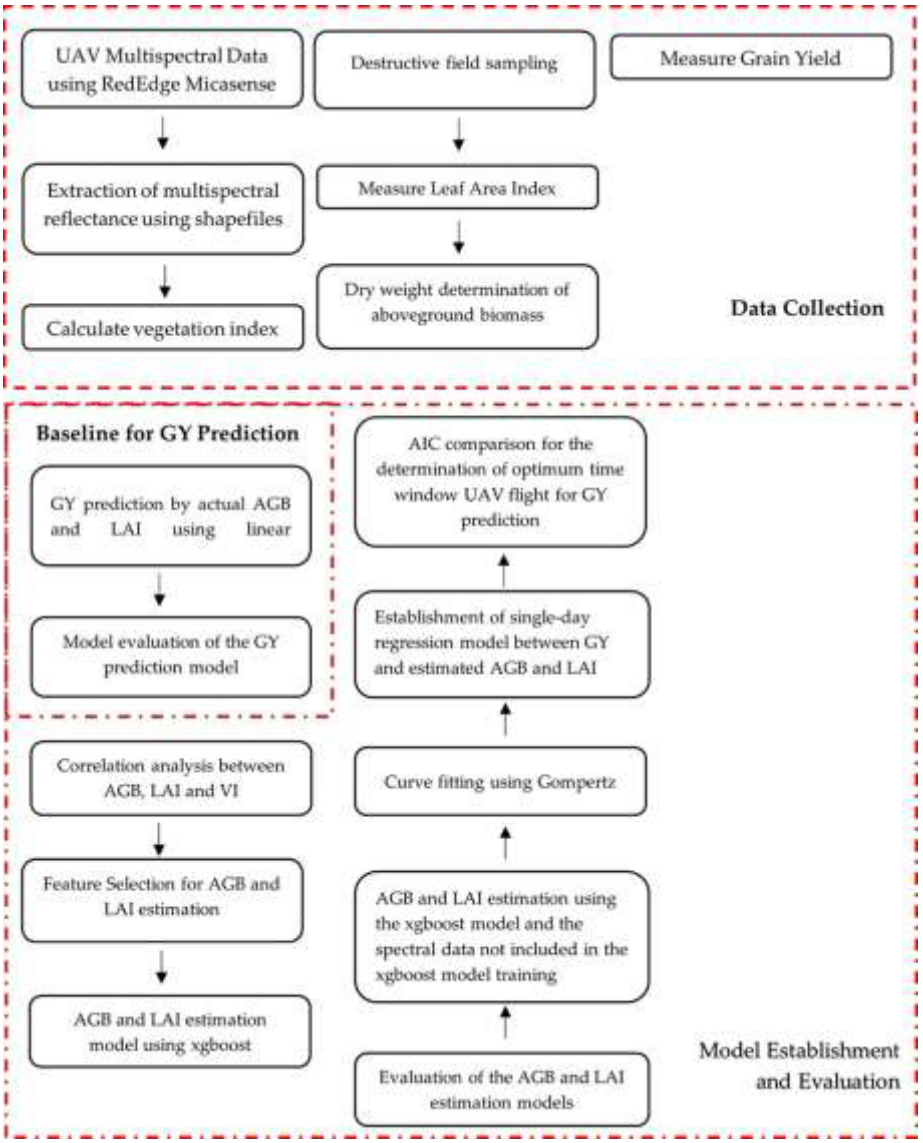

Figure 1. Workflow of the study.

2.1. Study Area

The study site is located at the Togo Field, Field Science Research Center of the Nagoya University in Hatajiri, Morowa District, Togo, Aichi Prefecture, Japan (35°06'37.1"N 137°04'59.4"E) (Figure 2).

Aichi Prefecture belongs to a humid subtropical climate zone. During the growing season, the average monthly total sunshine duration is 165.38 h, and the average monthly total precipitation is 223.35, and the average daily temperature is 25.7 °C [36]. The primary soil type is ultisols.

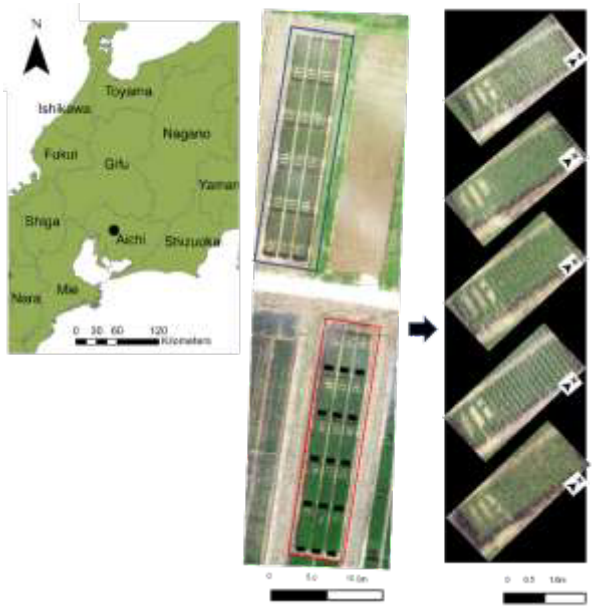

Figure 2. Location of the study site in Aichi, Japan. Orthomosaic image of the two experimental trials: trial with no fertilizer (in blue box) and trial with fertilizer (red box). On the right, from the top to bottom, are the plot images clipped from the orthomosaic image of rice cultivars, namely, Aichinokaori, Hatsushimo, Asahi, Nakate Shinsenbon, and Nikomaru.

2.2. Experimental Design

Two experimental trials, namely, a trial with no fertilizer and a trial with fertilizer, were conducted in 2020 and 2021, involving five japonica cultivars with different heading times and plant architectures, Aichinokaori, Asahi, Hatsushimo, Nakate Shinsenbon, and Nikomaru (Figure 2). These cultivars were divided into two groups at the study site: the early-heading group (Aichinokaori, Nakate Shinsenbon, and Nikomaru) and the late-heading group (Asahi and Hatsushimo). Nakate Shinsenbon has a large number of small-sized panicles with a short plant stature; and Nikomaru has a small number of large-sized panicles with a tall plant stature, and Aichinokaori, Asahi, and Hatsushimo have an intermediate stature. Basal fertilization was carried out according to local practices for the fertilizer

trials, and top-dressing was not performed for both trials. The amount of fertilizer applied in the fertilizer plot was 48 kg N, 34 kg P, and 44 kg K per hectare. The plot size was 1.68 m × 5.52 m with a 24 cm plant spacing. The experiments were laid out in a randomized complete block design with three replications.

2.3. Field Data Collection

AGB was sampled for each cultivar at different growth stages: (1) tillering stage, (2) stem elongation, (3) booting stage and (4) heading stage. The tillering stage is referred to as the late tillering stage (V8); the stem elongation stage is when the panicle branches have formed (R1); the booting stage is the flag leaf collar formation (R^2); and the heading stage is when one or more florets of the main stem panicle achieve anthesis (R4) [37].

Sampling was conducted after the UAV flight for spectral data collection (Table 1). Four adjacent hills of rice plants were sampled in each plot. The number of tillers per sampled hill was counted and separated into leaves and stems. The detached leaves were used to determine the LAI using an area meter, AAM-9 (Hayashi Denko co ltd., Tokyo, Japan). After measuring the leaf area, the detached plant parts were oven-dried at 70 °C for 48 h until a constant weight was attained and weighed. LAI determination was carried out only until the booting stage. Grain yield was measured at physiological maturity. Eight hills per plot were harvested. The grains were cleaned, and weighed, and the grain yield was converted to ton/ha.

Table 1. UAV flight and sampling dates for the corresponding growth stages of the two-year experiment trials.

Growth Stage	2020 UAV Flight Date (DAT)	2021 UAV Flight Date (DAT)
	Aichinokaori	
Tillering	21-July (49)	31-July (52)
Stem Elongation	11-August (70)	18-August (70)
Booting	17-August (76)	25-August (77)
Heading	25-August (84)	31-August (83)
	Asahi	
Tillering	29-July (57)	5-August (57)
Stem Elongation	11-August (70)	18-August (70)
Booting	23-August (82)	31-August (83)
Heading	11-September (101)	9-September (92)
	Hatushimo	
Tillering	21-July (49)	28-July (49)
Stem Elongation	5-August (64)	11-August (63)
Booting	23-August (82)	31-August (83)

Heading	11-September (101)	9-September (92)
	Nakate Shinsenbon	
Tillering	15-July (43)	22-July (43)
Stem Elongation	29-July (57)	5-August (57)
Booting	17-August (76)	20-August (72)
Heading	25-August (84)	31-August (83)
	Nikomaru	
Tillering	21-July (49)	28-July (49)
Stem Elongation	5-August (64)	11-August (63)
Booting	17-August (76)	25-August (77)
Heading	25-August (84)	9-September (92)

2.4. UAV Image Acquisition and Preprocessing

This study utilized a UAV system: Matrice 210 RTK v2 with a Zenmuse X7 50 mm camera (DJI, Shenzhen, Guangdong, China) and Micasense RedEdge-MX sensors on board. The multispectral bands used in this study were the following: blue (475 ±32 nm), green (560 ± 27 nm), red (668 ±14 nm), red edge (717 ± 12 nm), and near-IR (842 ± 57 nm). The flight altitude was 20.0 m with a forward overlap of 80% and a side overlap of 75%. The shooting mode was hovering with a flight speed of 1.2 m/s. The approximate resolution was 0.20 cm/pix.

For each UAV flight, the sensors were calibrated using a Calibrated Reflectance Panel (CRP) provided by the sensor manufacturer according to its instructions. UAV flights were conducted between 10:00 am and 4:00 pm under windless and clear-sky conditions once a week until the heading stage. The number of UAV flights used in this study was 11 in 2020 and 17 in 2021.

The acquired images were ortho-mosaicked using the Pix4D mapper software (Pix4D SA, Prilly, Switzerland) to generate the spectral reflectance images of the experimental plots and georeferenced using ground control points.

An ortho-mosaicked true (RGB) image was used to create a region of interest (ROI). A shapefile consisting of circular polygons with a 10 cm radius corresponding to each hill of rice plants served as the ROI.

The reflectance images were then rasterized using the ‘raster’ [38] package in R. The ortho-mosaicked reflectance images were clipped into smaller raster images covering the experimental plot and cut for individual hills using the ROI shapefile. The mean values of reflectance from the clipped hill images were calculated. A total of 24 vegetation indices (Table A1) were calculated using different combinations of the mean values of the five spectral reflectance images.

2.5. Data Analysis

Data from rice growing seasons (2020 and 2021) were pulled together to comprise the whole dataset for the study—the study was composed of three prediction models for each cultivar. To establish a baseline for predicting grain yield by AGB and LAI, a linear regression model was conducted using repeated k-fold cross-validation (k = 3) provided by the 'caret' package in R [39]. A regression model for each growth stage was conducted to determine which growth stage can best predict grain yield. The growth stage corresponding to the model with the lowest RMSE in the model evaluation using an independent test dataset was considered as the optimum growth stage for predicting grain yield using AGB and LAI.

A correlation analysis was performed between AGB, LAI, and VIs using the 'corrplot' [40] package in R, and VIs were chosen as the feature variable for further XGBoost modeling. Since the XGBoost algorithm cannot handle high-dimensional data, the top ten correlated VIs were used to estimate AGB and LAI.

The 'xgboost' package in R [41] was used to train the XGBoost model to estimate AGB and LAI. A hold-out method was used with 70% as the training dataset and 30% as the independent test dataset. With the training dataset, the model was trained by a repeated k-fold cross-validation method (k = 3, 10 times). The optimum estimation model was determined using the lowest RMSE as the evaluation metric criterion.

The XGBoost algorithm is a boosting ensemble machine learning algorithm combining boosted trees' features and the gradient descent method with regularization functions. In the tree-based learning method, a prediction is made by creating a regression tree based on a decision tree score. Therefore, correlated features do not necessarily influence the performance of XGBoost. Then, the weak learners in the regression tree are given more weight in the next iteration. This is done by incorporating the prediction of the residuals or errors of the prior regression tree into the new regression tree. Then, a regularization parameter is included in the new regression tree to account for the increase in the complexity of the model. The gradient descent method minimizes the cost function, which measures the error between the predicted and observed values.

To further explain the prediction process, feature importance was summarized using SHAP (SHapley Additive exPlanations) from the 'SHAPforxgboost' package in R [42]. The independent test dataset was evaluated using the normalized RMSE.

To achieve an optimized prediction model using XGBoost, there are several tuning parameters that can be explored as described by [41,43]. This study attempted to optimize the following parameters: (1) max depth, which is the depth of the decision tree, which means a tree must have features equal to the number of depths to create a prediction; (2) colsample by tree, which is the number of features supplied to a tree.

The estimation models for AGB and LAI were then utilized to predict the AGB and LAI across the growth period using the VIs calculated from other UAV flights not used in the training data for the estimation models. A predicted value corresponding to the extracted ROI of one hill was eliminated when it was less than 85% of the preceding predicted value and the records with less than 3 predicted values were removed from the next analyses. The remaining predicted AGB and LAI were fitted into the Gompertz growth curve using the 'drc' package in R [44] to interpolate AGB and LAI values at 1 to 100 DAT using 0.1 as the starting value (DAT 0) for AGB and LAI. Then, to determine which days were the optimum time window for conducting a UAV flight, a single-day linear regression model between grain yield and the predicted AGB and LAI was conducted using the 'caret' package in R [34] by a repeated k-fold cross-validation method (k = 3, 10 times). In total, 960 records of AGB and grain yield, and 720 records of LAI were used in our study, but only 48 were used for each stage per cultivar. Training single-day linear regression models with a limited number of data can lead to overfitting and inaccurate results. To expand the yield data quantitatively and to eliminate the chance success produced by bias in data partitioning, we conducted a trial of 10 repeats of 3 CVs. The Akaike information criteria (AIC) score was computed for each regression models using the 'AICcmodavg' package in R [45]. The AIC weights were then calculated for each of the 100 regression models based on the regression model with the lowest AIC score. The DAT values corresponding to the regression models with an AIC weight of fewer than 1.0 units were considered the optimum time window for the UAV flights. The single-day regression models that fall in this criterion are considered the models that can best estimate the target variable, grain yield. A smoothing method, namely, LOESS (locally weighted scatterplot smoothing), in the 'ggplot2' [46] package in R was used to determine the trend

in the single-day regression series. In this smoothing method, the R^2 for a single-day regression was recalculated based on the R^2 values of the nearby R^2 data points. The nearby data points were set at 50% of the total R^2 data points.

3. Results

3.1. Relationship of AGB and LAI with Grain Yield

Five rice cultivars with different architectures and heading timings were used in this study and grown at different fertilizer levels to ensure diversity in the data. The AGB, LAI, and grain yields differed between the five rice cultivars on a hill basis (Figures 3 and 4), suggesting that the grain yield prediction model for each cultivar is reasonable. In 2020, there were no significant varietal differences in AGB as observed from the high AGB variability within a cultivar while in 2021, varietal differences in AGB were observed with less AGB variability within a cultivar. On the other hand, the AGB between cultivars in the fertilizer trial showed similar AGB variability patterns in both years. AGB was also higher in the fertilizer trial compared to the trial with no fertilizer, regardless of years.

The range of LAI values per growth stage was similar among cultivars in the fertilizer trial except with Aichinokaori in 2020 and Nakate Shinsenbon in 2021 (Figure 3 e, f). Higher LAI values were observed among cultivars in 2020 than in 2021. LAI measured from the fertilizer trial was also higher than in the trial with no fertilizer. Higher LAI variability within a cultivar was also observed in the fertilizer trial, especially, at later growth stages (Figure 3 g, h).

Grain yields across cultivars showed slight variation in the trial with no fertilizer compared to grain yields in the fertilizer trial. In 2020, Aichinokaori had a lower grain yield than Hatsushimo and Nikomaru while in 2021, Hatsushimo had a higher grain yield than Nakate Shinsenbon. Aichinokaori had the lowest grain yield across trials and years (Figure 4 a–d).

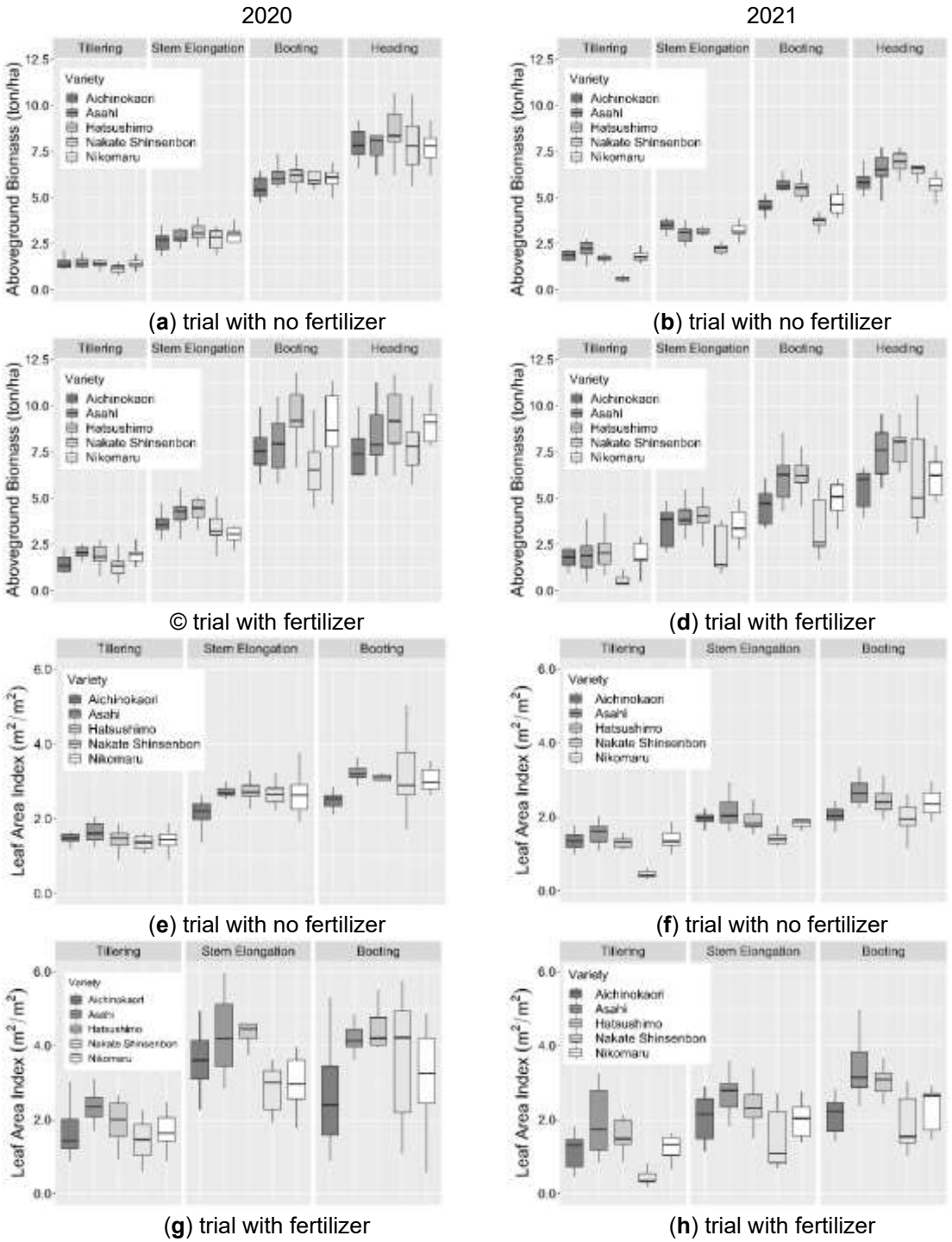

(**a**) trial with no fertilizer (**b**) trial with no fertilizer

© trial with fertilizer (**d**) trial with fertilizer

(**e**) trial with no fertilizer (**f**) trial with no fertilizer

(**g**) trial with fertilizer (**h**) trial with fertilizer

Figure 3. Aboveground biomass (ton/ha) of five cultivars grown in 2020 and 2021 in the (**a**, **b**) trial with no fertilizer and (**c**, **d**) trial with fertilizer. Leaf area index (m^2/m^2) of five cultivars grown in 2020 and 2021 in the (**e**, **f**) trial with no fertilizer and (**g**, **h**) trial with fertilizer.

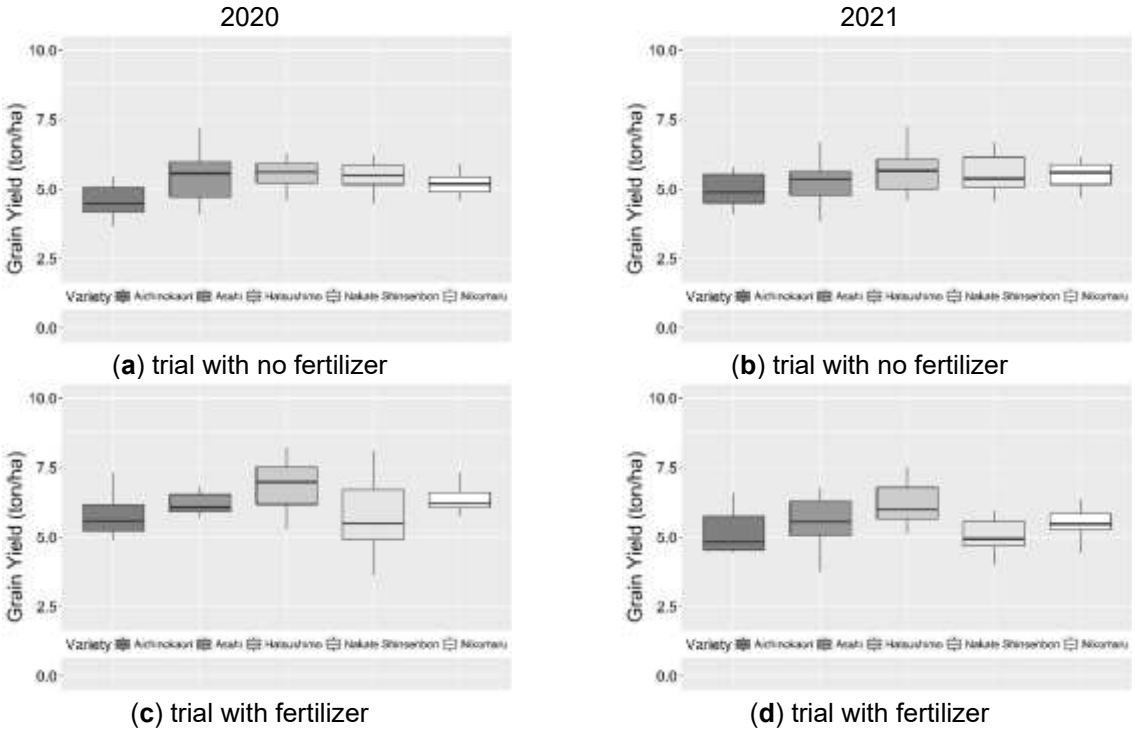

(**a**) trial with no fertilizer (**b**) trial with no fertilizer

(**c**) trial with fertilizer (**d**) trial with fertilizer

Figure 4. Grain yield (ton/ha) of five rice cultivars grown in 2020 and 2021 in the (**a**, **b**) trial with no fertilizer and (**c**, **d**) trial with fertilizer.

Simple linear regression modeling between grain yield and the actual AGB and LAI was conducted to determine the varietal difference and establish a baseline for predicting grain yield by AGB and LAI. Grain yield could be predicted using the actual AGB and LAI by accounting for the 19.0 to 53.0% variation in the grain yield (Figure 5). In this study, grain yield could be optimally predicted from the actual AGB and LAI at the stem elongation stage for all the cultivars used except Nikomaru in this study. From these results, it may be possible to develop a model to estimate yield using LAI and AGB at a particular timing.

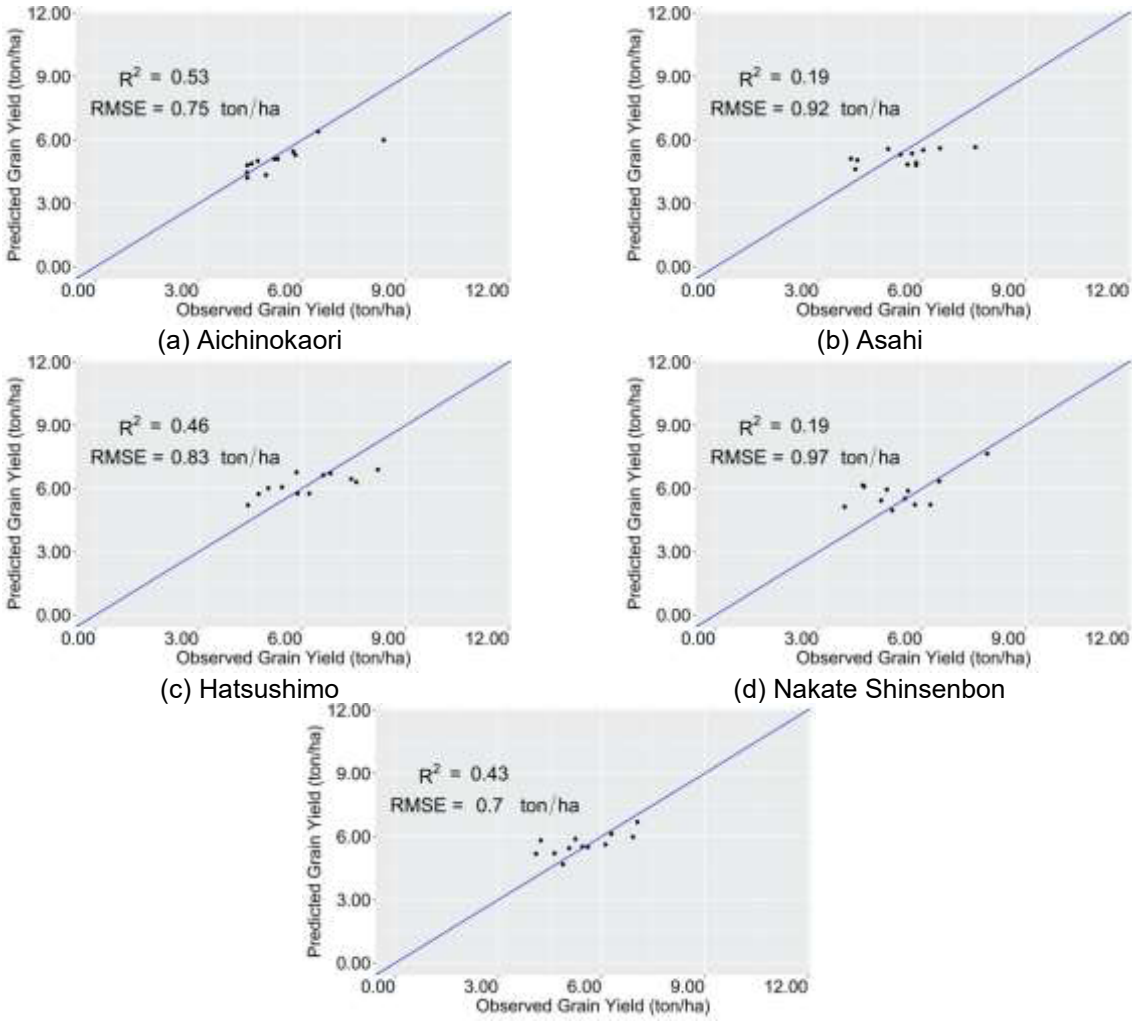

Figure 5. Model validation of the linear regression model between grain yield and actual AGB and LAI of the five rice cultivars — (**a**) Aichinokaori, (**b**) Asahi, (**c**) Hatsushimo, (**d**) Nakate Shinsenbon, and (**e**) Nikomaru, at the optimum growth stage. The optimum growth stage was determined by selecting the growth stage corresponding to the simple linear model that resulted in the lowest RMSE in the model validation. Cultivars Aichinokaori, Asahi, Hatsushimo, and Nakate Shinsenbon were optimally predicted at the stem elongation stage, while Nikomaru was optimally predicted at the tillering stage.

3.2. AGB and LAI Estimation

Based on the results of the yield estimation model using the actual LAI and AGB, it was thought that LAI and AGB could be used for yield estimation. For the estimation of LAI and AGB using UAVs, a model was developed to estimate AGB and LAI from VIs obtained from the flights.

In this study, 24 VIs were calculated from reflectance images, but since there were too many to include all of them in the XGBoost model to estimate LAI and AGB, VIs were selected to be used as explanatory variables. To select the VIs for AGB and LAI estimation modeling, a correlation analysis was performed between AGB, LAI, and VIs (Tables A2 and A3). The AGB of Nakate

Shinsenbon had the highest range of the top ten (10) correlated VIs (R^2: 0.772–0.806), followed by the AGB of cultivar Nikomaru (R^2: 0.679–0.752). Medium levels of correlation were found between the VIs and AGB of cultivars Asahi (R^2: 0.538–0.698) and Aichinokaori (R^2: 0.528–0.621). The AGB of cultivar Hatsushimo showed the lowest correlation (R^2: 0.447–0.631) (Table A2).

The LAI was positively correlated with the different VIs (Table A3). The correlation coefficient of the top ten (10) VIs highly correlated with the LAI of Nakate Shinsenbon ranged from 0.772 to 0.818 in R^2. Medium levels of correlation were found for Asahi (R^2: 0.681–0.805), Hatsushimo (R^2: 0.665–0.810), and Nikomaru (R^2: 0.609–0.707). Aichinokaori had the lowest correlation (R^2: 0.553–0.674).

Using the top ten (10) correlated VIs indicated in Tables A2 and A3, an AGB and LAI estimation model was developed using XGBoost. The different hyperparameters of the XGBoost model were tuned to obtain the optimum estimation for each cultivar (Tables A4 and A5). For some select cultivars, the AGB and LAI estimation models tuned using the lowest RMSE selection method showed decreased prediction performance when evaluated using the test data (Table 2, Figures 6, and 7). The AGB estimation model for Hatsushimo and the LAI estimation models for Asahi, Hatsushimo, and Nakate Shinsenbon showed a lower R^2 when estimating the target variables in the test dataset. A higher number of feature variables per tree and depth of trees may result in an estimation model that finds patterns particular to the sample used for building the prediction, resulting in overfitting (Tables A4 and A5).

In contrast, LAI estimation models that used 50% of the feature variables, and regression tree depths of five and three did not show overfitting: AGB estimation models for Aichinokaori, Asahi, Nakate Shinsenbon, and Nikomaru, and LAI estimation models for Aichinokaori and Nikomaru.

Table 2. R^2 and RMSE results of the cross-validated estimation model for aboveground biomass (ton/ha) and leaf area index (m^2/m^2) using XGBoost models.

Cultivar	Aboveground Biomass (Ton/ha)				Leaf Area Index (m^2/m^2)			
	Training Result		Test Result		Training Result		Test Result	
	R^2	RMSE	R^2	Normalized RMSE	R^2	RMSE	R^2	Normalized RMSE
Aichinokaori	0.66 ± 0.07	1.43	0.78	0.26	0.46 ± 0.05	0.65	0.71	0.20
Asahi	0.67 ± 0.07	1.50	0.66	0.29	0.85 ± 0.09	0.48	0.57	0.29
Hatsushimo	0.72 ± 0.07	1.54	0.56	0.36	0.84 ± 0.08	0.61	0.65	0.27
Nakate Shinsenbon	0.85 ± 0.09	1.24	0.83	0.29	0.82 ± 0.08	0.56	0.63	0.39
Nikomaru	0.75 ± 0.07	1.21	0.80	0.25	0.55 ± 0.05	0.65	0.73	0.22

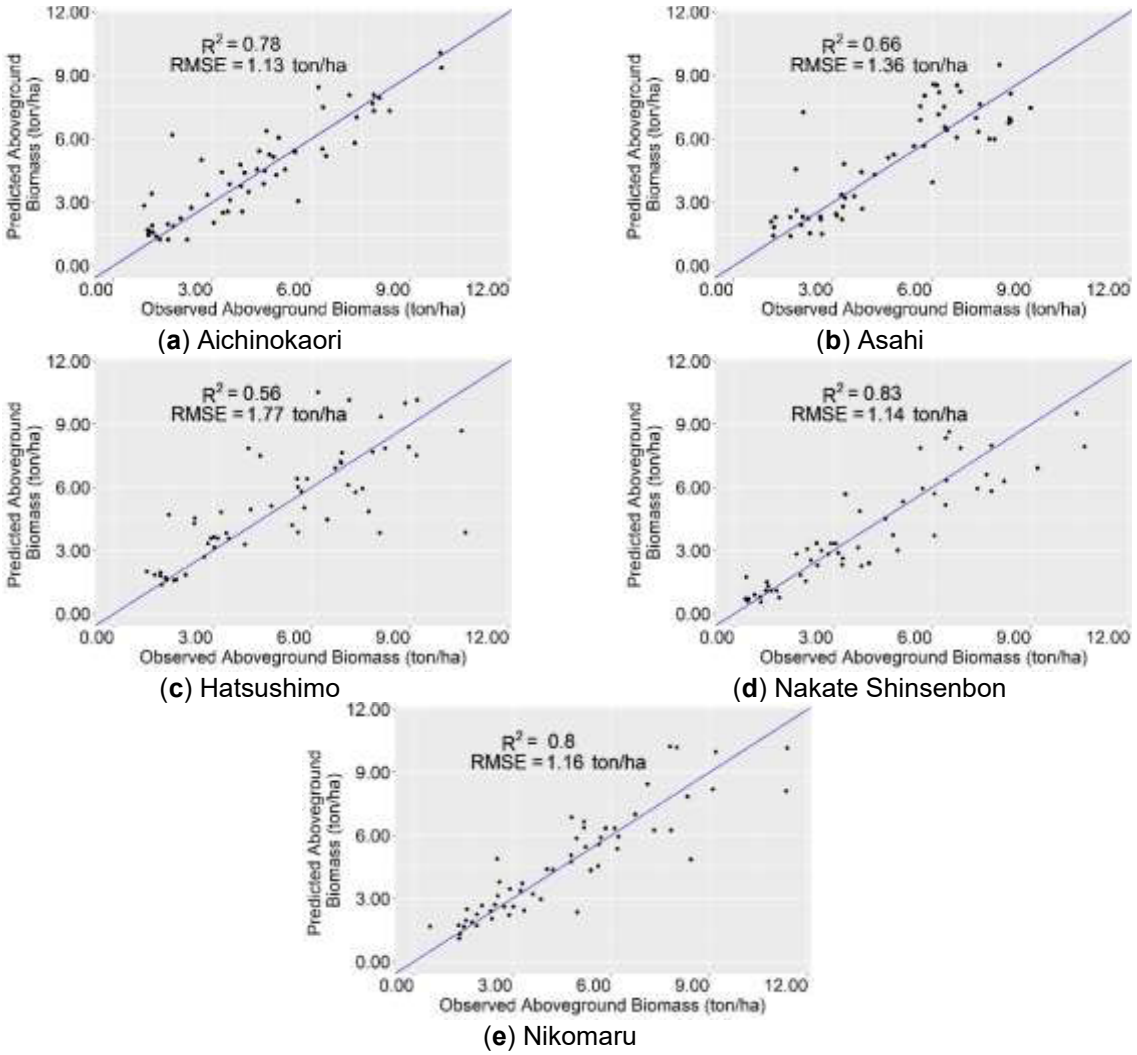

(**a**) Aichinokaori (**b**) Asahi

(**c**) Hatsushimo (**d**) Nakate Shinsenbon

(**e**) Nikomaru

Figure 6. Model evaluation of AGB estimation model using the test dataset for cultivars (**a**) Aichinokaori, (**b**) Asahi, **(c)** Hatsushimo, (**d**) Nakate Shinsenbon, and (**e**) Nikomaru.

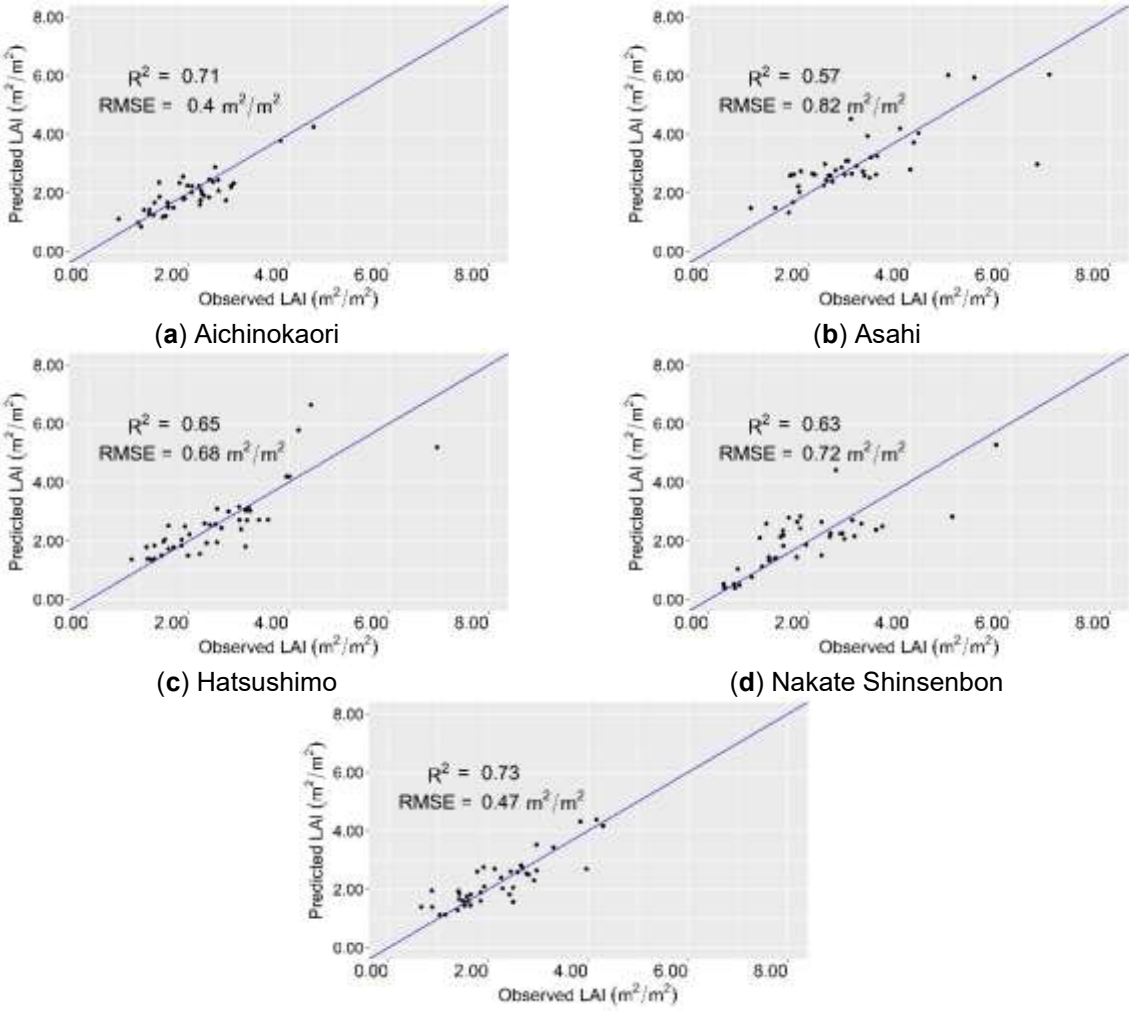

Figure 7. Model evaluation of LAI estimation model using the test dataset for cultivars (**a**) Aichinokaori, (**b**) Asahi, (**c**) Hatsushimo, (**d**) Nakate Shinsenbon, and (**e**) Nikomaru.

The XGBoost model has a variable importance computation that summarizes the feature variables' level of influence on the training process to predict AGB and LAI based on the parameter gain of a feature variable in the prediction process. The parameter gain measures the relative contribution of a feature variable in a tree created in the model. A higher gain value of a feature close to other features indicates that the former feature is more critical in the prediction. The relative importance of the correlated VIs in the AGB estimation models for each cultivar was calculated (Figure 8). All of the feature variables used in the training of the XGBoost model were significantly correlated with AGB, with varying correlations (Table A2).

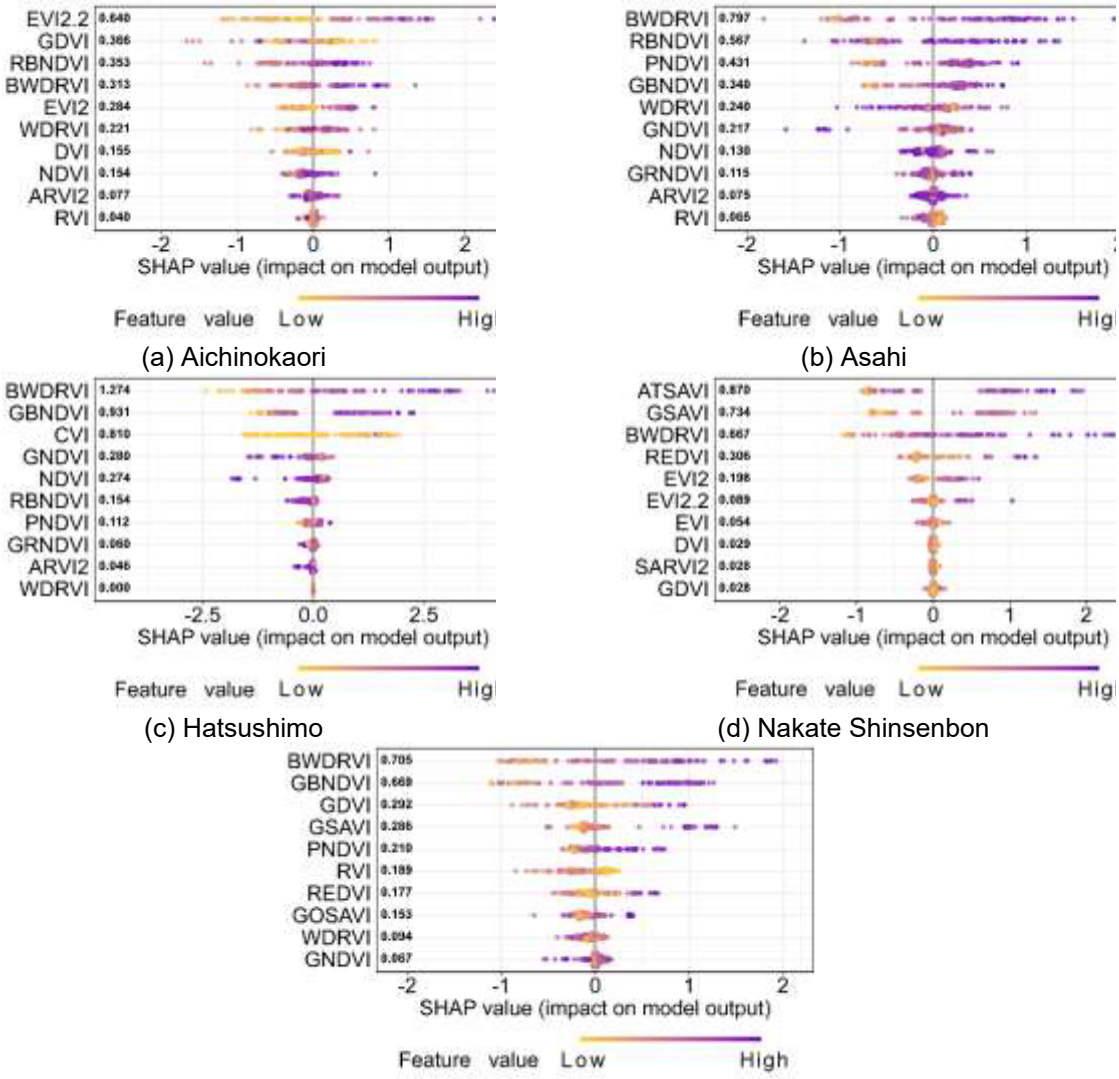

Figure 8. Variable importance in the AGB estimation model for cultivars (a) Aichinokaori, (b) Asahi, (c) Hatsushimo, (d) Nakate Shinsenbon, and (e) Nikomaru.

Comparing the levels of correlation of VIs to the levels of importance in the XGBoost model showed a difference in trend. There were VIs with a medium correlation with AGB, but they showed the highest level of importance in the XGBoost model. In particular, the variable importance of the AGB estimation model for Aichinokaori showed that EVI2.2 was the essential feature in the prediction (Figure 8a). Likewise, the variable importance of the AGB estimation model for Nakate Shinsenbon showed that ATSAVI was the most crucial feature in the prediction model (Figure 8d) but was the least correlated VI with AGB among the ten VIs (Table A2) used in the training process. However, it should be noted that this difference in feature ranking was compensated by making the most correlated VIs the second most important feature in XGBoost, as seen in the variable importance of

the AGB estimation models for Asahi, Hatsushimo, and Nikomaru. Nevertheless, the variable importance of the AGB estimation models for other cultivars such as Asahi, Hatsushimo, and Nikomaru showed that BWDRVI was the essential feature, which was also the VI most correlated with AGB (Table A2). The SHAP values of the AGB estimation models show that at least four feature variables per estimation model did not influence the prediction.

The variable importance in the LAI estimation model for each cultivar is shown in Figure 9a–e. The topmost vital features in the training process of the LAI estimation models were the VIs in the middle in the order of ascending correlation with LAI. The least correlated VIs also ranked the lowest in variable importance, such as GRNDVI in the estimation model for Hatsushimo and NDVI in the estimation model for Nikomaru. Similar to the AGB estimation models, the most correlated VIs were the second most important feature in the variable importance for the LAI estimation model.

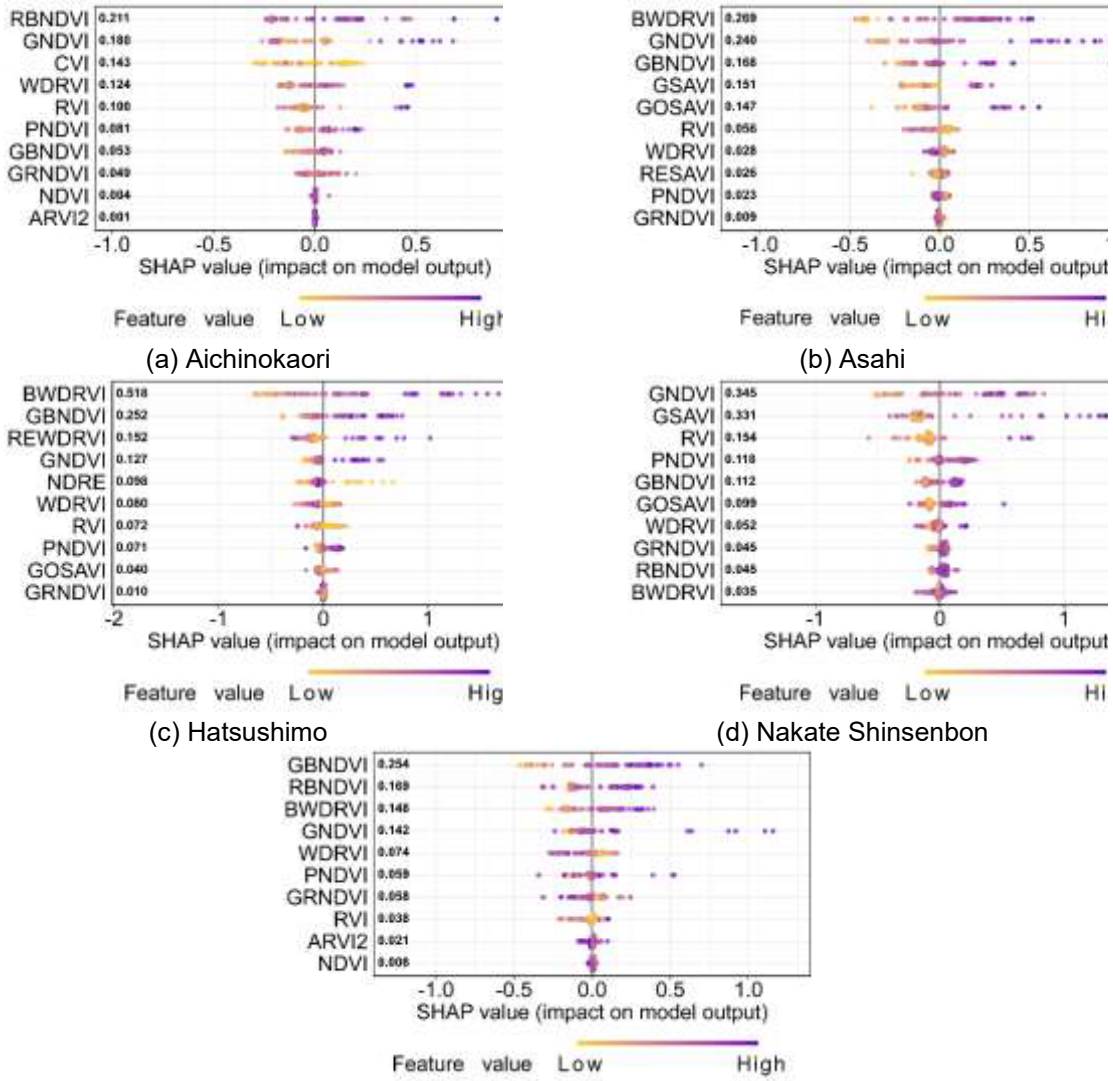

Figure 9. Variable importance in the LAI estimation model for cultivars (a) Aichinokaori, (b) Asahi, (c) Hatsushimo, (d) Nakate Shinsenbon, and (e) Nikomaru.

3.3. VI-Estimated AGB and LAI Fitted to the Gompertz Growth Curve

Aerial photography by UAV flights was conducted once a week until heading, and by using the reflectance data and the estimation model described above, it is possible to estimate changes in AGB and LAI for each rice cultivar over the growing season. The estimated AGB and LAI of each flight day were fitted to the Gompertz growth curve (Figures 10 and 11). Although the pattern of growth varied by year and fertilizer conditions, the relative growth trends for each cultivar were common. In our study, Hatsushimo was the fastest growing cultivar, with relatively high AGB and LAI at 85 DAT. At the same time, Nikomaru was the slowest growing cultivar, with a low AGB and LAI at the early growth stage. To evaluate the accuracy of the estimation and curve fitting, the estimated AGB and

LAI values for each cultivar, year, and trial were compared to the actual values of AGB at the heading stage and LAI at the booting stage. Based on this comparison, the highest accuracy for AGB estimation was observed in Nikomaru, while the lowest accuracy was observed in Asahi. The estimation for LAI across years and trials showed that the highest accuracy was observed in Asahi, and the lowest accuracy was observed in Hatsushimo (data not shown).

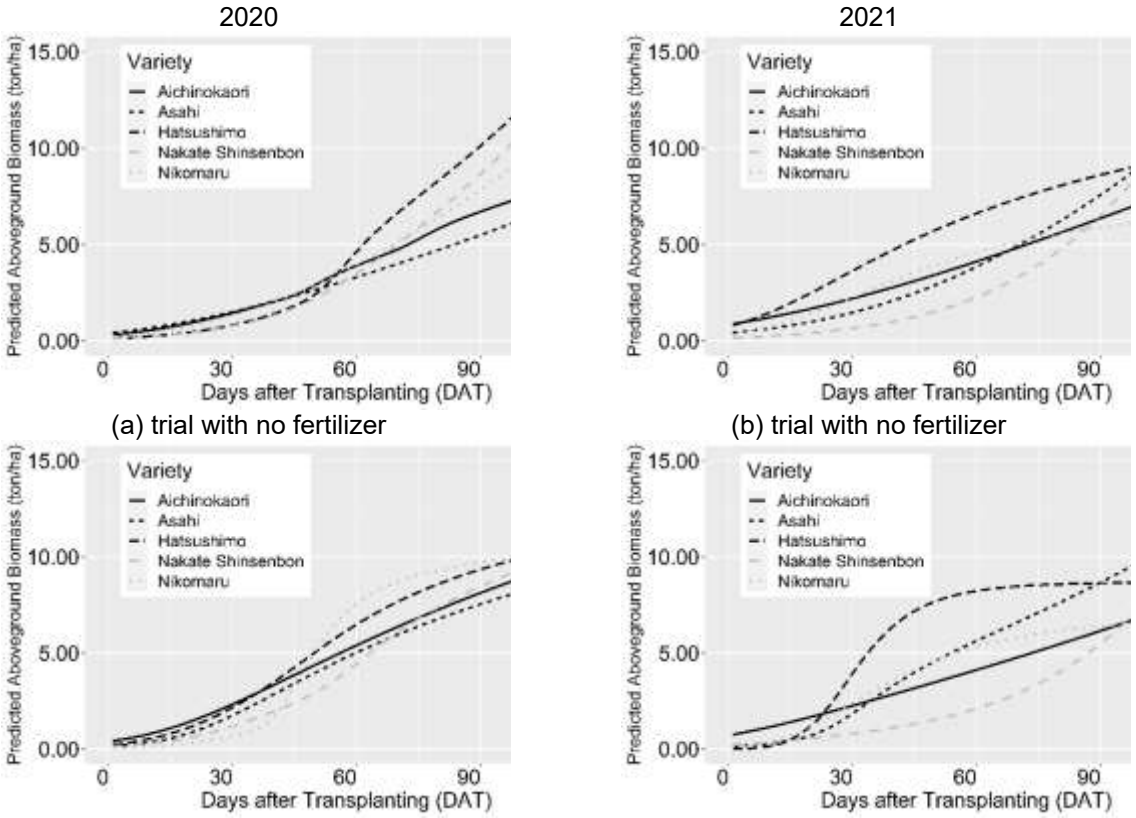

(a) trial with no fertilizer (b) trial with no fertilizer

(c) trial with fertilizer (d) trial with fertilizer

Figure 10. Estimated aboveground biomass (ton/ha) of five cultivars grown in 2020 and 2021 in the trial with no fertilizer (a, b) and trial with fertilizer (c, d).

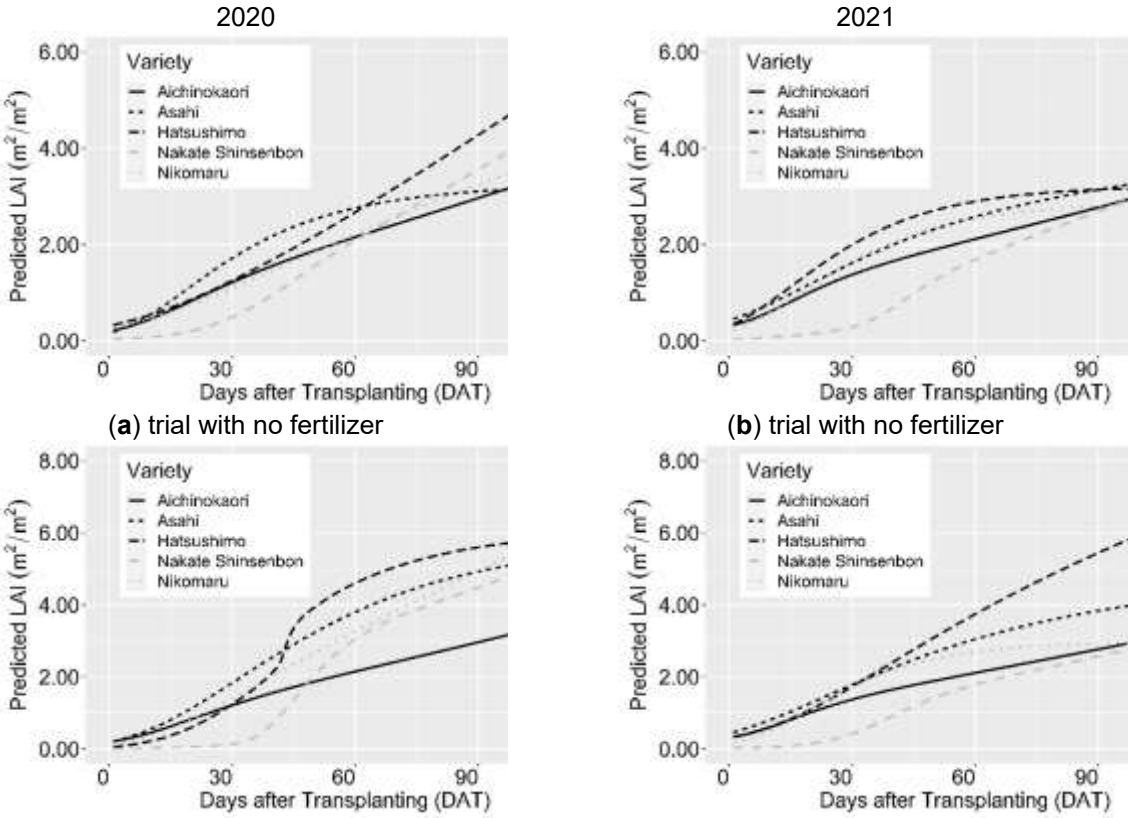

(**a**) trial with no fertilizer (**b**) trial with no fertilizer

(**c**) trial with fertilizer (**d**) trial with fertilizer

Figure 11. Estimated leaf area index (m^2/m^2) of five cultivars grown in 2020 and 2021 in the trial with no fertilizer (a, b) and trial with fertilizer (c, d).

3.4. Grain Yield Prediction Using VI-Estimated AGB and LAI

To identify the best time of year for UAV yield estimation, the linear regression between grain yield and VI-estimated AGB and LAI per day which fitted into the Gompertz growth curve was established for each cultivar on daily basis. A repeated k-fold cross-validation was performed to determine the regression function of the VI-estimated AGB and LAI per day for grain yield (Figure A1a–e, Figure 12). In the case of the linear regression with no parameter tuning, the mean R^2 values were also the R^2 of the final model for each single-day regression.

Using the VI-estimated AGB and LAI, the RMSE of grain yield prediction across cultivars varied throughout the growth period, and the lowest RMSE values were observed at same DAT of the highest R^2 peak (Figures 12 and A1 a-e). However, the strength of the grain yield prediction differed between cultivars. The VI-estimated AGB and LAI could explain only 10% and 30% of the grain yield variation for cultivars Aichinokaori and Hatsushimo, and 40–50% for Asahi, Nakate Shinsenbon, and Nikomaru. The optimum time window for UAV flights was 42–87 DAT without

referring to the actual growth stage dates observed in the study. Correspondingly, the RMSE values in these periods (25, 35, and 85 DAT) were also relatively higher but the RMSE values did not fluctuate strongly compared to the R^2 series, particularly in cultivars Aichinokaori and Asahi (Figure A1 a, b). In contrast, Hatsushimo and Nikomaru had a wide range of RMSE values (0.74 – 1.66 ton/ha and 0.46 – 1.16 ton/ha, respectively) which makes the determination of the optimum time window necessary for accurate grain yield prediction.

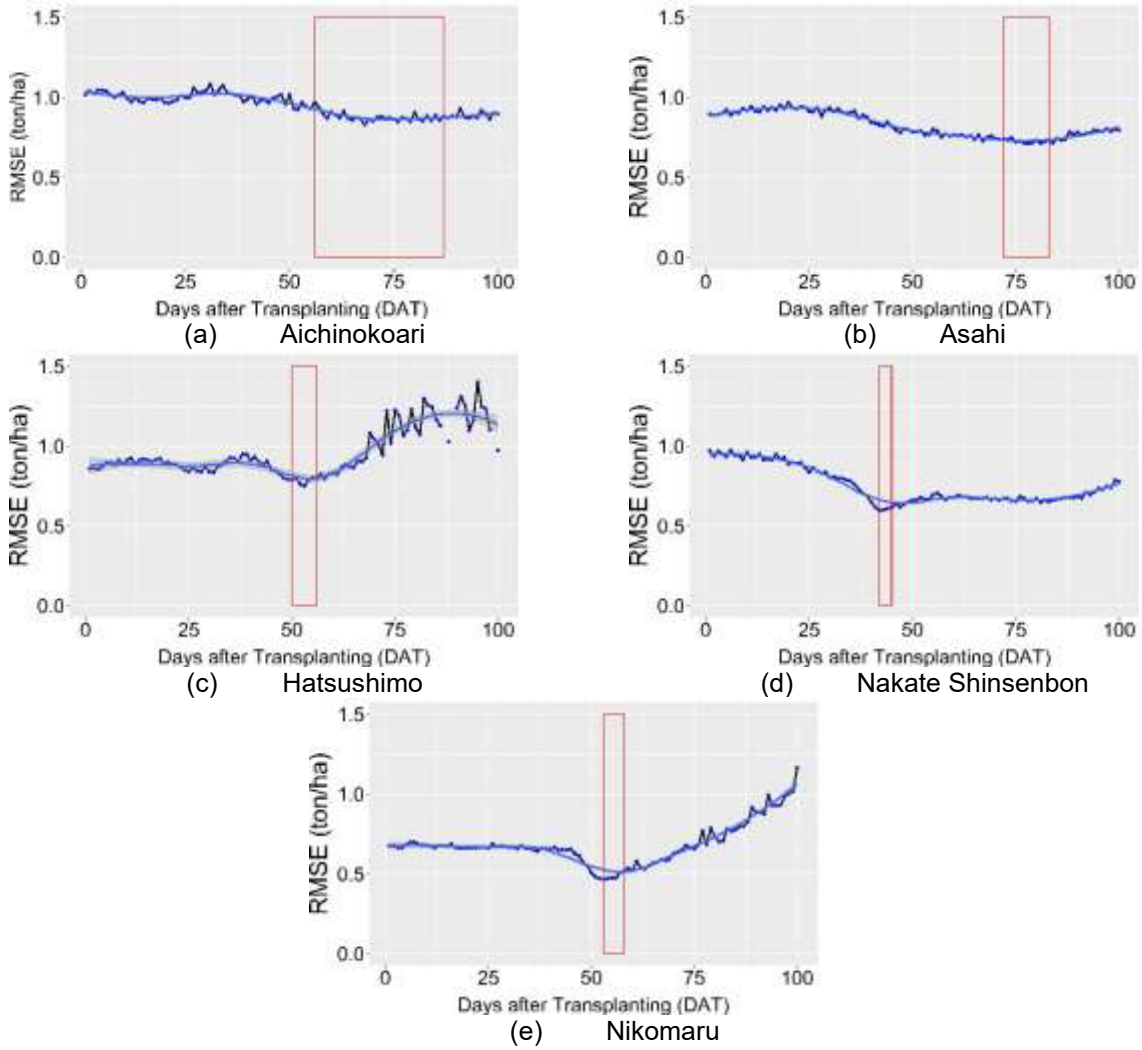

Figure 12. RMSE result of the training dataset of the single-day regression model between grain yield and VI-estimated AGB and LAI of the five rice cultivars. The red box indicates the optimum time window for UAV flights as determined from the AIC score comparison. The black line indicates the mean RMSE values from the repeated k-fold cross-validation conducted for each single-day regression. The darker blue line indicates the smoothed RMSE values that can be expected from the plotted RMSE series derived from the repeated k-fold cross-validation. The smoothed RMSE values were determined by using the LOESS (locally weighted scatterplot smoothing) method. The lighter blue region indicates the range of smoothed RMSE values to be expected 95% of the time from each single-day regression. (a) Aichinokaori; (b) Asahi; (c) Hatsushimo; (d) Nakate Shinsenbon; (e) Nikomaru.

Using the AIC, the optimum single-day regression model can be determined for each cultivar by calculating the AIC weights. The DAT values whose AIC weights are less than 1.0 units are considered the optimum time window for the UAV flight (Figure 12). Concerning the growth stage dates in the 2020 and 2021 rice seasons, the training process showed that the cultivars had different optimum time windows. For Aichinokaori, the optimum time window was 57–87 DAT, corresponding to the stem elongation to heading stages. The optimum time window was observed at 72–83 DAT for Asahi, coinciding with the stem elongation to booting stages. For Hatsushimo, the optimum time

window was 50–56 DAT, corresponding to the stem elongation stage. Nakate Shinsenbon's optimum time window was 42–45 DAT, coinciding with the stem elongation stage. For Nikomaru, the optimum time window was 53–58 DAT, corresponding to the stem elongation stage.

The independent test dataset evaluated the prediction models corresponding to the optimum time windows (Figure 13 a–e). The results show that prediction models corresponding to the optimum time window for cultivars Asahi and Nikomaru did not generalize well on the unseen dataset in R^2. The grain yield prediction model for Nakate Shinsenbon performed better than the previous two cultivars (RMSE = 0.52 ton/ha). On the other hand, a prediction model for cultivar Hatsushimo showed a better performance compared to the other cultivars. The prediction model for Aichinokaori at a later optimum time window showed a good prediction performance (RMSE = 0.61 ton/ha). Asahi was found to have a higher RMSE in the independent test dataset and the prediction error (RMSE = 1.04 ton/ha) was two times higher than the prediction error of the other cultivars.

The difference between the result of the training dataset and the independent test dataset in the single-day regression model were attributed to the following factors: (1) the k-fold cross validation method that we employed and (2) the prediction errors that were carried over by the AGB/LAI estimation models and the Gompertz growth curve to the single-day regression model. The large reduction of R^2 from the training dataset (optimum time graph) to the independent test dataset might be due to the low sampling size of the independent test dataset

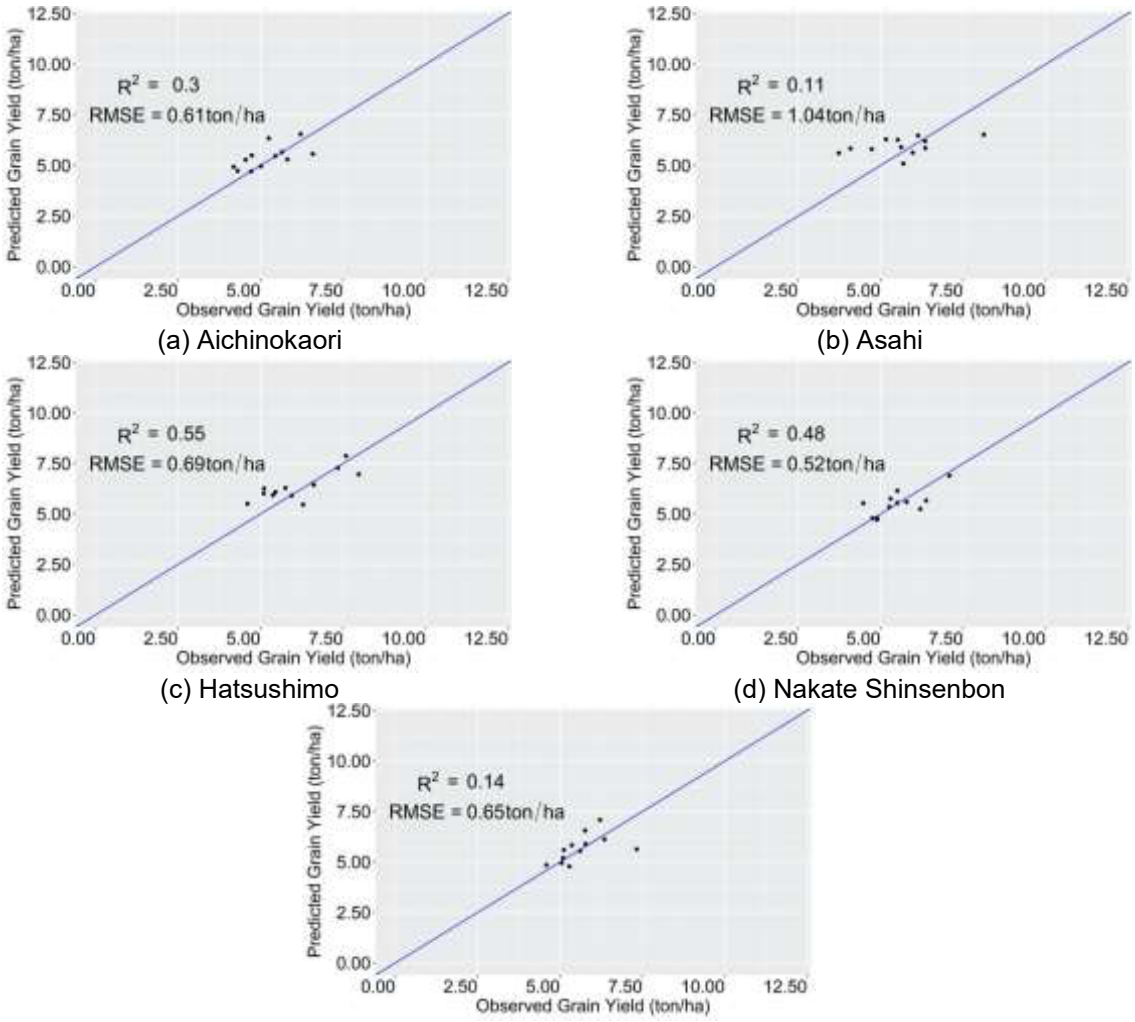

(a) Aichinokaori

(b) Asahi

(c) Hatsushimo

(d) Nakate Shinsenbon

(e) Nikomaru

Figure 13. Model evaluation of the optimum single-day regression model using the test dataset between grain yield and VI-estimated aboveground biomass and leaf area index of the five rice cultivars, (a) Aichinokaori, (b) Asahi, (c) Hatsushimo, (d) Nakate Shinsenbon, and (e) Nikomaru.

4. Discussion

Based on the research results, we developed a model to estimate AGB and LAI based on the reflectance obtained from UAV flights (Figures 6 and 7) and to provide the optimal time window to fly UAVs for yield prediction using the AGB and LAI for five rice cultivars based on the AIC weight of the single-day regression models (Figures 12 and A1).

Although the relationship between the in-season AGB and grain yield is continuously studied and can be generalized, a higher grain yield has been observed in rice cultivars that produce AGB before the heading stage [47], while the opposite is true for other cultivars [48]. With this, the selection of cultivars and the timing of UAV flights are critical concerns in grain yield prediction. Thus, a grain yield prediction model for each tested cultivar was developed to determine if a similar optimum time window relative to the growth stage for UAV flights can be obtained for different rice cultivars (Figures 5 and 12). In this study, UAVs were used to estimate AGB and LAI, and the estimated values were used to search for suitable flight times for yield estimation.

To estimate the appropriate time for yield estimation using UAVs, we conducted yield estimation on a hill basis. Because the spatial arrangement of the leaves is different from that of the population as a plot, it is assumed that the reflectance obtained from the plant will be different from that obtained from the community. However, it is quite possible that the reflectance obtained from individual plants will show a similar trend to that of a community composed of plants of comparable growth.

In a previous study [23], the grain yield prediction model determined the correlated multi-temporal VIs calculated from the UAV-derived multispectral images and employed a multi-linear regression model to predict grain yield. The same research also observed that VIs correlated with LAI were good predictors of grain yield. However, an LAI estimation model from these correlated VIs was not developed. The results from that study showed that the optimum times for UAV flights were as follows: combined UAV flights at the booting and heading stages, and combined UAV flights at the jointing and booting stages. Another study [22] used the field estimated AGB and leaf chlorophyll content (LCC) to predict grain yield. The results showed that destructive AGB sampling can predict grain yield, with the R^2 ranging from 0.69 to 0.75. The same paper used VIs and UAV-derived canopy structural information such as canopy height to predict the rice grain yield.

The previous research above showed that actual plant parameters, such as AGB and LAI, and the VIs derived from UAVs are feasible for grain yield prediction. This study investigated the relationship between AGB, LAI, VIs, and grain yield, and AGB and LAI estimation models were developed (Figures 6 and 7). Then, the AGB and LAI estimates were simulated using the Gompertz growth curve to see the AGB and LAI dynamics (Figures 10 and 11). These dynamics were then examined for their relationship with grain yield to determine the optimum time where these estimates can predict grain yield.

Considering the linear relationship of the selected VIs with the AGB and LAI of the five cultivars, several remarks about the model establishment were made (Tables A2 and A3). Using VIs with a smaller range of correlation coefficient values at a high level of correlation with the target variable can result in a better model accuracy than using VIs with a smaller range of correlation coefficient values at a medium level of correlation with the target variable. This was shown by comparing the AGB estimation model for Nakate Shinsenbon with that of Aichinokaori and Asahi, and the LAI estimation for Nakate Shinsenbon with that of Aichinokaori. VIs with a broader range of correlation values at medium to low levels of correlation with the target variable can result in a similar or better model accuracy than VIs with a smaller range of correlation coefficient values. The LAI estimation model for Hatsushimo was better than the LAI estimation model for Nikomaru.

Before the XGBoost model training for AGB and LAI estimation, feature selection was conducted using correlation analysis to determine feature variables—VIs — that linearly correlated with AGB and LAI (Tables A2 and A3). Even though some cultivars had similar correlated VIs, no two had the same set of correlated VIs. Among the VIs used in the AGB estimation models of the different cultivars, BWDRVI was the most common highly correlated VI. In past research, BWDRVI has provided good contrast between soybean soil and plant leaves at the maturity stage [49]. Other correlated VIs observed in this study confirm the findings of previous research in rice AGB estimation, where modified normalized vegetation indices showed a high correlation with AGB [50]. On the other hand, the LAI of the five rice cultivars also showed a high correlation with the modified normalized difference vegetation indices. A similar research result has been observed between the LAI of rice and VIs such as GBNDVI and GNDVI [51]. Like the previous research, this study also shows that

GBNDVI and GNDVI were more correlated with LAI than NDVI. The correlation analysis to select VIs for AGB and LAI estimations seemed reliable and reasonable.

The AGB and LAI can be estimated with good model accuracy using XGBoost (Table 2). Previous research on the estimation of aboveground forest biomass showed that the random forest algorithm (R^2 = 0.71) works better than stochastic gradient boosting (R^2 = 0.60) [52]. In this study, the model evaluation using test datasets of the XGBoost models for AGB estimation resulted in an R^2 ranging from 0.565 to 0.827. For the LAI estimation models, this resulted in an R^2 ranging from 0.574 to 0.727. Comparing the model performances between the AGB estimation and LAI estimation in this study shows that AGB estimation models had better accuracy than LAI estimation models. Using the UAV-derived VIs, AGB estimation models showed less overfitting than LAI estimation models (Table 2).

XGBoost and stochastic gradient boosting utilize the gradient descent method to find the minimum cost function for predicting the target. However, the XGBoost algorithm has regularization as one of its booster parameters, which prevents the overfitting of prediction models (Tables A4 and A5). The AGB estimation model for Hatsushimo used 90% of the feature variables to build regression trees, as represented by the booster parameter colsample_bytree. On the other hand, LAI estimation models for Asahi, Hatsushimo, and Nakate Shinsenbon had higher depths of regression trees at 10. A higher number of feature variables per tree and depth of trees may result in an estimation model that finds patterns particular to the sample used for building the prediction, resulting in overfitting. Much earlier research conducted in remote sensing for AGB and LAI estimation demonstrated that AGB estimation is more suited to remote sensing than LAI estimation [53]. Nevertheless, comparing the NRMSE results of the test dataset showed that all the AGB and LAI estimation models of the five cultivars had good levels of model accuracy (Table 2). Moreover, the variable importance shown through the SHAP plots indicates that boosting the ensemble algorithm can be an excellent strategy to predict AGB and LAI when variation in correlations between the VIs and target exists in the training process (Figures 8 and 9).

After the AGB and LAI estimation, each cultivar's grain yield prediction model was developed using the VI-estimated AGB and LAI fitted into the Gompertz growth curve (Figures 10 and 11). Comparing the accurate estimations of the growth curve fitted, AGB and LAI estimates from the

NRMSE of the AGB and LAI estimation models showed a difference in varietal performance (data not shown). Cultivars Aichinokaori and Nikomaru had higher accuracy in the test dataset than in the datasets from the growth curve fitting. In contrast, cultivars Asahi and Nakate Shinsenbon had higher accuracy in the dataset from the growth curve fitting than in the test dataset. The cultivar Hatsushimo showed the lowest accuracy for both datasets.

Using the single-day VI-estimated AGB and LAI simulated from the growth curve, a single-day regression was conducted to predict grain yield. The optimum time window for UAV flights was determined indicating good model accuracy based on the AIC weights (Figures 12 and A1). Cultivars such as Asahi, Hatsushimo, and Nakate Shinsenbon had optimum time windows at the stem elongation stage. Aichinokaori had an optimum time window at the initial heading stage, while Nikomaru had an optimum time window at the tillering stage. A similar optimum growth stage was observed in the grain yield prediction model using the actual AGB and LAI (Figure 5a–e), except for Aichinokaori, which could be predicted at the stem elongation stage using the actual AGB and LAI, or at the later growth stage using the VI-estimated AGB and LAI.

By evaluating the performances of single-day regression models using the VI-estimated AGB and LAI (Figures 13 a-e) and the grain yield prediction using the actual AGB and LAI (Figures 5 a-e) on an independent test dataset, the following results were observed: (1). —the grain yields of cultivars Hatsushimo and Nakate Shinsenbon were better predicted using the VI-estimated AGB and LAI; (2) the grain yield prediction of cultivars Aichinokaori and Nikomaru were better using the actual AGB and LAI, and (3) the grain yield prediction of cultivar Asahi could not be predicted well by either VI-estimated AGB and LAI or the actual AGB and LAI. These results show that using AGB and LAI was not sufficient enough to accurately predict the rice grain yield for the all cultivar (e.g. Asahi).

Concerning each cultivar's AGB and LAI estimations (Table 2), the accurate time window for UAV flights to predict grain yield could be determined. However, the percent variation in grain yield that can be explained still depends on the correlation of the VIs with AGB and LAI and the robustness of the machine learning algorithm. The optimum time windows determined in this study are consistent with previous studies for the pre-heading to initial heading stages [22, 26], and our results suggest that the lengths of the optimal time windows for each cultivar differed from 4 to 31 days (Figures 12 and A1). In practical terms, a longer optimum time window for UAV flights is an advantage as flight

days will be flexible. A shorter time window will make UAV flights a time-constraint, especially in cases where unfavorable weather conditions prevent UAV flights.

This study shows that a robust boosting ensemble machine learning algorithm—in this case, XGBoost can be used to estimate agronomic traits, namely, AGB and LAI. Then, using the developed estimation models, AGB and LAI can be calculated using the UAV-derived reflectance data gathered during the entire growth period. The estimated AGB and LAI throughout the growth period determined the optimum time window for the UAV flights. The simulated VI-estimated AGB and LAI dynamics allowed for grain yield prediction at any point throughout the growth period. This method will enable researchers to save resources and time for numerous UAV flights to predict grain yield from UAV-derived reflectance data.

5. Conclusion

The aims of this study were to (1) predict rice yield by using the estimated aboveground biomass (AGB) and leaf area index (LAI) until the heading stage from vegetation indices (VIs), and (2) determine the optimal sensing time in estimating AGB and LAI using VIs for yield prediction.

The AGB and LAI estimation models from the VIs using the XGBoost algorithm resulted in an R^2 ranging from 0.565 to 0.827 and 0.574 to 0.727, respectively, and the VI-estimated AGB and LAI predicted grain yield better than the actual AGB and VI for cultivars Hatsushimo and Nakate Shinsenbon (RMSE: 0.69 ton/ha and 0.52 ton/ha, respectively). The actual AGB and LAI predicted grain yields of Aichinokaori and Nikomaru (RMSE: 0.75 ton/ha and 0.7 ton/ha, respectively) better than the VI-estimated AGB and LAI while the grain yield of Asahi could not be predicted well by both methods. The optimum time window for UAV flights was at the stem elongation stage for cultivars Asahi, Hatsushimo, and Nakate Shinsenbon and at the initial heading stage for Aichinokaori ranging from 4 to 31 days.

These results indicate that the accuracy of rice grain yield estimation using the VI-s estimated AGB and LAI and the suitable period for yield estimation are cultivar dependent. On the other hand, due to the small number of cultivars tested in this study, it is not clear whether this model specificity is due to differences in plant architecture and panicle traits. Further research should be conducted on multiple cultivars using these UAV-derived features to develop a generalized yield estimation model that is tolerant of differences among rice cultivars.

5. Appendix

Table A1. List of vegetation indices used in the study.

Vegetation Index	Formula	References
Atmospherically Resistant Vegetation Index 2 (ARVI2)	$-0.18 + 1.17[(NIR - R) / (NIR + R)]$	[54]
Adjusted Transformed Soil Adjusted VI (ATSAVI)	$a[(NIR - a \times R - b) / (a \times NIR + R - a \times b + X(1 + a^2))]$	[55]
Blue-Wide Dynamic Range Vegetation Index (BWDRVI)	$(0.1NIR - B) / (0.1NIR + B)$	[54]
Chlorophyll Vegetation Index (CVI)	$NIR \times (R/G^2)$	[56]
Difference Vegetation Index (DVI)	$NIR - R$	[23]
Enhanced Vegetation Index (EVI)	$2.5[(NIR - R) / ((NIR + 6R - 7.5B) + 1)]$	[57]
Enhanced Vegetation Index 2 (EVI2)	$2.4[(NIR - R) / (NIR + R + 1)]$	[58]
Enhanced Vegetation Index 2-2 (EVI2-2)	$2.5[(NIR - R) / (NIR + 2.4R + 1)]$	[59]
Green-Blue Normalized Difference Vegetation Index (GBNDVI)	$[NIR - (G + B)] / [NIR + (G + B)]$	[60]
Green Difference Vegetation Index (GDVI)	$NIR - G$	[61]
Green Normalized Difference Vegetation Index (GNDVI)	$(NIR - G) / (NIR + G)$	[62]
Green Optimal Soil Adjusted Vegetation Index (GOSAVI)	$(1 + 0.16) \times (NIR - G) / (NIR + G + 0.16)$	[63]
Green-Red Normalized Difference Vegetation Index (GRNDVI)	$[NIR - (G + R)] / [NIR + (G + R)]$	[61]
Green Soil Adjusted Vegetation Index (GSAVI)	$1.5(NIR - G) / (NIR + G + 0.5)]$	[64]
Normalized Difference Red-Edge (NDRE)	$(NIR - RE) / (NIR + RE)$	[65]
Normalized Difference Vegetation Index (NDVI)	$(NIR - R) / (NIR + R)$	[51]
Pan Normalized Difference Vegetation Index (PNDVI)	$[NIR - (G + R + B)] / [NIR + (G + R + B)]$	[66]
Red-Blue Normalized Difference Vegetation Index (RBNDVI)	$[NIR - (R + B)] / [NIR + (R + B)]$	[67]
Red Edge Difference Vegetation Index (REDVI)	$NIR - RE$	[68]
Red Edge Soil Adjusted Vegetation Index (RESAVI)	$1.5(NIR - RE) / (NIR + RE + 0.5)]$	[69]
Red Edge Wide Dynamic Range Vegetation Index (REWDRVI)	$(a \times NIR - RE) / (a \times NIR + RE)$ $(a = 0.12)$	[70]
Ratio Vegetation Index (RVI)	NIR/R	[71]
Soil and Atmospherically Resistant Vegetation Index 2 (SARVI2)	$2.5(NIR - R) / (1 + NIR + 6R - 7.5B)]$	[72]
Wide Dynamic Range Vegetation Index (WDRVI)	$(a \times NIR - R) / (a \times NIR + R)$ $(a = 0.12)$	[73]

R = red reflectance; G = green reflectance; B = blue reflectance; NIR = near infrared reflectance; RE = red-edge reflectance.

Table A2. Pearson correlation coefficient between aboveground biomass (ton/ha) and vegetation indices across growth stages.

	Aichinokaori	Asahi	Hatsushimo	Nakate Shinsenbon	Nikomaru
ARVI2	**0.569** ***	**0.538** ***	**0.531** ***	0.641 ***	0.586 ***
ATSAVI	0.499 ***	0.413 ***	0.319 ***	**0.779** ***	0.605 ***
BWDRVI	**0.621** ***	**0.698** ***	**0.631** ***	**0.789** ***	**0.752** ***
CVI	0.049	0.087	**0.447** ***	0.136	0.486 ***
DVI	**0.535** ***	0.427 ***	0.345 ***	**0.788** ***	0.665 ***
EVI	0.516 ***	0.413 ***	0.308 ***	**0.800** ***	0.629 ***
EVI2	**0.532** ***	0.419 ***	0.319 ***	**0.807** ***	0.650 ***
EVI2.2	**0.539** ***	0.431 ***	0.330 ***	**0.818** ***	0.658 ***
GBNDVI	0.435 ***	**0.578** ***	**0.625** ***	0.714 ***	**0.700** ***
GDVI	**0.527** ***	0.433 ***	0.369 ***	**0.787** ***	**0.682** ***
GNDVI	0.343 ***	**0.524** ***	**0.619** ***	0.660 ***	**0.680** ***
GOSAVI	0.472 ***	0.445 ***	0.404 ***	**0.772** ***	**0.679** ***
GRNDVI	0.436 ***	**0.550** ***	**0.592** ***	0.690 ***	0.668 ***
GSAVI	0.508 ***	0.428 ***	0.358 ***	**0.798** ***	**0.680** ***
NDRE	0.260 ***	0.327 ***	0.306 ***	0.582 ***	0.551 ***
NDVI	**0.569** ***	**0.538** ***	**0.531** ***	0.641 ***	0.586 ***
PNDVI	0.484 ***	**0.581** ***	**0.603** ***	0.721 ***	**0.690** ***
RBNDVI	**0.603** ***	**0.590** ***	**0.565** ***	0.692 ***	0.638 ***
REDVI	0.508 ***	0.437 ***	0.351 ***	**0.806** ***	**0.684** ***
RESAVI	0.447 ***	0.393 ***	0.292 ***	0.758 ***	0.634 ***
REWDRVI	0.276 ***	0.327 ***	0.295 ***	0.595 ***	0.577 ***
RVI	**0.528****	**0.518****	0.446***	0.691***	**0.683****
SARVI2	0.516***	0.413***	0.308***	**0.800****	0.629***
WDRVI	**0.575****	**0.569****	**0.529****	0.717***	**0.676****

*** Significant at the 0.01 level of significance. VIs in bold character were used in the XGBoost model training.

Table A3. Pearson correlation coefficient between leaf area index (m^2/m^2) and vegetation indices across growth stages.

	Aichinokaori	Asahi	Hatsushimo	Nakate Shinsenbon	Nikomaru
ARVI2	**0.562*****	0.616***	0.607***	0.717***	**0.609*****
ATSAVI	0.396***	0.636***	0.581***	0.706***	0.516***
BWDRVI	0.535***	**0.736*****	**0.760*****	**0.777*****	**0.707*****
CVI	**0.582*****	0.645***	0.499***	0.394***	0.417***
DVI	0.362***	0.605***	0.572***	0.683***	0.429***
EVI	0.376***	0.626***	0.567***	0.695***	0.436***
EVI2	0.376***	0.623***	0.577***	0.689***	0.455***
EVI2.2	0.385***	0.640***	0.589***	0.710***	0.472***
GBNDVI	**0.571*****	**0.797*****	**0.727*****	**0.782*****	**0.688*****
GDVI	0.393***	0.648***	0.592***	0.717***	0.467***
GNDVI	**0.553*****	**0.805*****	**0.724*****	**0.754*****	**0.677*****
GOSAVI	0.484***	**0.762*****	**0.665*****	**0.752*****	0.589***
GRNDVI	**0.586*****	**0.768*****	**0.706*****	**0.782*****	**0.666*****
GSAVI	0.443***	**0.715*****	0.627***	**0.732*****	0.527***
NDRE	0.286***	0.619***	**0.658*****	0.621***	0.562***
NDVI	**0.562*****	0.616***	0.607***	0.717***	**0.609*****
PNDVI	**0.593*****	**0.770*****	**0.720*****	**0.795*****	**0.680*****
RBNDVI	**0.563*****	0.654***	0.649***	**0.738*****	**0.645*****
REDVI	0.379***	0.671***	0.622***	0.691***	0.480***
RESAVI	0.385***	**0.697*****	0.639***	0.662***	0.511***
REWDRVI	0.345***	0.652***	**0.718*****	0.652***	0.586***
RVI	**0.674*****	**0.718*****	**0.810*****	**0.849*****	**0.649*****
SARVI2	0.376***	0.626***	0.567***	0.695***	0.436***
WDRVI	**0.628*****	**0.681*****	**0.732*****	**0.817*****	**0.675*****

*** Significant at the 0.01 level of significance. VIs in bold character were used in the XGBoost model training.

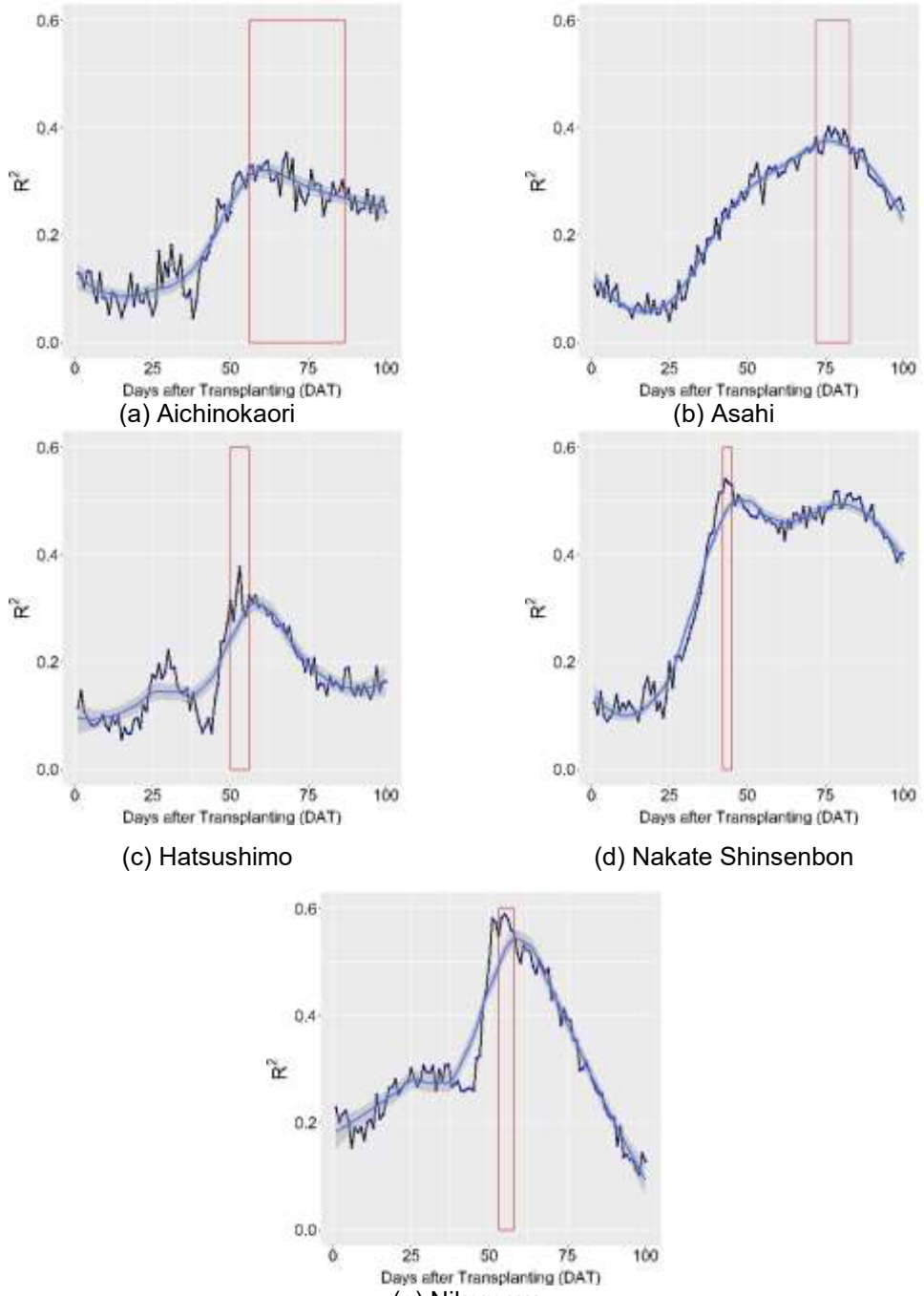

(a) Aichinokaori (b) Asahi

(c) Hatsushimo (d) Nakate Shinsenbon

(e) Nikomaru

Figure A1. R^2 result of the training dataset of the single-day regression model between grain yield and VI-estimated AGB and LAI of the five rice cultivars. The red box indicates the optimum time window for UAV flights as determined from the AIC score comparison. The black line indicates the mean R^2 values from the repeated k-fold cross-validation conducted for each single-day regression. The darker blue line indicates the smoothed R^2 values that can be expected from the plotted R^2 series derived from the repeated k-fold cross-validation. The smoothed R^2 values were determined by using the LOESS (locally weighted scatterplot smoothing) method. The lighter blue region indicates the range of smoothed R^2 values to be expected 95% of the time from each single-day regression. (a) Aichinokaori; (b) Asahi; (c) Hatsushimo; (d) Nakate Shinsenbon; (e) Nikomaru.

Table A4. Tuned booster parameters for optimizing the XGBoost model for the AGB estimation of five rice cultivars using the lowest RMSE as the selection criterion.

Cultivar	Eta	max_ depth	Gamma	colsample_ bytree	min_ child_weight	sub sample	N rounds
Aichinokaori	0.1	5	0.1	0.8	1	1	100
Asahi	0.1	5	0.1	0.5	1	1	100
Hatsushimo	0.1	3	0.1	0.9	1	1	100
Nakate Shinsenbon	0.1	3	0.1	0.5	1	1	100
Nikomaru	0.1	5	0.1	0.5	1	1	100

Table A5. Tuned booster parameters for optimizing the XGBoost model for the LAI estimation of five rice cultivars using the lowest RMSE as the selection criterion.

Cultivar	Eta	max_ depth	Gamma	colsample_ bytree	min_ child_weight	subsample	N rounds
Aichinokaori	0.1	3	0.1	0.6	1	1	100
Asahi	0.1	10	0.1	0.8	1	1	100
Hatsushimo	0.1	10	0.1	0.6	1	1	100
Nakate Shinsenbon	0.1	10	0.1	0.8	1	1	100
Nikomaru	0.1	5	0.1	0.5	1	1	100

6. References

1. Hu, P.; Chapman, S.C.; Wang, X.; Potgieter, A.; Duan, T.; Jordan, D.; Guo, Y.; Zheng, B. Estimation of Plant Height Using a High Throughput Phenotyping Platform Based on Unmanned Aerial Vehicle and Self-Calibration: Example for Sorghum Breeding. *Eur. J. Agron.* **2018**, *95*, 24–32, doi:10.1016/j.eja.2018.02.004.
2. Tao, H.; Feng, H.; Xu, L.; Miao, M.,; Yang, G.; Yang, X.; Fan, L. Estimation of the Yield and Plant Height of Winter Wheat Using UAV-Based Hyperspectral Images. *Sensors* **2020**, *20*, 1231.
3. Madec, S.; Baret, F.; De Solan, B.; Thomas, S.; Dutartre, D.; Jezequel, S.; Comar, A High-Throughput Phenotyping of Plant Height: Comparing Unmanned Aerial Vehicles and Ground LiDAR Estimates. *Front. Plant Sci.* **2002**, *8*,1-14, doi:10.3389/fpls.2017.02002.
4. Gong, Y.; Yang, K.; Lin, Z.; Fang, S.; Wu, X.; Zhu, R.; Peng, Y. Remote Estimation of Leaf Area Index (LAI) with Unmanned Aerial Vehicle (UAV) Imaging for Different Rice Cultivars throughout the Entire Growing Season. *Plant Methods* **2021**, *17*, 88, doi:10.1186/s13007-021-00789-4.
5. Hasan, U.; Sawut, M.; Chen, S. Estimating the Leaf Area Index of Winter Wheat Based on Unmanned Aerial Vehicle RGB-Image Parameters. *Sustainability* **2019**, *11*, 6829, doi:10.3390/su11236829.
6. Roosjen, P. P.; Brede, B.; Suomalainen, J. M.; Bartholomeus, H. M.; Kooistra, L.; Clevers, J. G. Improved Estimation of Leaf Area Index and Leaf Chlorophyll Content of a Potato Crop Using Multi-Angle Spectral Data – Potential of Unmanned Aerial Vehicle Imagery. *International Journal.of Applied Earth Observation and Geoinformation* **2018**, *66*, 14–26.
7. Yue, J.; Yang, G.; Tian, Q.; Feng, H.; Xu, K.; Zhou, C. Estimate of Winter-Wheat above-Ground Biomass Based on UAV Ultrahigh-Ground-Resolution Image Textures and Vegetation Indices. *ISPRS Journa of Photogrammetry in Remote Sensing.* **2019**, *150*, 226–244, doi:10.1016/j.isprsjprs.2019.02.022.
8. Niu, Y.; Zhang, L.; Zhang, H.; Han, W.; Peng, X. Estimating Above-Ground Biomass of Maize Using Features Derived from UAV-Based RGB Imagery. *Remote Sensing.* **2019**, *11*, 1261.
9. Lu, N.; Zhou, J.; Han, Z.; Li, D.; Cao, Q.; Yao, X.; Tian, Y.; Zhu, Y.; Cao, W.; Cheng, T. Improved Estimation of Aboveground Biomass in Wheat from RGB Imagery and Point Cloud Data Acquired with a Low-Cost Unmanned Aerial Vehicle System. *Plant Methods* **2019**, *15*, 17, doi:10.1186/s13007-019-0402-3.
10. Yang, H.; Li, F.; Wang, W.; Yu, K. Estimating Above-Ground Biomass of Potato Using Random Forest and Optimized Hyperspectral Indices. *Remote Sensing.* **2021**, *13*, 2339, doi:10.3390/rs13122339.
11. Zhang, J.; Cheng, T; Guo, W.; Xu, X.; Qiao, H.; Xie, Y.; Ma, X. Leaf Area Index Estimation Model for UAV Image Hyperspectral Data Based on Wavelength Variable Selection and Machine Learning Methods. *Plant Methods.* **2021**.*17*, 1–14.
12. Osco, L.P.; Junior, J.M.; Ramos, A.P.M.; Furuya, D.E.G.; Santana, D.C.; Teodoro, L.P.R.; Gonçalves, W.N.; Baio, F.H.R.; Pistori, H.; Junior, C.A. da S.; et al. Leaf Nitrogen Concentration and Plant Height Prediction for Maize Using UAV-Based Multispectral Imagery and Machine Learning Techniques. *Remote Sensing.* **2020**, *12*, 3237, doi:10.3390/rs12193237.
13. Prasad, N.R.; Patel, N.R.; Danodia, A.; Manjunath, K.R. Comparative Performance of Semi-Empirical Based Remote Sensing and Crop Simulation Model for Cotton Yield Prediction. *Model. Earth Syst. Environ.* **2022**, 8, 1733–1747, doi:10.1007/s40808-021-01180-x.
14. Rehmani, M. I. A.; Ding, C.; Li, G.; Ata-Ul-Karim, S. T.; Hadifa, A.; Bashir, M. A.; Ding, Y. Vulnerability of Rice Production to Temperature Extremes during Rice Reproductive Stage in Yangtze River Valley, China. *J. King Saud Univ.-Sci.* **2021**, *33*, 101599, doi:10.1016/j.jksus.2021.101599.
15. Rehmani, M. I. A.; Wei, G.; Hussain, N.; Ding, C.; Li, G.; Liu, Z.,; Ding, Y. Yield and Quality Responses of Two Indica Rice Hybrids to Post-Anthesis Asymmetric Day and Night Open-Field Warming in Lower Reaches of Yangtze River Delta. *Field Crops Res.* **2014**, *156*, 231–241.
16. Onwuchekwa-Henry, C.B.; Ogtrop, F.V.; Roche, R.; Tan, D.K.Y. Model for Predicting Rice Yield from Reflectance Index and Weather Variables in Lowland Rice Fields. *Agriculture* **2022**, *12*, 130, doi:10.3390/agriculture12020130.
17. Ge, H.; Ma, F.; Li, Z.; Du, C. Grain Yield Estimation in Rice Breeding Using Phenological Data and Vegetation Indices Derived from UAV Images. *Agronomy* **2021**, *11*, 2439, doi:10.3390/agronomy11122439.

18. Freeman, K.W.; Girma, K.; Arnall, D.B.; Mullen, R.W.; Martin, K.L.; Teal, R.K.; Raun, W.R. By-Plant Prediction of Corn Forage Biomass and Nitrogen Uptake at Various Growth Stages Using Remote Sensing and Plant Height. *Agron. J.* **2007**, *99*, 530–536, doi:10.2134/agronj2006.0135.
19. Rahman, M.M.; Crain, J.; Haghighattalab, A.; Singh, R.P.; Poland, J. Improving Wheat Yield Prediction Using Secondary Traits and High-Density Phenotyping Under Heat-Stressed Environments. *Front. Plant Sci.* **2021**, *12*, 1977, doi:10.3389/fpls.2021.633651.
20. Barzin, R.; Pathak, R.; Lotfi, H.; Varco, J.; Bora, G.C. Use of UAS Multispectral Imagery at Different Physiological Stages for Yield Prediction and Input Resource Optimization in Corn. *Remote Sens.* **2020**, *12*, 2392, doi:10.3390/rs12152392.
21. Johansen, K.; Morton, M.J.L.; Malbeteau, Y.; Aragon, B.; Al-Mashharawi, S.; Ziliani, M.G.; Angel, Y.; Fiene, G.; Negrão, S.; Mousa, M.A.A.; et al. Predicting Biomass and Yield in a Tomato Phenotyping Experiment Using UAV Imagery and Random Forest. *Front. Artif. Intell.* **2020**, *3*.
22. Wan, L.; Cen, H.; Zhu, J.; Zhang, J.; Zhu, Y.; Sun, D.; Du, X.; Zhai, L.; Weng, H.; Li, Y.; et al. Grain Yield Prediction of Rice Using Multi-Temporal UAV-Based RGB and Multispectral Images and Model Transfer – a Case Study of Small Farmlands in the South of China. *Agric. For. Meteorol.* **2020**, *291*, 108096, doi:10.1016/j.agrformet.2020.108096.
23. Zhou, X.; Zheng, H.B.; Xu, X.Q.; He, J.Y.; Ge, X.K.; Yao, X.; Cheng, T.; Zhu, Y.; Cao, W.X.; Tian, Y.C. Predicting Grain Yield in Rice Using Multi-Temporal Vegetation Indices from UAV-Based Multispectral and Digital Imagery. *ISPRS J. Photogramm. Remote Sens.* **2017**, *130*, 246–255, doi:10.1016/j.isprsjprs.2017.05.003.
24. Wang, F.; Yi, Q.; Hu, J.; Xie, L.; Yao, X.; Xu, T.; Zheng, J. Combining Spectral and Textural Information in UAV Hyperspectral Images to Estimate Rice Grain Yield. *Int. J. Appl. Earth Obs. Geoinformation* **2021**, *102*, 102397, doi:10.1016/j.jag.2021.102397.
25. Zhou, J.; Lu, X.; Yang, R.; Chen, H.; Wang, Y.; Zhang, Y.; Huang, J.; Liu, F. Developing Novel Rice Yield Index Using UAV Remote Sensing Imagery Fusion Technology. *Drones* **2022**, *6*, 151, doi:10.3390/drones6060151.
26. Harrell, D.L.; Tubaña, B.S.; Walker, T.W.; Phillips, S.B. Estimating Rice Grain Yield Potential Using Normalized Difference Vegetation Index. *Agron. J.* **2011**, *103*, 1717–1723, doi:10.2134/agronj2011.0202.
27. Fassnacht, F.E.; Hartig, F.; Latifi, H.; Berger, C.; Hernández, J.; Corvalán, P.; Koch, B. Importance of Sample Size, Data Type and Prediction Method for Remote Sensing-Based Estimations of Aboveground Forest Biomass. *Remote Sens. Environ.* **2014**, *154*, 102–114, doi:10.1016/j.rse.2014.07.028.
28. Kanke, Y.; Tubana, B.; Dalen, M.; Harrell, D. Evaluation of Red and Red-Edge Reflectance-Based Vegetation Indices for Rice Biomass and Grain Yield Prediction Models in Paddy Fields. *Precis. Agric.* **2016**, *17*, doi:10.1007/s11119-016-9433-1.
29. Perros, N.; Kalivas, D.; Giovos, R. Spatial Analysis of Agronomic Data and UAV Imagery for Rice Yield Estimation. *Agriculture* **2021**, *11*, 809, doi:10.3390/agriculture11090809.
30. Bouras, E. houssaine; Jarlan, L.; Er-Raki, S.; Balaghi, R.; Amazirh, A.; Richard, B.; Khabba, S. Cereal Yield Forecasting with Satellite Drought-Based Indices, Weather Data and Regional Climate Indices Using Machine Learning in Morocco. *Remote Sens.* **2021**, *13*, 3101, doi:10.3390/rs13163101.
31. Kang, Y.; Ozdogan, M.; Zhu, X.; Ye, Z.; Hain, C.; Anderson, M. Comparative Assessment of Environmental Variables and Machine Learning Algorithms for Maize Yield Prediction in the US Midwest. *Environ. Res. Lett.* **2020**, *15*, 064005, doi:10.1088/1748-9326/ab7df9.
32. Shah, A.; Agarwal, R.; Baranidharan, B. Crop Yield Prediction Using Remote Sensing and Meteorological Data. In Proceedings of the 2021 International Conference on Artificial Intelligence and Smart Systems (ICAIS); March **2021**; pp. 952–960.
33. Archontoulis, S.V.; Miguez, F.E. Nonlinear Regression Models and Applications in Agricultural Research. *Agron. J.* **2015**, *107*, 786–798, doi:10.2134/agronj2012.0506.
34. Ismail, Z.; Khamis, A.; Jaafar, M. Fitting Nonlinear Gompertz Curve to Tobacco Growth Data. *J. Agron.* **2003**, *2*, doi:10.3923/ja.2003.223.236.
35. Kataoka, T.; Kaneko, T.; Okamoto, H.; Hata, S. Crop Growth Estimation System Using Machine Vision. In Proceedings of the Proceedings 2003 IEEE/ASME International Conference on Advanced Intelligent Mechatronics (AIM 2003); July **2003**; Vol. 2, pp. b1079-b1083 vol.2.
36. Japan Meteorological Agency. Tables of Climatological Normals (1991–2020). Accessed on 27 May 2022. https://www.data.jma.go.jp/stats/data/en/normal/normal.html.

37. Counce, P.; Keisling, T.; Mitchell, A. A Uniform, Objective, and Adaptive System for Expressing Rice Development. *Crop Sci. - CROP SCI* **2000**, *40*, doi:10.2135/cropsci2000.402436x.
38. Hijmas, R.J. raster: Geographic Data Analysis and Modeling. R package version. 3.5-15. **2022**, https://CRAN.R-project.org/package=raster
39. Kuhn, M. Building Predictive Models in R Using the Caret Package. *J. Stat. Softw.* **2008**, *28*, 1–26, doi:10.18637/jss.v028.i05.
40. Wei, T.; Simko, V.; Levy, M.; Xie, Y.; Jin, Y.; Zemla, J. Package 'Corrplot.' *Statistician* **2017**, *56,* 1-18.
41. Chen, T.; He, H.T.; Benesty, M.; Khotilovich, V.; Tang, Y.; Cho, H.; Chen, K.; Mitchell, R.; Cano, I.; Zhou, T.; Li, M.; Xie, J.; Lin, M.; Geng, Y.; Li, Y.; Yuan, J. xgboost: Extreme Gradient Boosting. R package version 1.6.0.1. **2022**, https://CRAN.R-project.org/package=xgboost
42. Yang, L. and Just, A. SHAPforxgboost: SHAP Plots for 'XGBoost'. R package version 0.1.1. **2021**, https://CRAN.R-project.org/package=SHAPforxgboost
43. Srinivas, P.; Katarya, R. HyOPTXg: OPTUNA Hyper-Parameter Optimization Framework for Predicting Cardiovascular Disease Using XGBoost. *Biomed. Signal Process. Control* **2022**, *73*, 103456, doi:10.1016/j.bspc.2021.103456.
44. Ritz, C.; Baty, F.; Streibig, J.C.; Gerhard, D. Dose-Response Analysis Using R. *PLOS ONE* **2015**, *10*, e0146021, doi:10.1371/journal.pone.0146021.
45. Mazerolle, M.J. AICcmodavg: Model selection and multimodel inference based on (Q)AIC(c). R package version 2.3-1. **2020**, https://cran.r-project.org/package=AICcmodavg
46. Wickham, H. ggplot2: Elegant Graphics for Data Analysis. Springer-Verlag New York, **2016**. https://ggplot2.tidyverse.org
47. Pan, Y.; Gao, S.; Xie, K.; Lu, Z.; Meng, X.; Wang, S.; Lu, J.; Guo, S. Higher Radiation Use Efficiency Produces Greater Biomass Before Heading and Grain Yield in Super Hybrid Rice. *Agronomy* **2020**, *10*, 209, doi:10.3390/agronomy10020209.
48. Pieters, A.J.; El Souki, S.; Nazar, C. Growth, Yield and Nitrogen Allocation in Two Rice Cultivars under Field Conditions in Venezuela. *Interciencia* **2006**, *31*, 671–676.
49. Zhou, J.; Yungbluth, D.; Vong, C.N.; Scaboo, A.; Zhou, J. Estimation of the Maturity Date of Soybean Breeding Lines Using UAV-Based Multispectral Imagery. *Remote Sens.* **2019**, *11*, 2075, doi:10.3390/rs11182075.
50. Cen, H.; Wan, L.; Zhu, J.; Li, Y.; Li, X.; Zhu, Y.; Weng, H.; Wu, W.; Yin, W.; Xu, C.; et al. Dynamic Monitoring of Biomass of Rice under Different Nitrogen Treatments Using a Lightweight UAV with Dual Image-Frame Snapshot Cameras. *Plant Methods* **2019**, *15*, 32, doi:10.1186/s13007-019-0418-8.
51. Wang, F.; Huang, J.; Tang, Y.-L.; Wang, X. New Vegetation Index and Its Application in Estimating Leaf Area Index of Rice. *Rice Sci.* **2007**, *14*, 195–203, doi:10.1016/S1672-6308(07)60027-4.
52. Ghosh, S.M.; Behera, M.D. Aboveground Biomass Estimation Using Multi-Sensor Data Synergy and Machine Learning Algorithms in a Dense Tropical Forest. *Appl. Geogr.* **2018**, *96*, 29–40, doi:10.1016/j.apgeog.2018.05.011.
53. Casanova, D.; Epema, G.F.; Goudriaan, J. Monitoring Rice Reflectance at Field Level for Estimating Biomass and LAI. *Field Crops Res.* **1998**, *55*, 83–92, doi:10.1016/S0378-4290(97)00064-6.
54. Sonobe, R.; Yamaya, Y.; Tani, H.; Wang, X.; Kobayashi, N.; Mochizuki, K. Crop Classification from Sentinel-2-Derived Vegetation Indices Using Ensemble Learning. *J. Appl. Remote Sens.* **2018**, *12*, 1, doi:10.1117/1.JRS.12.026019.
55. Zhang, J.; He, Y.; Yuan, L.; Liu, P.; Zhou, X.; Huang, Y. Machine Learning-Based Spectral Library for Crop Classification and Status Monitoring. *Agronomy* **2019**, *9*, 496, doi:10.3390/agronomy9090496.
56. Clevers, J.G.P.W.; Kooistra, L.; Van den Brande, M.M.M. Using Sentinel-2 Data for Retrieving LAI and Leaf and Canopy Chlorophyll Content of a Potato Crop. *Remote Sens.* **2017**, *9*, 405, doi:10.3390/rs9050405.
57. Xiao, X.; Boles, S.; Liu, J.; Zhuang, D.; Frolking, S.; Li, C.; Salas, W.; Moore, B. Mapping Paddy Rice Agriculture in Southern China Using Multi-Temporal MODIS Images. *Remote Sens. Environ.* **2005**, doi:10.1016/j.rse.2004.12.009.
58. Qiu, B.; Li, W.; Tang, Z.; Chen, C.; Qi, W. Mapping Paddy Rice Areas Based on Vegetation Phenology and Surface Moisture Conditions. *Ecol. Indic.* **2015**, *56*, 79–86, doi:10.1016/j.ecolind.2015.03.039.

59. Jiang, Z.; Huete, A.; Didan, K.; Miura, T. Development of a Two-Band Enhanced Vegetation Index without a Blue Band. *Remote Sens. Environ.* **2008**, *112*, 3833–3845, doi:10.1016/j.rse.2008.06.006.
60. Qiu, C.; Liao, G.; Tang, H.; Liu, F.; Liao, X.; Zhang, R.; Zhao, Z. Derivative Parameters of Hyperspectral NDVI and Its Application in the Inversion of Rapeseed Leaf Area Index. *Appl. Sci.* **2018**, *8*, 1300.
61. Kang, Y.; Nam, J.; Kim, Y.; Lee, S.; Seong, D.; Jang, S.; Ryu, C. Assessment of Regression Models for Predicting Rice Yield and Protein Content Using Unmanned Aerial Vehicle-Based Multispectral Imagery. *Remote Sens.* **2021**, *13*, 1508, doi:10.3390/rs13081508.
62. Teal, R.K.; Tubana, B.; Girma, K.; Freeman, K.W.; Arnall, D.B.; Walsh, O.; Raun, W.R. In-Season Prediction of Corn Grain Yield Potential Using Normalized Difference Vegetation Index. *Agron. J.* **2006**, *98*, 1488–1494, doi:10.2134/agronj2006.0103.
63. Marin, D.B.; Ferraz, G.A. e S.; Guimarães, P.H.S.; Schwerz, F.; Santana, L.S.; Barbosa, B.D.S.; Barata, R.A.P.; Faria, R. de O.; Dias, J.E.L.; Conti, L.; et al. Remotely Piloted Aircraft and Random Forest in the Evaluation of the Spatial Variability of Foliar Nitrogen in Coffee Crop. *Remote Sens.* **2021**, *13*, 1471, doi:10.3390/rs13081471.
64. Candiago, S.; Remondino, F.; De Giglio, M.; Dubbini, M.; Gattelli, M. Evaluating Multispectral Images and Vegetation Indices for Precision Farming Applications from UAV Images. *Remote Sens.* **2015**, *7*, 4026–4047, doi:10.3390/rs70404026.
65. Tian, Y.C.; Yao, X.; Yang, J.; Cao, W.X.; Hannaway, D.B.; Zhu, Y. Assessing Newly Developed and Published Vegetation Indices for Estimating Rice Leaf Nitrogen Concentration with Ground- and Space-Based Hyperspectral Reflectance. *Field Crops Res.* **2011,** *120(2)*, 299-310**.** https://doi.org/10.1016/j.fcr.2010.11.002.
66. Xu, R.; Zhao, S.; Ke, Y. A Simple Phenology-Based Vegetation Index for Mapping Invasive Spartina Alterniflora Using Google Earth Engine. *IEEE J. Sel. Top. Appl. Earth Obs. Remote Sens.* **2021**, *14*, 190–201, doi:10.1109/JSTARS.2020.3038648.
67. Tanaka, S.; Goto, S.; Maki, M.; Akiyama, T.; Muramoto, Y.; Yoshida, K. Estimation of leaf chlorophyll concentration in winter wheat [*Triticum aestivum*] before maturing stage by a newly developed vegetation index- rbNDVI. *J. Jpn. Agric. Syst. Soc. Jpn.* **2007** *4,* 297-303.
68. Zha, H.; Miao, Y.; Wang, T.; Li, Y.; Zhang, J.; Sun, W.; Feng, Z.; Kusnierek, K. Improving Unmanned Aerial Vehicle Remote Sensing-Based Rice Nitrogen Nutrition Index Prediction with Machine Learning. *Remote Sens.* **2020**, *12*, 215, doi:10.3390/rs12020215.
69. Cao, Q.; Miao, Y.; Wang, H.; Huang, S.; Cheng, S.; Khosla, R.; Jiang, R. Non-Destructive Estimation of Rice Plant Nitrogen Status with Crop Circle Multispectral Active Canopy Sensor. *Field Crops Res.* **2013**, *154*, 133–144, doi:10.1016/j.fcr.2013.08.005.
70. Lu, J.; Miao, Y.; Shi, W.; Li, J.; Hu, X.; Chen, Z.; Wang, X.; Kusnierek, K. Developing a Proximal Active Canopy Sensor-Based Precision Nitrogen Management Strategy for High-Yielding Rice. *Remote Sens.* **2020**, *12*, 1440, doi:10.3390/rs12091440.
71. Zhu, Y.; Yao, X.; Tian, Y.; Liu, X.-J.; Cao, W. Analysis of Common Canopy Vegetation Indices for Indicating Leaf Nitrogen Accumulations in Wheat and Rice. *Int. J. Appl. Earth Obs. Geoinformation* **2008**, *10*, 1–10, doi:10.1016/j.jag.2007.02.006.
72. Basso, B.; Cammarano, D. Remotely Sensed Vegetation Indices: Theory and Applications for Crop Management. *Rivista Italiana di Agrometeorologia*, **2004**. *1(5)*, 36-53.
73. Cao, Y.; Li, G.L.; Luo, Y.K.; Pan, Q.; Zhang, S.Y. Monitoring of Sugar Beet Growth Indicators Using Wide-Dynamic-Range Vegetation Index (WDRVI) Derived from UAV Multispectral Images. *Comput. Electron. Agric.* **2020**, *171*, 105331, doi:10.1016/j.compag.2020.105331.

Chapter VI: General Discussion

Abstract: Spectral and textural features of UAV-derived multispectral images were utilized to estimate rice AGB, LAI, and grain yield. The study attempted to associate AGB and LAI estimates in predicting rice grain yield, including determining the optimum time window of UAV flight for predicting grain yield. This chapter aimed to summarize the improvement in AGB, and LAI estimation models and the grain yield prediction model established in the study. Results show that a reasonable estimate of rice AGB can be achieved using Random Forest and adding vegetation fraction cover to VIs. Rice LAI was best estimated using Random Forest and Type I texture index. The optimum time window for UAV flight varied, with cultivars ranging from 4 to 31 days between the tillering and the initial heading stages. Grain yield prediction using cumulative VIs taken at booting and heading stages resulted in comparable predictions from VI-estimated AGB and LAI, depending on the cultivars. Results of the entire study suggest that model algorithm and feature construction are important in improving the estimation of crop parameters, AGB and LAI, and grain yield prediction.

---

1. Introduction

The agricultural production system requires crop data derived from fast and reliable techniques. The main goal of rice crop production is to produce a sustainable and profitable grain yield and attaining such a goal must involve integrated crop management. Generally, crop producers would select agricultural inputs such as seeds, fertilizers, and water management strategies that are proven to provide high grain yield returns. However, such claims were tested on rice field trials whose conditions may differ from a prospective farm, despite multi-location trials conducted for such agricultural inputs or techniques. Thus, site-specific rice crop management was promoted to ensure the applicability of agricultural innovations to a particular rice production area.

The site-specific crop management further improved with the introduction of precision agriculture, which promotes the precise application of fertilizers and pesticides by characterizing the farm at the small plot and hill levels. Doing so requires methods that are fast and provide accurate and precise data. The remote sensing method is one approach to acquiring such crop data. Even with

remote sensing methods, optimization of the method is required to ensure the reliability of the data and applicability for crop management use.

Moreover, regular crop field data collection using remote sensors is an alternative, time-saving method but will be more profitable if it can be utilized in forecasting field crop conditions. Crop prediction will allow a more proactive way of managing crops. If significant yield losses can be predicted at a particular time of the crop growth duration, necessary mitigating measures can be implemented. However, considering crop has its physiological mechanism, it is necessary to determine when and to what extent crop prediction is feasible.

Crop prediction of grain yield and non-yield components requires understanding the cultivars, environment, and interaction between the two. It means that crop and environmental variables are essential components of crop prediction. However, environmental variables such as weather data can only be meaningful if crop prediction is developed at regional and national levels.

Developing crop prediction models complementary to site-specific crop management is thus challenging. The potential of using remote sensing methods in crop prediction should be evaluated, as it can provide a higher temporal and spatial resolution than the traditional sampling method. Introducing the Unmanned Aerial Vehicle (UAV) in the market provided a better opportunity to gather crop data that seems to suit farm-level crop management. Multispectral cameras onboard UAVs provide a vegetation index that highlights vegetation that can be used for crop estimation.

Crop estimation estimates grain yield and other crop parameters such as leaf area index and aboveground biomass. Including sources of variation for the crop, parameters are also essential for an effective crop estimation model.

The study established model workflows to improve estimation models of yield-related traits such as leaf area index (LAI) and aboveground biomass (AGB) and prediction model of grain yield to determine if crop prediction using remote sensing methods alone can give reliable and reasonable estimates for crop management. Improvement of the models was established by examining other UAV-derived variables, feature selection methods, and machine learning methods. In addition, the optimum time window for UAV flight to predict rice grain yield was determined. The entire dataset utilized to develop the estimation models in the study was derived from two-year rice experimental trials in 2020 and 2021, involving two fertility levels and five rice cultivars.

This chapter aimed to describe the effect of remote sensing variables in estimating AGB and LAI estimates and predicting grain yield. Also, the chapter aimed to discuss the merit of determining the optimum time window for UAV flight in grain yield prediction.

2. Leaf Area Index

The effect of combining the texture and spectral features of UAV-derived multispectral images using different feature selections and machine learning methods in rice LAI estimation was evaluated. Two types of texture indices were developed from the GLCM-based texture metrics. These were 1). Type I: texture indices derived from the transformation of the optimized bands, and 2). Type II: texture indices derived from the transformation of texture metrics with each metric optimized according to band and angle. Results have shown that combining texture and the spectral index could improve LAI estimation when the Type I texture index is used. However, the Type II texture index was a poor LAI estimator. All the feature selection methods did not significantly influence the estimation performance. In research done by [4], rice LAI estimation using VIs derived from multispectral images was improved by adding a textural index calculated from the GLCM-based textures. The random forest (RF) algorithm best estimates rice LAI using NIR and red edge-based vegetation indices [5]. Feature selection using RF was also found to give reliable LAI estimates compared to other feature selection methods [6].

However, the feature selection method and machine learning models in this study had comparable rice LAI estimation performances. The difference in the estimation model between Type I and Type II was due to the optimization performed in the texture indices. VIs and Type I texture indices had similar performance because of almost similar transformation between VIs and Type I texture index. The difference in the estimation model was due to the optimization performed in the texture indices. VIs and Type I texture indices had similar performance because of almost similar transformation between VIs and Type I texture index.

3. Aboveground biomass estimation

Rice AGB is an essential indicator of crop productivity. The rice AGB estimation model was improved by adding Vegetation Fraction Cover (VF) as a feature variable to the AGB- estimation model using Vegetation Index (VI). Its effect on the rice AGB estimation was evaluated. AGB was

sampling at different growth stages from tillering to heading stage following UAV flights, involving two fertility trials and five rice cultivars. VIs were generated from raw reflectance from the multispectral cameras on board the UAV. VF was extracted using the threshold-based segmentation method to classify the plant from the non-plant components in the multispectral images. Feature selection and machine learning were also applied in the estimation model. Feature selection such as Recursive Feature Elimination (RFE), z-test, and M-statistic while machine learning models were Random Forest (RF), Support Vector Regression (SVR), and Extreme Gradient Boost (XGBoost). Results demonstrated that combining VIs with VF slightly improved the AGB estimation model, regardless of feature selection methods. AGB estimation model using RFE and z-test selected feature variables performed better than M-statistic selected features. Likewise, RF and XGBoost showed comparable performance in estimating AGB, while SVR had poor estimation performance regardless of the feature selection method.

3.1. Effect of Feature Variables

In a review article published by [2], AGB estimation using UAV systems was reported that VIs could estimate AGB with good performance when structural variables and variables regarding volume were included in the model. It is because the growth stage indicated by changes in the structure highly affects the performance of AGB estimation. In this study, VI was combined with the Vegetation Fraction Cover. Ideally, one threshold value should be set for each VIs between non-plant and plant areas in the ROI. However, the difference in the illumination over the whole area made it difficult to discriminate between plant and non-plant areas through VI values.

Regardless, only one threshold value for each field trial for all the UAV flights conducted. It is practical to set only one threshold value for each field trial to apply it throughout the crop growth period. VF was generated from a single threshold method, ExG-ExR or the Excess Green Index. Previous research showed that Excess Green performs well in binarizing plant images [3]. Instead of generating VF from each VI, only one VI was used to adjust the VI values at the tillering stage to improve its correlation with AGB. As the results in Chapter 2 suggest, VI taken at tillering stage had a lower correlation with AGB. Also, results show that combining VF with VI slightly improved AGB estimation across growth stages.

3.2. Effect of Feature Selection

Image analyses can deal with the differences in brightness in one image. A local adaptive threshold is a technique that considers brightness variation in a field image. The technique relies on the standard deviation of the binary image, and it binarizes images on a set window size or region in a raster image rather than the whole image. However, instead of focusing on the brightness variation of one field trial, given a definite ROI in the field, the study focused on the ability of the VI to have mean values distinct for different treatment factors. In the study, the treatment factor considered for separability of VI was the fertility trials, No fertilizer, and Fertilizer trials. It is assumed that the AGB variation observed was due to the fertility level and was accounted for in the separability values of VIs. Atmospheric and soil-insensitive VIs were found to have good separability at tillering and heading stages. However, when these VIs were used in estimating AGB, the model evaluation was relatively poor compared to the model with VI selected from correlation analysis and the RFE method. These results suggest that the separability of VI is not a good estimator of LAI in rice.

3.3. Comparison of Machine Learning

The machine learning methods, MLR, SVR, RF, and XGBoost, were employed to estimate AGB. The results suggest that XGBoost and RF had a comparative model performance. Both ML develop regression trees as part of the training process. Their difference is the regularization function that can be optimized in the XGBoost. Moreover, RF has fewer tuning parameters than XGBoost, which makes a shorter running time for RF.

The study on rice AGB estimation concentrated on the following: (1) difference between groups of VIs in terms of correlation with AGB and separability of treatment. The results showed that atmospheric and soil-insensitive VIs did not improve AGB estimation compared to VIs known for saturation, such as NDVI. VIs separability varies with the growth stage, with tillering stage showing the best separability score. There was decreased separability of Normalized VI as the crop reached canopy closure, while atmospheric and soil-insensitive VIs had good separability at tillering and heading stages.

The results show that RFE did not select atmospheric and soil-insensitive VIs, while M-statistic and z-test methods selected those VIs. This indicates that the M-statistic and z-test select features

are distinctly different based on the separability of treatment factors and correlation with the target variable, AGB. On the other hand, RFE selected VIs based on the set of features that resulted in the lowest RMSE, disregarding the multicollinearity of feature variables. Multicollinearity of variables results in unstable estimation models as the value of one feature variable is affected by another. However, the results suggest that multicollinearity does not necessarily result in an unstable estimation model.

4. Grain Yield Prediction Model

The prediction model predicted rice grain yield by directly using multitemporal VIs. The correlation of grain yield to numerous VIs was examined in the study. Across growth stages, correlations were low. Recursive feature elimination was performed to select VIs that can potentially achieve low RMSE values. Random Forest performed better than Multiple Linear, Support Vector, and Ridge regressions. It was observed that different numbers of VIs are required for each growth stage, with the heading stage requiring more than 15 VIs to achieve low RMSE values. However, comparing the prediction model with five VIs and the model with 14 VIs selected from the recursive elimination method (RFE) performed using multitemporal VIs showed comparable results.

The selected VIs are GARI, CVI, GRNDVI, NDRE, and REWDRVI. GARI and GRNDVI have normalized VIs with an additional one band that minimizes the saturation effect of the red band in the VI. These are the blue band for GARI and the green band for GRNDVI. The canopy does not highly absorb in blue and green regions compared to the red band, thus avoiding the narrow VI values at later growth stages, indicating a non-saturation effect. On the other hand, NDRE and REWDRVI have normalized VIs with red and red-edge bands in their transformations, respectively. The normalization of the band reflectance prevents the NDRE from having a wide variation of values compared to ratio-based VIs. On the other hand, the normalization and the red-edge component of the REWDRVI make it less sensitive to differences in canopy LAI. Thus, its values can represent the optimal variation in the grain yield with less noise in the dataset.

Transformation of VIs or VI variables as cumulative VI values at four and two growth stages did not substantially increase grain yield prediction. However, the cumulative VI values taken at the booting and heading stage showed relatively better prediction among the VI variables.

5. Relation of Grain Yield to AGB and LAI Estimation

Using VI-estimated yield-related traits such as AGB and LAI to predict rice grain yield was evaluated. AGB and LAI were estimated using VIs correlated to them at different growth stages. The estimation models were trained using XGBoost, and hyperparameters were optimized to achieve the lowest RMSE result. The study aimed to determine the optimum time window of UAV flight, and the optimum DAT determined from the single-day regression models was evaluated for their performance in predicting grain yield. Our result suggests that grain yield can be predicted by VI-estimated AGB and LAI depending on the cultivar. Some cultivars can be predicted well, but others cannot be predicted well by both actual and VI-estimated AGB and LAI, such as Asahi.

Low prediction performance indicates the high residuals between predicted and actual values. If the difference between the two is high, the predictors employed have no relationship with the target variable, for it does not reflect the variation of the target variable. Although low prediction performance is also considered dependent on the data splitting between training and test dataset, cross-validation helped in allowing the model to train with as much data variation as possible. However, overfitting is a possible drawback. Nevertheless, when a training process has controlled the possible drawbacks, an underfit model would only mean that the predictors are not enough to predict the grain yield. However, recall, the predictors in the grain yield prediction model were VI-estimated crop estimates whose prediction errors from the crop estimation models were carried on to the grain yield prediction model.

When the optimum time window for UAV flight was determined, the AIC scores were calculated from the single-regression models developed for each variety. Only presented was the model evaluation of the single regression models whose DAT (days after transplanting) was included in the identified time window. Different cultivars had different grain yield prediction performances. Some cultivars were predicted poorly using actual VIs, VI-estimated AGB and LAI, and actual AGB and LAI values.

The low prediction in some cultivars such as Asahi and Nakate Shinsenbon can be explained by the Analysis of Variance and F-test between the categorical variables, fertility level, discrete variable, year and continuous variables, actual LAI, AGB, and grain yield. The actual AGB and LAI were discretized to compare their variances with grain yield.

When random data splitting is applied to select the training dataset, it is assumed that the variation in the training and test dataset is representative of the whole dataset and has the same variance. The F-test's significance would determine if the variation in the grain yield is related to the variation of the predictor. If the F-test for a categorical variable is not significant, then the categorical variable does not explain the variation of the grain yield. Thus, discretization of the continuous variables, LAI and AGB, was done to establish a probability distribution to detect better the relationship between LAI, AGB, and grain yield.

ANOVA and F-Test using the actual AGB and LAI showed that different cultivars had different significant F-tests (Tables A1-5). Results show that cultivars with a more significant F-test had better prediction performance. However, the high number of F-tests was reduced when a high number of significant interactions was observed. This is because the interactions were not considered in the single-regression model. Aichinokaori had a significant difference in grain yield according to discretized LAI and AGB, while Hatsushimo had few significant variations but had only one significant interaction. On the other hand, Asahi had a lower number of significant F-tests. When the variation of the dependent variable, grain yield, according to the levels of an independent categorical variable, is insignificant, it implies that the independent variable cannot explain the variations observed in the grain yield.

The significance of grain yield in terms of AGB variation indicates that AGB is a good predictor of grain yield. The comparison between cultivars also shows that the significance of grain yield at LAI variation cannot compensate for the lack of significance at AGB variation. Although the reported R^2 of rice grain yield prediction in other research was less than 0.50, an R^2 of less than 0.60 is still low. Studies conducted by [7,8] concluded that higher grain yield is attributed to the harvest index than biomass production, indicating that AGB production may not be enough predictor for rice grain yield. An underestimation of grain yield is more likely to decrease prediction performance than overestimation, as shown between Nakate Shinsenbon and Hatsushimo. A yield-LAI model developed by [9] demonstrated that rice grain yield could be predicted with an $R^2 = 0.945$. However, our study suggests that LAI may not predict grain yield at a similarly high R^2.

6. Conclusion

Crop estimation models using UAV-derived variables were examined for their potential to aid rice crop management. The study consisted of four components: (1) AGB estimation model, (2) LAI estimation model, (3) grain yield prediction model and (4) determination of the optimum time window of UAV flights to predict grain yield with the use of AGB and LAI estimates from UAV-derived variables.

The results of the entire study suggest that AGB estimation was improved by including vegetation fraction cover (VF) estimated using a color index and threshold-based image segmentation method. Random forest and XGBoost had comparable AGB estimation performance. Type I texture index improved LAI estimation compared to VIs. VF was not used to improve LAI estimation as VF is equivalent to LAI. Texture index was not used in improving the AGB estimation model because AGB estimation focused only on two spectra, plant and the non-plant component of the UAV image, that the threshold-based segmentation method can manage.

The optimum time window for UAV flight varies with the cultivars used in the study. The optimum time window ranged from 4 to 31 days between tillering to the initial heading stages. Cultivars such as Asahi cannot be predicted using actual and VI-estimated AGB and LAI. The determined optimum time window for UAV flights can be applied in remote sensing using satellites for a more accurate and cost-efficient grain yield prediction. This approach is different from other crop prediction models utilizing remote sensing data. With this approach, data collection is reduced without lowering the accuracy of the prediction, instead optimizing the data collection for UAV-based remote sensing.

The results from directly predicting grain yield using multiple VIs selected from recursive feature elimination show that a low correlation between grain yield and VIs still resulted in prediction performance comparable to the grain yield prediction model developed from VI-estimated AGB and LAI. This was observed when the prediction model was developed for each cultivar, and some cultivars performed better when grain yield was directly predicted from cumulative VI values. The results indicate the following (1) prediction performance highly depends on the model algorithm used even with low correlations between the variables; a robust algorithm can detect data patterns that are beyond the simple correlation between variables, and (2) feature selection method is an important aid in improving prediction by reducing prediction time by removing redundant features that would likely result in similar performance with a model having lower dimensions, (3) the use of estimated values

for another prediction model may result in higher prediction error as the estimated values transfer the error to the next prediction model but can be improved by removing sources of variations that can lead to overfitting.

The study observed this by developing prediction models for each cultivar, as some cultivars performed better than others. Given these results, grain yield may be predicted using VIs directly or by using VI-estimated AGB and LAI, provided that the significant source of variations is optimally represented and minimized in the model. Failure in doing so requires a reduction in the complexity of the model by developing a prediction model without the apparent source of variation. In the case of this study, it was the varietal effect in the model. Nevertheless, both prediction models, grain yield-VI and grain yield-VI, estimated AGB & LAI resulted in optimally predicting grain yield between tillering to initial heading stages, depending on the cultivars. It is better than predicting grain yield at ripening stages where changes in crop management would not likely bring grain yield improvement.

The entire study's results can be considered during rice crop management. The improved AGB and LAI estimate from UAV-derived variables across growth stages can be used to evaluate if the current nutrient management is effective. Field evaluation time of rice crop breeding for better LAI might be shortened by utilizing the LAI estimation model using UAV-derived spectral and texture variables. Moreover, the AGB estimation model using VI and Vegetation Fraction Cover (VF) can guide breeders to identify nutrient-use efficient cultivars without AGB sampling at mid-season, wherein the need for topdressing is evaluated.

7. Appendix

Table A1. Analysis of variance for the grain yield of Aichinokaori as affected by year, fertility level, and growth stage.

	Df	Sum Sq	Mean Sq	F value	Pr(>F)
lai_disc	2	4.31	2.156	4.09	0.01954
trial	1	11.57	11.571	21.95	8.58E-06
Year	1	24.28	24.282	46.064	7.47E-10
agb_disc	5	2.74	0.548	1.04	0.398105
Growth_stage	2	9.74	4.871	9.24	0.000204
lai_disc:trial	1	0.29	0.291	0.552	0.459311
lai_disc:year	2	4.26	2.131	4.043	0.020403
trial:year	1	1.04	1.041	1.976	0.162851
lai_disc:agb_disc	9	8.45	0.939	1.781	0.080712
trial:agb_disc	4	1.2	0.3	0.569	0.685362
year:agb_disc	4	5.34	1.335	2.532	0.044792
lai_disc:Growth_stage	1	0.81	0.807	1.53	0.218873
trial:Growth_stage	2	3.52	1.762	3.342	0.039234
year:Growth_stage	2	5.26	2.63	4.989	0.008548
agb_disc:Growth_stage	1	0.04	0.041	0.077	0.781916
lai_disc:trial:year	1	0.12	0.116	0.219	0.640455
trial:year:agb_disc	1	1.13	1.128	2.141	0.1465
Residuals	103	54.3	0.527		

Table A2. Analysis of variance for the grain yield of Asahi as affected by year, fertility level, and growth stage.

	Df	Sum Sq	Mean Sq	F value	Pr(>F)
lai_disc	2	6.38	3.19	6.24	0.00278
trial	1	27.72	27.722	54.226	4.94E-11
year	1	5.81	5.805	11.355	0.00107
agb_disc	5	1.39	0.277	0.542	0.74382
Growth_stage	2	2.02	1.008	1.972	0.14448
lai_disc:trial	1	0.01	0.007	0.013	0.9093
lai_disc:year	2	1.79	0.895	1.751	0.17877
trial:year	1	0.51	0.508	0.993	0.32128
lai_disc:agb_disc	6	4.4	0.733	1.434	0.2092
trial:agb_disc	4	1.75	0.438	0.856	0.49298
year:agb_disc	5	1.41	0.282	0.552	0.73613
lai_disc:Growth_stage	3	1.49	0.496	0.97	0.41022
trial:Growth_stage	2	0.56	0.28	0.547	0.58034
year:Growth_stage	2	0.7	0.349	0.683	0.50737
agb_disc:Growth_stage	2	0.96	0.478	0.935	0.39578
lai_disc:trial:year	1	0.4	0.403	0.789	0.37646
lai_disc:trial:agb_disc	1	0	0	0	0.98448
trial:year:agb_disc	1	0.32	0.325	0.635	0.42747
Residuals	101	51.63	0.511		

Table A3. Analysis of variance for the grain yield of Hatsushimo as affected by year, fertility level, and growth stage.

	Df	Sum Sq	Mean Sq	F value	Pr(>F)
lai_disc	2	6.68	3.34	4.421	0.014347
trial	1	79.84	79.84	105.743	2.00E-16
year	1	10.02	10.02	13.267	0.000421
agb_disc	5	4.54	0.91	1.203	0.312822
Growth_stage	2	3.19	1.59	2.112	0.126066
lai_disc:trial	1	0	0	0.001	0.974748
lai_disc:year	1	0.07	0.07	0.094	0.760365
trial:year	1	4.62	4.62	6.123	0.014941
lai_disc:agb_disc	6	4.76	0.79	1.05	0.397323
trial:agb_disc	4	2.29	0.57	0.757	0.555702
year:agb_disc	4	1.51	0.38	0.501	0.734742
lai_disc:Growth_stage	2	0.01	0	0.006	0.993532
trial:Growth_stage	2	1.38	0.69	0.916	0.403325
year:Growth_stage	1	0.53	0.53	0.699	0.405008
agb_disc:Growth_stage	2	1	0.5	0.661	0.518608
lai_disc:trial:year	1	0.21	0.21	0.273	0.602471
lai_disc:year:agb_disc	1	1.39	1.39	1.835	0.178461
trial:year:agb_disc	1	0.05	0.05	0.061	0.804924
Residuals	105	79.28	0.76		

Table A4. Analysis of variance for the grain yield of Nakate Shinsenbon as affected by year, fertility level, and growth stage.

	Df	Sum Sq	Mean Sq	F value	Pr(>F)	
lai_disc	2	18.1	9.05	11.277	3.69E-05	
trial	1	0.02	0.016	0.02	0.888277	
year	1	8.5	8.501	10.593	0.001532	
agb_disc	5	1.84	0.367	0.457	0.807037	
Growth_stage	2	31.22	15.608	19.45	6.67E-08	
lai_disc:trial	2	11.61	5.806	7.235	0.001143	
lai_disc:year	1	0.02	0.018	0.022	0.881664	
trial:year	1	2.71	2.712	3.379	0.068881	.
lai_disc:agb_disc	5	6.74	1.348	1.679	0.146108	
trial:agb_disc	5	6.24	1.248	1.555	0.17941	
year:agb_disc	3	1.16	0.387	0.482	0.695493	
lai_disc:Growth_stage	3	3.5	1.166	1.453	0.231818	
trial:Growth_stage	2	13.48	6.739	8.397	0.000416	
year:Growth_stage	1	0.04	0.039	0.049	0.825678	
agb_disc:Growth_stage	3	0.31	0.102	0.127	0.943819	
lai_disc:trial:year	1	1.62	1.619	2.017	0.158535	
lai_disc:trial:agb_disc	1	0.16	0.165	0.205	0.651585	
Residuals	104	83.46	0.803			

Table A5. Analysis of variance for the grain yield of Nikomaru as affected by year, fertility level, and growth stage.

	Df	Sum Sq	Mean Sq	F value	Pr(>F)
lai_disc	2	8.45	4.226	9.368	0.000191
trial	1	20.84	20.836	46.185	8.74E-10
year	1	7.52	7.517	16.662	9.18E-05
agb_disc	5	5.41	1.082	2.399	0.042608
Growth_stage	2	3.8	1.902	4.216	0.017549
lai_disc:trial	2	1.98	0.991	2.196	0.116724
lai_disc:year	2	5.03	2.515	5.575	0.005108
trial:year	1	0.24	0.237	0.525	0.470545
lai_disc:agb_disc	6	8.54	1.423	3.155	0.007194
trial:agb_disc	4	2.51	0.628	1.392	0.242503
year:agb_disc	4	0.24	0.059	0.132	0.970389
lai_disc:Growth_stage	3	0.05	0.017	0.037	0.990235
trial:Growth_stage	2	2.02	1.011	2.24	0.111939
year:Growth_stage	1	0.25	0.254	0.562	0.455296
agb_disc:Growth_stage	3	0.59	0.198	0.439	0.725453
lai_disc:trial:year	1	0.01	0.009	0.021	0.8854
lai_disc:trial:agb_disc	2	1.71	0.856	1.896	0.155621
trial:year:agb_disc	2	0.53	0.267	0.592	0.55532
trial:year:Growth_stage	1	1.17	1.172	2.597	0.110314
lai_disc:agb_disc:Growth_stage	1	3.19	3.186	7.062	0.009207
Residuals	97	43.76	0.451		

8. References

1. Zhang, Z.-H.; Li, P.; Wang, L.-X.; Hu, Z.-L.; Zhu, L.-H.; Zhu, Y.-G. Genetic Dissection of the Relationships of Biomass Production and Partitioning with Yield and Yield Related Traits in Rice. *Plant Science.* **2004**, *167(1)*, 1–8, doi:10.1016/j.plantsci.2004.01.007.
2. G. Poley, L.; J. McDermid, G. A Systematic Review of the Factors Influencing the Estimation of Vegetation Aboveground Biomass Using Unmanned Aerial Systems. *Remote Sensing.* **2020**, *12(7)*, 1052, doi:10.3390/rs12071052.
3. Zhang, D.; Mansaray, L.R.; Jin, H.; Sun, H.; Kuang, Z.; Huang, J. A Universal Estimation Model of Fractional Vegetation Cover for Different Crops Based on Time Series Digital Photographs. *Computers and Electronics in Agriculture.* **2018**, *151*, 93–103, doi:10.1016/j.compag.2018.05.030.
4. Yang, K.; Gong, Y.; Fang, S.; Duan, B.; Yuan, N.; Peng, Y.; Wu, X.; Zhu, R. Combining Spectral and Texture Features of UAV Images for the Remote Estimation of Rice LAI throughout the Entire Growing Season. *Remote Sensing.* **2021**, *13(15)*, 3001, doi:10.3390/rs13153001.
5. Wang, L.; Chang, Q.; Yang, J.; Zhang, X.; Li, F. Estimation of Paddy Rice Leaf Area Index Using Machine Learning Methods Based on Hyperspectral Data from Multi-Year Experiments. *PlosS one.* **2018**, *13(12)*, e0207624, doi:10.1371/journal.pone.0207624.
6. Chen, Z.; Jia, K.; Xiao, C.; Wei, D.; Zhao, X.; Lan, J.; Wei, X.; Yao, Y.; Wang, B.; Sun, Y.; et al. Leaf Area Index Estimation Algorithm for GF-5 Hyperspectral Data Based on Different Feature Selection and Machine Learning Methods. *Remote Sensing.* **2020**, *12(13)*, 2110, doi:10.3390/rs12132110.
7. Yang, W.; Peng, S.; Laza, R.C.; Visperas, R.M.; Dionisio-Sese, M.L. Grain Yield and Yield Attributes of New Plant Type and Hybrid Rice. *Crop Science.* **2007**, *47(4)*, 1393–1400, doi:10.2135/cropsci2006.07.0457.
8. Mohamad, O.; Suhaimi, O.; Abdullah, M. Z. The relationships between harvest index, grain yield and biomass in rice. *MARDI Research Journal*. **1994**, 22(1), 29-3, https://citeseerx.ist.psu.edu/viewdoc/download?doi=10.1.1.1045.1417&rep=rep1&type=pdf
9. Aboelghar, M.; Arafat, S.; Abo Yousef, M.; El-Shirbeny, M.; Naeem, S.; Massoud, A.; Saleh, N. Using SPOT Data and Leaf Area Index for Rice Yield Estimation in Egyptian Nile Delta. *Egyptian Journal of Remote Sensing and Space Science.* **2011**, *14(2)*, 81–89, doi:10.1016/j.ejrs.2011.09.002.

Acknowledgement

I would like to express my deepest appreciation and gratitude to the following people who have greatly helped through this.

To my adviser, Dr. Shunsaku Nishiuchi, for the advices, encouragements, and guidances that he provided to me. Thank you so much sensei.

To the members of my guidance committee, Dr. Kazuyuki Doi, Dr. Yoshiaki Inukai, Dr. Mikio Nakazono, and Dr. Jun Murase for their time, effort, and suggestions to improve the manuscript.

To the Ministry of Education, Culture, Sports, Science and Technology (MEXT) through the Japanese Government (Monbukagakusho: MEXT) Scholarship for the generosity in providing scholarship that allowed me to pursue my graduate studies.

To all the Graduate School of Bioagricultural Sciences staff for the accommodation, guidance and assistance for the completion of all the requirements of my graduate study.

To all my groupmates in the laboratory, Ms. Kobayashi, Mr. Kato, Mr. Inoue, Mr. Nakata, Mr. Takata, and Mr. Shibata and to all the students in the laboratory, Information Sciences in Agricultural Lands, for all the support and company, thank you.

To Mr. Mizuno, Ms. Kuwahata, and all the staff of the Meidai Nojo for all the administrative and fieldwork support they provided.

To all my fellow Filipino and foreign students in Nagoya University, for all the support and advices.

To my family, Mommy, Daddy and ate Mariz for their unwavering support. Thank you for supporting me all these years.

And above all, to God who made everything possible. To God be the glory.